UNCLASSIFIED

AD NUMBER

AD821818

NEW LIMITATION CHANGE

TO

Approved for public release, distribution unlimited

FROM

Distribution authorized to U.S. Gov't. agencies and their contractors; Critical technology; Sep 1967. Other requests shall be referred to Air Force Flight Dynamics Laboratory, Research and Technology Division, Wright-Patterson AFB, OH, 45433.

AUTHORITY

AEEDL ltr, 23 Jan 1973

THIS PAGE IS UNCLASSIFIED

AFFDL-TR-67-128

AD821818

ANALYTICAL STUDY OF AIR DATA EQUATIONS FOR A HEMISPHERICAL PRESSURE PROBE THROUGH THE HYPERSONIC MACH NUMBER RANGE

David J. Romeo
Cornell Aeronautical Laboratory, Inc.

Technical Report AFFDL-TR-67-128

September 1967

This document is subject to special export controls and each transmittal to foreign governments or foreign nationals may be made only with prior approval of the Air Force Flight Dynamics Laboratory, Wright-Patterson Air Force Base, Ohio 45433.

Air Force Flight Dynamics Laboratory
Research and Technology Division
Air Force Systems Command
Wright-Patterson Air Force Base, Ohio

NOTICES

When Government drawings, specifications, or other data are used for any purpose other than in connection with a definitely related Government procurement operation, the United States Government thereby incurs no responsibility nor any obligation whatsoever; and the fact that the Government may have formulated, furnished, or in any way supplied the said drawings, specifications, or other data, is not to be regarded by implication or otherwise as in any manner licensing the holder or any other person or corporation, or conveying any rights or permission to manufacture, use, or sell any patented invention that may in any way be related thereto.

Copies of this report should not be returned to the Research and Technology Division unless return is required by security considerations, contractual obligations, or notice on a specific document.

ANALYTICAL STUDY OF AIR DATA EQUATIONS FOR A HEMISPHERICAL PRESSURE PROBE THROUGH THE HYPERSONIC MACH NUMBER RANGE

David J. Romeo
Cornell Aeronautical Laboratory, Inc.

FOREWORD

This report was prepared by Cornell Aeronautical Laboratory, Inc. under USAF Contract No. AF33(615)-3554. The contract was initiated under Project No. 8222, Task No. 822207. The work was administered under the direction of the Air Force Flight Dynamics Laboratory, Research and Technology Division. Mr. William E. Ross served as project engineer over the initial portion of the program, and Mr. Ralph Guth served during the latter phase of the study.

This report covers work conducted from March 1966 through June 1967.

The interest and helpful suggested of the Air Force contract project engineers, R. Guth and W. E. Ross, are gratefully acknowledged. Appreciation is also expressed to Miss N. Robinson and to Mrs. S. Sweet for their extensive work in performance of the calculations and in preparation of the final report.

This report has been reviewed and is approved.

H. W. BASHAM
Chief, Control Elements Branch
Flight Control Division
AF Flight Dynamics Laboratory

ABSTRACT

Air data outputs obtainable from pressure measurements on a hemispherical probe have been investigated analytically through the Hypersonic Mach number range. Angles of attack from +50° to -20° and angles of sideslip to ±15° are considered using a five orifice probe (one centerline, two each in angle of attack and angle of sideslip planes). Emphasis is put on the hypersonic regime, wherein air data outputs are shown to be obtainable by using a simplified set of equations. Specifically, vehicle attitude can be obtained from pressure inputs alone; true air speed can be obtained with the additional input of free stream density. Pressure expressions used to obtain attitude angle for the hypersonic regime are found to be acceptable for Mach numbers as low as . 5. Expressions for determining the uncertainties in the air data outputs resulting from both pressure measurement error and simplifying assumptions used in deriving the air data equations are presented. Discussions on the capability of determining vehicle altitude and Mach number with inputs of hemisphere pressure and free stream density are given. Finally, air data output errors resulting from changes in nose shape due to material ablation are also considered.

TABLE OF CONTENTS

TABLE OF CONTENTS (Cont'd)

LIST OF FIGURES

LIST OF FIGURES (Cont'd)

LIST OF FIGURES (Cont'd)

LIST OF SYMBOLS

a	Speed of sound, ft. /sec.
C	Pressure error or uncertainty, $\Delta P / P$
C_p	Specific heat at constant pressure, $ft^2/sec^2\ °R$
d	Orifice diameter, inches
D	Probe diameter, inches
h	Altitude, ft.; also enthalpy, ft^2/sec^2
K	Empirical constant in P_s/q relation
Δl	Nose recession distance due to ablation, inches
m	Mass, slugs
M	Mach number
n	Exponent in pressure distribution expression
N	Normal force, pounds
P	Pressure, $pounds/ft^2$
q	Free stream dynamic pressure, $\frac{1}{2}\rho_\infty U_\infty^2$, $pounds/ft^2$
r	Probe radius, $D/2$, inches
R	Gas constant, 1716.3 $ft^2/sec^2\ °R$
S	Area, ft^2
t	Time, sec.
T	Temperature, °R
u, v, w	Velocity components in x, y, z axes system; Figure 1
U_i	Indicated air speed
U_∞	Free stream velocity (true air speed), ft/sec
$U_{\infty, N}$	Free stream velocity component normal to probe surface, ft/sec
x, y, z	Righthanded orthogonal body axes system, Figure 1
Z	Imperfect gas law constant, $P/\rho RT$

Preceding Page Blank

α	Angle of attack
β	Angle of sideslip
γ	Angle between axis of symmetry and some given orifice in x-y plane, also ratio of specific heats
δ, ϵ	Angles used in defining attitude angles
θ	Angle between stagnating streamline and some given orifice location
ρ	Density, slugs/ft^3
ϕ	Angle between axis of symmetry and some given orifice in x-z plane

SUBSCRIPTS

1-4	Various orifice locations
r	Values behind normal shock
s	Stagnation values
∞	Free stream values

NOTE: Bars over symbols, e.g. $\overline{U_\infty}$, indicate vector quantities; primes, e.g. n', indicate ablation perturbed quantities.

SECTION I

INTRODUCTION

Air data, as used in this report, means information describing the attitude, air speed, Mach number and altitude of a flight vehicle. In this study, assumed air data inputs are pressure measurements on a hemispherical probe, with and without the additional input of free stream density. The probe in a typical flight usage could well be the nose (on the order of a half-foot diameter) of the flight vehicle, and it will be assumed to be free of pressure perturbation due to other vehicle components.

Instrumentation and techniques used to obtain air data at subsonic, transonic, and low supersonic Mach numbers are highly developed. A bibliography of this work is presented in Reference (1). At these speeds, the conventional approach has been to equip the flight vehicle with external probes provided with sensors which measure stagnation pressure and indicated static pressures, local flow angles and total temperature. That information can be related to free stream values of static pressure, angle of attack and sideslip and temperature to provide data on the relationship of the aircraft to the atmosphere through which it is flying as well as data on the atmosphere itself. It is normal practice to design probes and locate static sources on the vehicle which by themselves introduce minimum errors in the measurement of stagnation and static pressures over the flight range of interest. Once installed on a vehicle, the air data computer is designed to correct for the so-called position errors of the flight vehicle.

To speeds of about Mach 2 or Mach 3, these errors may be regarded as perturbations to the basic measurement and corrections as determined from full-scale flight tests and wind tunnel tests are applied. At high supersonic-hypersonic Mach numbers, however, the conditions are vastly different. Hypersonic flows are characterized by strong shock wave systems lying close to the body surface; hence, air data, static pressure, for example, cannot be obtained through small corrections to some measurement. Total or stagnation temperature measurement is subject to real gas effects and proper interpretation of stagnation enthalpy from this measurement is difficult (see Reference 2).

In the past half dozen years or so, much valuable experimental information has been obtained concerning air data at supersonic Mach numbers -- particularly with regard to vehicle attitude on X-15 flights, see, for example, References (3-8). Attitude angle for these flights was measured using rotating hemispherical null seeking pressure probe. This investigation was undertaken in order to describe fully the maximum utility of a simple fixed position pressure-instrumented hemisphere probe at high Mach numbers, and also to consider the maximum obtainable air data outputs obtainable from this sensor at the lower Mach numbers.

Although the study considered air data investigation over the range of Mach numbers up to 20 for altitudes to 300,000 feet, because of present air data needs for hypersonic cruise as well as lifting re-entry vehicles, emphasis was put on the high Mach number range. Furthermore, of the air data outputs defined above, primary emphasis, again because of present needs, was given to vehicle

attitude (angles of attack and sideslip) and velocity (true air speed). Specifically, the study consisted of defining the equations needed to describe the pressure distribution over a hemisphere, particularly in the hypersonic range, and then using these equations developing expressions for the air data outputs, (angle of attack, true air speed, etc.). Throughout the study, frequent use of error analysis was employed in order to assess not only the usefulness of the various expressions, but as a useful tool in determining orifice location, and the validity of simplifying assumptions.

The air data investigation presented herein was written such that similar air data outputs (e.g. α and β) are grouped in individual sections. Angle of attack and angle of sideslip are discussed in Section II. True air speed and indicated air speed investigations are given in Section III. Mach number and altitude because of their similar dependence on the input of free stream density are both considered in Section IV. A cursory examination of the degree of nose ablation for a typical flight case and the effect of this ablation on the air data attitude equations is given in Section V. Each section was written with the intent of making it a fairly complete discussion in itself of the particular air data output being considered.

Results are given in forms which can be easily assessed for accuracy and/or modifications for a particular application. Suggestions for additional work, primarily experimental, to further develop the usefulness of this air data probe are given.

SECTION II

VEHICLE ATTITUDE ANGLE

1. DEFINITION OF VEHICLE ATTITUDE ANGLE AND AXIS SYSTEM

Consider a body at some arbitrary attitude with respect to the free stream velocity vector $\bar{U}_\infty$, as shown in Figure 1. To describe the attitude of the body with respect to this velocity vector an axis reference system is defined. This system, employs the body axes (see e.g. Reference 3) and is a right-handed orthogonal set with the origin at the body center of gravity (c.g.). A longitudinal plane of symmetry for the body is assumed. Then the axes are:

x - in the plane of symmetry, directed longitudinally forward.

y - normal to the plane of symmetry, directed along the right wing.

z - in the plane of symmetry directed "down."

Further, let the projections of the velocity vector $\bar{U}_\infty$ on the body axes be called $\bar{u}$, $\bar{v}$, $\bar{w}$ for components along the x, y, and z axes, respectively.

The angles are now defined in terms of the velocity vector and its projections on the orthogonal body axes. Angle of attack, α, and angle of sideslip, β, are defined in the x-z and x-y planes, respectively, as:

angle of attack, $$\alpha = \cos^{-1}\frac{\bar{u}}{(u^2+w^2)^{1/2}} = \sin^{-1}\frac{\bar{w}}{(u^2+w^2)^{1/2}} \tag{1}$$

angle of sideslip, $$\beta = \cos^{-1}\frac{\bar{u}}{(w^2+v^2)^{1/2}} = \sin^{-1}\frac{\bar{v}}{(w^2+v^2)^{1/2}} \tag{2}$$

A third angle, δ, (herein unnamed) that is useful to define is:

$$\delta = \cos^{-1}\frac{(u^2+w^2)^{1/2}}{\bar{U}_\infty} = \sin^{-1}\frac{\bar{v}}{\bar{U}_\infty} \tag{3}$$

This angle δ has sometimes been called the angle of sideslip (see, for example, References 9-11). However, in this study, the sideslip angle is the angle defined by Equation (2). Note that while α and β are defined in the planes of the body axes, δ is not. Further note that δ is independent of angle of attack, i.e. the vector $(u^2 + w^2)^{1/2}$ remains constant as α varies; whereas β is not independent of α, since the vector, $\bar{u}$, varies as α varies. For this reason, δ will be used in the derivations of an expression for α in terms of the pressure distribution in the x-z plane, wherein, the pressure distribution in the x-y plane will subsequently be shown to be independent of δ.

2. ATTITUDE ANGLE DETERMINATION AT HYPERSONIC MACH NUMBERS

The capability (including accuracy, range of use, etc.) of the hemispherical pressure probe as used to measure angle of attack and angle of sideslip depends on the following factors;

1) The accuracy to which the pressures are known.

2) The correctness of the assumed pressure distributions.

3) The choice and degree of exactness of the derived attitude equations with consideration given to the selection of orifice locations.

Pressure accuracy, of course, is applicable to the entire Mach number range. The last two factors, however, require different analysis for different Mach number regimes. Since, as stated in the introduction, emphasis will be placed on the hypersonic Mach number regime, consideration is first given to this range and then to the lower Mach numbers.

a. Pressure Accuracy

The air data error equations developed are general enough to allow introduction of pressure errors of various magnitude, however, plus or minus one percent pressure errors are used in this study. One percent errors are not meant to represent present state of the art pressure transducer capability but rather are used solely for purposes of illustration and comparison. Present systems are better than one percent, perhaps one-fourth of one percent, thus conclusions as to the actual usefulness of a result are conservative.

b. Pressure Distribution at Hypersonic Mach Numbers

Pressure data obtained on a hemispherical nose can be thought of as two separate data inputs: pressure distribution and absolute pressure magnitude. Determination of attitude angles α and β will be seen to be independent of absolute magnitudes, dependent on distribution only.

The most widely accepted approximate method used to predict the pressure distribution on a hemisphere in hypersonic flow is the simple Newtonian impact flow theory. It is useful to consider the assumptions upon which the theory is based and to include herein its derivation.

Consider the streamline encountering the hemispherical surface at an angle θ (see sketch below). No mention is made of any shock process associated with the flow; it is assumed that none exists.

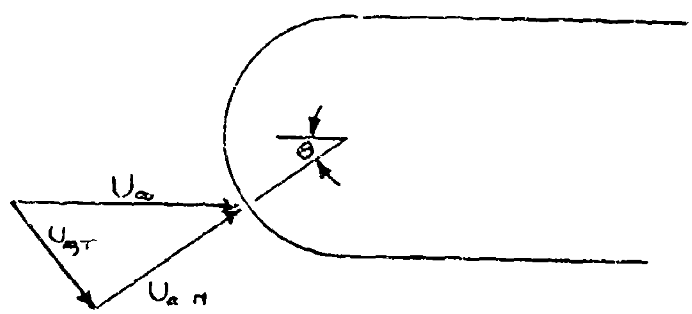

The only assumption that is made, and this constitutes the basis of the theory, is that the streamline must turn an angle $(90-\theta)$ upon impact with the body, and in so doing, all flow momentum normal to the surface, $m\,U_{\infty,N}$, is lost to the body, whereas the tangential component of momentum is entirely

conserved. Therefore, the normal force on the surface is

$$N = \frac{d}{dt}\left(m\, U_{\infty,N}\right) = U_{\infty,N}\,\frac{dm}{dt} \tag{4}$$

where the mass flow rate normal to the surface is

$$\frac{dm}{dt} = \rho_\infty U_{\infty,N}\, S \qquad \text{for area S.}$$

Notice the assumption of an incompressible fluid, ρ_∞ = Constant, is implied here.

Thus,
$$N = \rho_\infty U_{\infty,N}^{2}\, S \tag{5}$$

but
$$U_{\infty,N} = U_\infty \cos\theta \qquad \text{so the pressure at } \theta\text{ ,} \tag{6}$$

is
$$P = N/S$$

$$P = \rho_\infty U_\infty^{2} \cos^2\theta = 2\, q \cos^2\theta \tag{7}$$

where
$$q = \frac{1}{2}\rho_\infty U_\infty^{2}$$

is the pressure acting on the surface at θ . This is the Newtonian flow prediction. As the impact angle goes to zero, $\cos^2\theta \longrightarrow 1$, the fluid at this location stagnates and the Newtonian theory simply gives:

$$P_s/q = 2 \tag{8}$$

or P_s , the stagnation pressure, is equal to two times the dynamic pressure, q. The value of P_s is known experimentally to be incorrect. Quite often a modified Newtonian Theory,* whereby the value of $P/\cos^2\theta$ is set equal to a known stagnation pressure P_s at $\theta = 0$, is used in the pressure distribution prediction; i. e.,

$$P = P_s \cos^2\theta \tag{9}$$

The validity of this pressure distribution equation at high Mach numbers is next considered in view of analytical and experimental results.

Experimental pressure data taken in the Cornell Aeronautical Laboratory hypersonic shock tunnel (Reference 12) on a 12-inch diameter hemisphere cylinder at U_∞ = 14,000 fps is shown in Figure 2. These results are averaged data for approximately 14 tunnel runs, and are also shown corrected for the effects of the conical flow field in which the model was tested using the

* Suggested by L. Lees, IAS Preprint JJ4, 1955.

characteristic conical flow solutions of Reference (13). In conjunction with the experimental tests, a computer program for a real-reacting gas was used to predict the hemisphere pressure distribution for the test conditions of the program. Additionally, exact numerical solutions for an ideal gas (Reference 14) are shown in Figure 2.

Several important points are evident from Figure 2:

1) The corrected experimental data and the real gas solution at U_∞ = 14,000 fps are both in excellent agreement with the ideal gas solutions.

2) The ideal gas solutions are practically invariant with Mach number for $8 < M < 30$.

3) These curves lie below the $\cos^2 \theta$ curve, showing an inadequacy in using the modified Newtonian distribution.

In view of these results, the numerical real and ideal solutions and the experimental data are accepted as presenting the correct hypersonic hemispherical pressure distribution.

It was next decided to see how simply this distribution could be approximated. Of the numerous methods for approximating the pressure distribution (power series, trigonometric series, etc.). it was felt that a simple relation of the form

$$P = P_s \cos^n \theta \tag{10}$$

would best fit the purposes of the study. This is a straightforward choice since this relation is of the familiar Newtonian approximation form and requires only the generalization that the cosine exponent, n, is not assumed to be 2.0.

In Figure 3, P/p_s averaged from the numerical solutions is plotted versus $\cos \theta$ on log-log paper. Thus, if $P/p_s = \cos^n \theta$, we can write $\log P/p_s = n \log \cos \theta$ and n will be the slope of the curve. Fairing a straight line through these data produces a resulting slope of n = 2.24. Lines which bound the whole curve are seen to fall between 2.14 and 2.34. Thus, a maximum error in n of $\Delta n/n = \pm 0.1/2.24$ is assumed to exist. The curve $P/p_s = \cos^{2.24} \theta$ is also shown plotted in Figure 2 for comparison to the numerical and experimental results.

c. Attitude Equations at Hypersonic Mach Numbers

The pressure distribution selected for the hemisphere probe was seen to be of the form

$$P = P_s \cos^n \theta , \qquad n = 2.24 \tag{10}$$

where θ is the angle between the stagnation point and some orifice at which pressure P is measured. With reference to the body axis system defined in Section II. 1., the attitude angles α and β can be determined from this assumed pressure distribution and from the pressure measurements in the x-z and x-y planes, respectively.

Since the location of any orifice can be measured in terms of its angular displacement from the stagnation point, herein called the angle θ, for any orifice, i, the pressure, P_i can be expressed as a function of the stagnation pressure, P_s, and the cosine of the angle θ.

$$P_i = P_s \cos^n \theta \tag{10}$$

For an orifice in the x-z plane, (see Figure 1) say P_1

$$P_1 = P_s \cos^n \theta \tag{11}$$

but

$$\cos \theta = \bar{U}/\bar{U}_\infty \tag{12}$$

$$\cos \alpha = \bar{U}/(u^2 + w^2)^{1/2} \tag{13}$$

$$\cos \delta = (u^2 + w^2)^{1/2}/\bar{U}_\infty \tag{14}$$

so that

$$\cos \theta = \cos \alpha \cos \delta \tag{15}$$

or

$$P_1 = P_s \cos^n \alpha \cos^n \delta \tag{16}$$

This is a useful relation, since δ does not vary with attitude angle in the x-z plane; thus the pressure at any attitude location in this plane is independent of δ. Any pressure in the x-z plane is thus

$$P_i = P_s \cos^n \delta \cos^n (\alpha - \phi_i) \tag{17}$$

where ϕ_i is the orifice angular displacement from the x-axis, in the x-z plane.

The determination of sideslip angle β, as defined, is identically the same problem as the determination of α. All that is required to show this is the introduction and subsequent cancellation of an additional angle, say ϵ :

$$\epsilon = \cos^{-1} \frac{(u^2+v^2)^{1/2}}{\bar{U}_\infty} = \sin^{-1} \frac{\bar{w}}{\bar{U}_\infty} \tag{18}$$

such that the pressure distribution in the x-y plane is

$$P_j = P_s \cos^n \theta = P_s \cos^n (\beta + \phi_j) \cos^n \epsilon \tag{19}$$

As can be seen from Eq. (19), the distribution in the x-y plane is independent of ϵ as was the pressure distribution in the x-z plane independent of δ.

(1) Determination of Angle of Attack

The pressure on the hemisphere at some point in the x-z plane was seen to be

$$P = P_s \cos^n \theta = P_s \cos^n \delta \cos^n (\alpha - \phi) \tag{17}$$

where the angle δ is invariant in this plane. Thus, the pressure distribution in the x-z plane is independent of P_s and the angle δ. Similarly, an expression for α can be nondimensionalized to make it independent of $P_s \cos^n \delta$. Consider the pressure at three orifice locations in the x-z plane (see sketch, p. 9).

$$P_1 = P_s \cos^n \delta \cos^n(\alpha - \phi_1) \tag{17}$$

$$P_2 = P_s \cos^n \delta \cos^n \alpha \quad , \quad \phi_2 = 0 \tag{20}$$

$$P_3 = P_s \cos^n \delta \cos^n(\alpha - \phi_3) \tag{21}$$

$P_s \cos^n \delta$ is common to all three equations. Thus, Equations 17, 20 and 21 represent only two independent equations for the determination of unknowns $(P_s \cos^n \delta)$ and α, or three independent equations for the determination of $(P_s \cos^n \delta)$, α, and n if it is not assumed that n is known. For the hypersonic case where n is known, any two of the three equations are sufficient for the solutions of these two variables. However, the solution for α can make use of all three equations, if the inclusion of the third equation, although redundant, will decrease the uncertainty of α for given uncertainties in the individual pressure measurements. In general, then, the choice of two or three pressure measurements will depend on accuracy rather than need.

a. Angle of Attack Determined from Two Pressures

Equations 17 and 20 can be used to eliminate $P_s \cos^n \delta$ by either of the two formulations:

$$\frac{P_1 - P_2}{P_1 + P_2} = \frac{\cos^n(\alpha - \phi_1) - \cos^n \alpha}{\cos^n(\alpha - \phi_1) + \cos^n \alpha} \tag{22}$$

or

$$\frac{P_1}{P_2} = \frac{\cos^n(\alpha - \phi_1)}{\cos^n \alpha} \tag{23}$$

Equation (22) is shown plotted in Figure 4 for values of ϕ_1 chosen to cover the angle of attack range, remembering from Figure 3 that the pressure distribution, $P = P_s \cos^n \theta$, is valid only for θ up to about 65°.

The curves of Figure 4 demonstrate the sensitivity of the ratio $\left(\frac{P_1 - P_2}{P_1 + P_2}\right)$ to α for different values of ϕ_1 and can thus be used to select ϕ_1's that will minimize uncertainties in α due to uncertainties in measurements of P_1 and P_2. First of all, however, it is necessary to find an expression for the change in $\left(\frac{P_1 - P_2}{P_1 + P_2}\right)$ due to changes in P_1 and P_2. This is done by differentiating Equation (22)*:

$$d\left(\frac{P_1 - P_2}{P_1 + P_2}\right) = \frac{\partial\left(\frac{P_1 - P_2}{P_1 + P_2}\right)}{\partial P_1} dP_1 + \frac{\partial\left(\frac{P_1 - P_2}{P_1 + P_2}\right)}{\partial P_2} dP_2 \tag{24}$$

* To be complete, it should be considered that n also can have an uncertainty $n \pm \Delta n$; this uncertainty will be considered in the final error uncertainty equations.

SKETCH OF AIR DATA PROBE

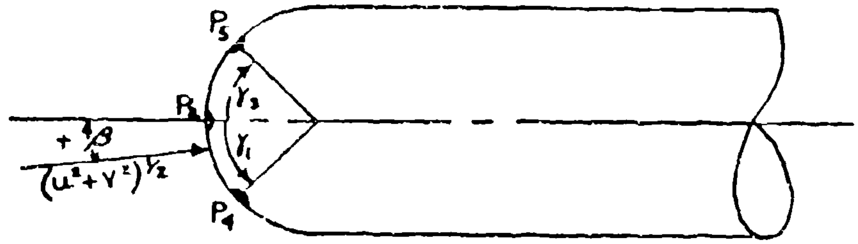

Top View x-y Plane

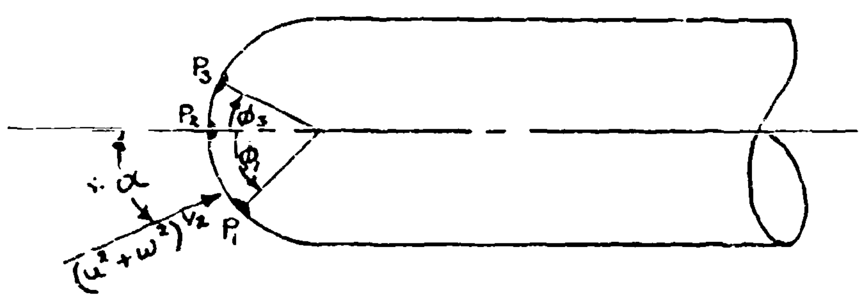

Side View x-z Plane

Where u, v, w are velocity projections on x, y and z axes, respectively (see Section II. 1.).

Performing the differentiation in Equation (24) and dividing through by Equation (22), results in

$$\frac{d\left(\frac{P_1 - P_2}{P_1 + P_2}\right)}{\frac{P_1 - P_2}{P_1 + P_2}} = \frac{2\,P_2\,dP_1}{(P_1 - P_2)(P_1 + P_2)} - \frac{2\,P_1\,dP_2}{(P_1 - P_2)(P_1 + P_2)} \tag{25}$$

Next, assume that $\frac{dP_1}{P_1} = \frac{\Delta P_1}{P_1}$, etc. Let $\frac{\Delta P_1}{P_1} = \frac{\Delta P_2}{P_2} = \pm C$ and consider the worst case, where all errors are accumulative (i.e., all plus or all minus). Equation (25) then reduces to

$$\frac{\Delta\left(\frac{P_1 - P_2}{P_1 + P_2}\right)}{\frac{P_1 - P_2}{P_1 + P_2}} = \frac{4\,C\,P_1\,P_2}{(P_1 - P_2)\,(P_1 + P_2)} \tag{26}$$

For various values of α and for the case of one percent pressure errors, $C = 0.01$, values of

$$\Delta\left(\frac{P_1 - P_2}{P_1 + P_2}\right) = \frac{4\,C\,P_1\,P_2}{(P_1 + P_2)^2} \tag{27}$$

were calculated. These increments were then added and subtracted to $\left(\frac{P_1 - P_2}{P_1 + P_2}\right)$ in Figure 4 to obtain values of $\pm\Delta\alpha$ (see sketch below).

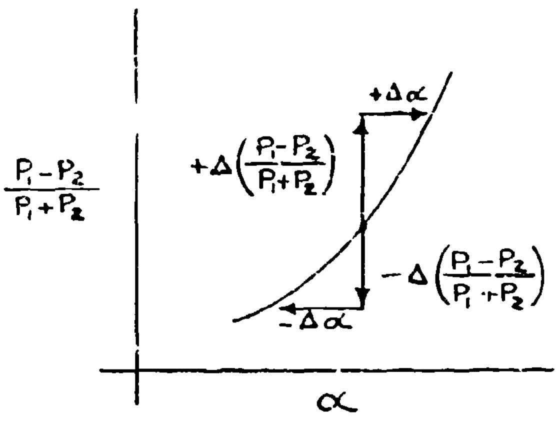

These values of $\pm\Delta\alpha$, obtained graphically, were then plotted versus α for the different ϕ's in Figure 5. As can be seen, the best choice of ϕ_1 that will cover the α range from -20° to 50° and maintain $(\alpha - \phi) \lesssim 65°$ is $\phi_1 = 45°$. For this case, $\Delta\alpha \sim \frac{1}{2}°$ for 1% errors in pressure over the entire α range.

Next, consider the alternate formulation of Equations (17) and

(20),

$$\frac{P_1}{P_2} = \frac{\cos^n(\alpha - \phi_1)}{\cos^n \alpha} \tag{23}$$

Equation (23) is plotted in Figure 6 for the ϕ_1 values considered in Figure 4. The uncertainty in α due to uncertainties in P_1 and P_2 was determined in the same manner as was done for Equation (22).

$$\frac{d(P_1/P_2)}{P_1/P_2} = \frac{dP_1}{P_1} - \frac{dP_2}{P_2} \tag{28}$$

and as before,

$$\frac{dP_1}{P_1} = \frac{dP_2}{P_2} = \frac{\Delta P}{P} = \pm C$$

$$\frac{\Delta(P_1/P_2)}{P_1/P_2} = \frac{\Delta P_1}{P_1} - \frac{\Delta P_2}{P_2} = 2C \tag{29}$$

or

$$\Delta\left(\frac{P_1}{P_2}\right) = 2C\,\frac{P_2}{P_1} \tag{30}$$

Using Equation (30), graphical values of $\Delta\alpha$ were obtained from Figure 6 and are shown plotted in Figure 7. Comparison of Figures 5 and 7 shows the results to be practically equivalent. Thus, Equation (22) presents no advantage in accuracy over Equation (23) and the simple relation

$$\frac{P_1}{P_2} = \frac{\cos^n(\alpha - \phi_1)}{\cos^n \alpha} \tag{23}$$

appears to be the better choice for angle of attack determination for the two pressure measurements. Furthermore, $\phi_1 = 45°$ is again the best choice of orifice locations. For this value of ϕ_1, Equation (23) reduces to

$$\frac{P_1}{P_2} = \left(\frac{1}{\sqrt{2}}\right)^n (1 + \tan\alpha)^n \;;\quad \phi_1 = 45° \tag{31}$$

which can now be solved directly for angle of attack.

$$\alpha = \tan^{-1}\left[\sqrt{2}\left(\frac{P_1}{P_2}\right)^{1/n} - 1\right]_{\phi_1 = 45°} \tag{32}$$

Equation (32), therefore, represents a closed form solution for α using only two pressure inputs in the x-z plane. Since this equation results in no loss in accuracy over the alternate orifice calibration, Equation (23), and has the advantage of a closed form solution in α, it has been selected as the most promising form for the two-pressure input case.

An analytical expression for angle of attack uncertainty can now be found by taking the total derivative of Equation (23), where we will now allow n to be uncertain. We will allow ϕ_1 to be variable, since we have not yet shown that $\phi_1 = 45°$ is an optimum location when n is allowed to vary. Equation (23) can be written as

$$\frac{P_1}{P_2} = \frac{\cos^n(\alpha - \phi_1)}{\cos^n \alpha} = (\cos\phi_1 + \sin\phi_1 \tan\alpha)^n \tag{33}$$

The total derivative of both sides of Equation (33) is taken, resulting in

$$\begin{aligned} 2C\left(\frac{P_1}{P_2}\right) = n\,(\cos\phi_1 + \sin\phi_1\tan\alpha)^{n-1} \sin\phi_1 \sec^2\alpha\, d\alpha \\ + (\cos\phi_1 + \sin\phi_1\tan\alpha)^n \log_e(\cos\phi_1 + \sin\phi_1\tan\alpha)\, dn \end{aligned} \tag{34}$$

Solving for $d\alpha$ produces

$$d\alpha = \frac{(\cos\phi_1 + \sin\phi_1\tan\alpha)}{\sin\phi_1}\frac{\cos^2\alpha}{n}\left[2C - \left[\log_e(\cos\phi_1 + \sin\phi_1\tan\alpha)\right]dn\right] \tag{35}$$

Next, assuming accumulative errors, and $d\alpha = \pm\Delta\alpha$, etc.

$$\Delta\alpha = (\cot\phi_1 + \tan\alpha)\frac{\cos^2\alpha}{n}\left[2C + \left[\log_e(\cos\phi_1 + \sin\phi_1\tan\alpha)\right]\Delta n\right] \tag{36}$$

Equation (36) is presented in Figure 8 for $\phi_1 = 15°$, $30°$, and $45°$ for $C = \Delta P/P$ of $\pm.01$ and for a constant value of Δn of $\pm.2$ for the purpose of selecting orifice location ϕ_1. Again, it was assumed that all errors would be accumulative. An orifice location of $\phi_1 = 45°$, as expected, is seen to produce the lowest uncertainty in $\Delta\alpha$. Actually, this error may simply decrease as ϕ_1 increases, however, 45° is just about an upper limit on ϕ_1 if we want to measure to minus 15° or 20° angle of attack. Next, the error dependence due to Δn is shown in Figure 9 for $\phi_1 = 45°$, where actual values of Δn were obtained as a function of α as follows. On a plot of the actual hemispherical pressure distribution (Figure 3), lines of $\cos^n\theta$ for various n's were drawn to intercept the curve at θ's up to 60°. Then for each θ, values of $\Delta n = 2.24 - n$ were obtained. These values were then used in Equation (36) for C = .01 to obtain the results shown in Figure 9. From Figure 9, it is seen that, up to about 45°, the $\Delta\alpha$ error due to the ΔP and Δn uncertainties is only about 6/10 of a degree, which is felt to be quite good. Furthermore, over this range the uncertainty in Δn alone is negligible as can be seen by the dotted curve which was plotted for $\Delta n = 0$, and which follows the solid curve up to 45°. Finally, for comparison, the graphically determined values of $\Delta\alpha$ from Figure 7 are also shown replotted on Figure 9; and it is seen that good agreement of the two methods of $\Delta\alpha$ determination is achieved.

b. Angle of Attack Determined from Three Pressures

In using Equations (17), (20) and (21) to determine α, it must be remembered that the assumed pressure distribution is valid only for about $\theta \leq 65°$, or $(\alpha - \phi)$ values somewhat less than 65°. Since α can be as large as 50°, ϕ_3 can be no less than about -15°; therefore, the total orifice spacing can be practically no greater than the spacing chosen for the two orifice case.

The three orifice calibration of α, however, can be compared to the two orifice calibration on the basis of accuracy and the method of pressure measurement. The formulation chosen

$$\frac{P_1 - P_2}{P_2 - P_3} = \frac{\cos^n(\alpha - \phi_1) - \cos^n(\alpha - \phi_2)}{\cos^n(\alpha - \phi_2) - \cos^n(\alpha - \phi_3)} \tag{37}$$

incorporates the use of pressure differentials, as opposed to absolute pressure measurements, which may be an advantage from an instrumentation standpoint. To cover the α range, the orifice locations were selected to be $\phi_1 = 45°$, $\phi_2 = 0°$, $\phi_3 = -15°$. For $\phi_3 = -15°$, the pressure distribution is valid up to $\alpha = 50°$, however, a singularity (i.e., $P_2 - P_3 \longrightarrow 0$) in the function as $\alpha \longrightarrow -7\frac{1}{2}$ limits the useful negative range. Equation (37) is shown plotted in Figure 10 where, for the ϕ's selected, the function reduces to

$$\frac{P_1 - P_2}{P_2 - P_3} = \frac{\left(\frac{\sqrt{2}}{2}\right)^n \left(1 + \tan\alpha\right)^n - 1}{1 - \left(.966 - .259 \tan\alpha\right)^n} \tag{38}$$

The error equation for this relation turns out to be

$$\frac{\Delta\left(\frac{P_1 - P_2}{P_2 - P_3}\right)}{\frac{P_1 - P_2}{P_2 - P_3}} = C\left[\frac{1}{1 - \frac{P_2}{P_1}} + \frac{1}{\frac{P_1}{P_2} - 1} + \frac{1}{1 - \frac{P_3}{P_2}} + \frac{1}{\frac{P_2}{P_3} - 1}\right] \tag{39}$$

or

$$\Delta\left(\frac{P_1 - P_2}{P_2 - P_3}\right) = C\left[\frac{P_1 + P_2}{P_1 - P_2} + \frac{P_2 + P_3}{P_2 - P_3}\right]\frac{P_1 - P_2}{P_2 - P_3} \tag{40}$$

The uncertainty in α, due to accumulative $C = \pm 0.01$ uncertainties in individual pressure measurements, is shown in Figure 11. As can be seen, the $\Delta\alpha$ uncertainties are larger than the two orifice formulation for most of the angle of attack range (compare Figures 7 and 11). From the standpoint of accuracy, therefore, the three orifice relation appears to be less desirable than the two orifice relation.

(2) Determination of Angle of Sideslip

Thus far the attitude angle equations, orifice selection, error equations, etc. have been evaluated for angle of attack determination. As pointed out in Section II. 1., however, there is no fundamental difference between the determination of angle of attack, α, or angle of sideslip, β. Thus, all discussion thus far written in Section II. 2. c. (1) for α orifice selection, etc. is equally applicable for β.

For the angle of attack equation, a ϕ_1 orifice located at 45° was seen to give the best P_1/P_2 relation for small α values. Therefore, although the β range is smaller than the angle of attack range, a location of γ_1 = 45° will similarly be the best choice for the β equation. Furthermore, the same arguments that showed the simple pressure ratio relation to be optimum holds equally well for β. The β equation is then, for γ_1 = 45° in the x-y plane

$$\beta = \tan^{-1}\left[\sqrt{2}\left(\frac{P_1}{P_2}\right)^{1/n} - 1\right]_{\gamma_1 = 45°} \tag{41}$$

and the error equation is

$$\Delta\beta = \left(\cot\gamma_1 + \tan\beta\right)\frac{\cos^2\beta}{n}\left[2C + \left[\log_e\left(\cos\gamma_1 + \sin\gamma_1\tan\beta\right)\right]\Delta n\right] \tag{42}$$

d. Attitude Equations at Large Angles of Attack

The attitude angle equations were derived for angle of attack usage up to approximately 50°. Thus, the choice of exponent n in

$$\frac{P}{P_s} = \cos^n\theta \tag{10}$$

was selected to minimize errors in α over this range. It is of some interest to investigate the errors in α at angles as large as 85°. This was done simply by extending Figure 3 to large θ's, Figure 12, and by using Equation (36) to generate Figure 13. Values of Δn used in Equation (36) were obtained in the same manner as was done to generate Figure 9.

From Figure 13, it is seen that, above about 50°, the angle of attack error $\Delta\alpha$ increases rapidly to rather large errors $\sim 6°$. However, the error in α, although large, would still allow use of the attitude equation

$$\alpha = \tan^{-1}\left[\sqrt{2}\left(\frac{P_1}{P_2}\right)^{1/n} - 1\right]_{\phi_1 = 45°} \tag{32}$$

for angles of attack as large as 85° with no discontinuities in the equation.

3. ATTITUDE ANGLE DETERMINATION OVER THE ENTIRE MACH NUMBER RANGE

The basic expression used in the derivation of the attitude equations at hypersonic Mach numbers in Section II. 2. c.,

$$P = P_s \cos^n \theta \tag{10}$$

was found to hold with sufficient accuracy with respect to both experimental data and theoretical solutions (Section II. 2. b.). Furthermore, it was found that the exponent n was equal to approximately 2.24. If Equation (10) is also satisfied at lower Mach numbers, nose pressures alone could continue to be used to obtain simple attitude angle expressions. To examine the validity of this pressure distribution relation at Mach numbers less than 6, data compiled in References (15) and (2) from the literature are shown in Figures 14 and 15.

These plots present P/P_s versus $\cos\theta$ on log scales; thus, a linear relation in P/P_s would indicate a distribution of the form $P/P_s = \cos^n\theta$ where the slope of the line would be equal to n. For the most part, Figures 14 and 15 do indeed show that a cosine relation provides a satisfactory approximation to the pressure distribution for Mach numbers as low as $M_\infty = .5$. The slopes of these curves (n), however, are not constant but are Mach number dependent. Values of n measured from Figures 14 and 15 are plotted as a function of M_∞ in Figure 16. The results of n correlate with M_∞ quite nicely. Furthermore, an extrapolation of the curve should satisfy the value of n (2.24) assumed to hold at hypersonic Mach numbers, which it appears to do reasonably well. This result is in good agreement with Reference (15) which showed a cosine exponent to vary from 1.5 to 2.3 in going from low supersonic to hypersonic Mach numbers; in that report, the exponent was defined through

$$\frac{P - \frac{1}{2}P_\infty}{P_s - \frac{1}{2}P_\infty} = \cos^n \theta \tag{43}$$

This equation differs slightly from the present correlation having the disadvantage of requiring a knowledge of free stream static pressure for attitude determination.

If Mach number was a known input, Figure 16 could be used to obtain n accurately enough to use the attitude expression,

$$\alpha = \tan^{-1}\left[\sqrt{2}\left(\frac{P_1}{P_2}\right)^{1/n} - 1\right] \tag{32}$$

Without being given M_∞, however, an expression for α is needed which is dependent on input nose pressure but independent of n. A relation of this form will now be developed.

Consider again the three basic pressure equations that can be written for three pressure inputs in the x-z (pitch) plane:

$$P_1 = P_s \cos^n\theta = P_s \cos^n \delta \cos^n(\alpha - \phi_1) \tag{17}$$

$$P_2 = P_s \cos^n\delta \cos^n\alpha \tag{20}$$

$$P_3 = P_s \cos^n\delta \cos^n(\alpha-\phi_3) \tag{21}$$

Pressures P_1, P_2 and P_3, are measured quantities and it is desired to find α. The quantities $(P_s \cos^n\delta)$, and n are also unknown, but three independent equations exist. First, $(P_s \cos^n\delta)$ is eliminated by dividing Equation (17) by Equation (20)

$$\frac{P_1}{P_2} = \left[\frac{\cos(\alpha-\phi_1)}{\cos\alpha}\right]^n \tag{23}$$

and Equation (21) by Equation (20).

$$\frac{P_3}{P_2} = \left[\frac{\cos(\alpha-\phi_3)}{\cos\alpha}\right]^n \tag{44}$$

Next, n can be eliminated by taking the log of Equations (23) and (44),

$$\log\left(\frac{P_1}{P_2}\right) = n \log\left[\frac{\cos(\alpha-\phi_1)}{\cos\alpha}\right] \tag{45}$$

$$\log\left(\frac{P_3}{P_2}\right) = n \log\left[\frac{\cos(\alpha-\phi_3)}{\cos\alpha}\right] \tag{46}$$

and then dividing Equation (45) by Equation (46).

$$\frac{\log(P_1/P_2)}{\log(P_3/P_2)} = \frac{\log\left(\cos(\alpha-\phi_1)/\cos\alpha\right)}{\log\left(\cos(\alpha-\phi_3)/\cos\alpha\right)} \tag{47}$$

Equation (47) expresses α as a function of only P_1, P_2 and P_3.

We now have an expression for angle of attack which is independent of n and requires only a pressure distribution of the form $P = P_s \cos^n\theta$, regardless of the value of n. A plot of this function for $\phi_1 = 45°$, $\phi_3 = -15°$ is given in Figure 17. For the case of $\phi_1 = 45°$, $\phi_3 = -45°$, Equation (47) reduces to

$$\frac{\log(P_1/P_2)}{\log(P_3/P_2)} = \frac{\log\frac{\sqrt{2}}{2}(1+\tan\alpha)}{\log\frac{\sqrt{2}}{2}(1-\tan\alpha)} \tag{47a}$$

Using Equation (47), it is possible, therefore, to obtain α (or β) independently of n. Once α (and β) are found, however, it is possible to obtain n by using Equation (32). Taking the log of both sides of Equation (32) and solving for n one obtains

$$n = \frac{\log(P_1/P_2)}{\log\left(\frac{1+\tan\alpha}{\sqrt{2}}\right)} \tag{48}$$

The necessity of knowing n even when α and β have already been determined will be seen in Section III wherein the calculation of stagnation pressure, P_s is required in order to obtain true and indicated air speed.

Equation (47) would appear to be very useful for $M_\infty \leq 6$, where n varies but is not known as an input. The usefulness of Equation (47) at hypersonic Mach numbers should also be considered. Obviously, an equation that can be used continuously over the whole Mach number range is more desirable than having separate equations which would cover incremental Mach number ranges. A comparison of calibration Equations (47) and (32) should consider the following:

1) Accuracy in α (or β) for given $\frac{\Delta P}{P}$ errors.
2) Range of use in α.
3) Simplicity of attitude expression.

Obviously, Equation (32) is the simpler, but to make a valid comparison of items 1) and 2), it is necessary to first attempt to optimize Equation (47) for accuracy and range of use for various orifice locations, as was done for Equation (32). A series of five different orifice locations were considered and are shown in Figures 17-21.

Before these figures are discussed, it is useful to consider first the errors in angle of attack which could result from errors in pressure measurements using Equation (47). Taking the total derivative of the left-hand side of Equation (47)

$$df(P) = \frac{1}{\log\left(\frac{P_3}{P_2}\right)}\left[\frac{\Delta P_1}{P_1} - \frac{\Delta P_2}{P_2}\right] - \frac{\log\left(\frac{P_1}{P_2}\right)}{\left[\log\left(\frac{P_3}{P_2}\right)\right]^2}\left[\frac{\Delta P_3}{P_3} - \frac{\Delta P_2}{P_2}\right] \tag{49}$$

for $\frac{dP_1}{P_1} = \frac{\Delta P_1}{P_1}$, etc. Equation (49) can also be written in terms of the angle relations

$$\Delta f(P) = \frac{1}{n\log\left(\frac{\cos(\alpha-\phi_3)}{\cos\alpha}\right)}\left[\frac{\Delta P_1}{P_1} - \frac{\Delta P_2}{P_2}\right] - \frac{\log\left(\frac{\cos(\alpha-\phi_1)}{\cos\alpha}\right)}{n\left[\log\left(\frac{\cos(\alpha-\phi_3)}{\cos\alpha}\right)\right]^2}\left[\frac{\Delta P_3}{P_3} - \frac{\Delta P_2}{P_2}\right] \tag{49a}$$

Dividing Equation (49) by $f(P)$ results in

$$\frac{\Delta f(P)}{f(P)} = \frac{1}{\log\left(\frac{P_1}{P_2}\right)}\left[\frac{\Delta P_1}{P_1} - \frac{\Delta P_2}{P_2}\right] - \frac{1}{\log\left(\frac{P_3}{P_2}\right)}\left[\frac{\Delta P_3}{P_3} - \frac{\Delta P_2}{P_2}\right] \tag{50}$$

or

$$\frac{\Delta f(P)}{f(P)} = \frac{1}{n\log\left(\frac{\cos(\alpha-\phi_1)}{\cos\alpha}\right)}\left[\frac{\Delta P_1}{P_1} - \frac{\Delta P_2}{P_2}\right] - \frac{1}{n\log\left(\frac{\cos(\alpha-\phi_3)}{\cos\alpha}\right)}\left[\frac{\Delta P_3}{P_3} - \frac{\Delta P_2}{P_2}\right] \tag{50a}$$

Next, for the right-hand side of Equation (47),

$$\frac{\Delta f(\alpha)}{f(\alpha)} = \frac{1}{\log\left(\frac{\cos(\alpha-\phi_1)}{\cos\alpha}\right)}\left(\tan\alpha - \tan(\alpha-\phi_1)\right) - \frac{1}{\log\left(\frac{\cos(\alpha-\phi_3)}{\cos\alpha}\right)}\left(\tan\alpha - \tan(\alpha-\phi_3)\right) \tag{51}$$

Equating Equations (50 a) and (51), i.e., $\frac{\Delta f(P)}{f(P)} = \frac{\Delta f(\alpha)}{f(\alpha)}$ and

solving for $\Delta\alpha$ results in

$$\Delta\alpha = \frac{\log(\cos\phi_3+\sin\phi_3\tan\alpha)\left[\frac{\Delta P_1}{P_1}-\frac{\Delta P_2}{P_2}\right]+\log(\cos\phi_1+\sin\phi_1\tan\alpha)\left[\frac{\Delta P_2}{P_2}-\frac{\Delta P_3}{P_3}\right]}{n\left[\log(\cos\phi_3+\sin\phi_3\tan\alpha)(\tan\alpha-\tan(\alpha-\phi_1))-\log(\cos\phi_1+\sin\phi_1\tan\alpha)(\tan\alpha-\tan(\alpha-\phi_3))\right]} \quad (52)$$

The numerator of Equation (52) is of the form

$$A\left[\frac{\Delta P_1}{P_1}-\frac{\Delta P_2}{P_2}\right]+B\left[\frac{\Delta P_2}{P_2}-\frac{\Delta P_3}{P_3}\right] \quad (53)$$

and it was found arithmetically that, when A and B have opposite signs, an error of $\frac{2\Delta P}{P}(A+B)$ could occur, whereas when A and B have like signs, the maximum possible error is $\frac{2\Delta P}{P}A$ or $\frac{2\Delta P}{P}B$, depending on whichever of A or B was numerically greater. Shown in Figures 22-26 are plots of $\Delta\alpha$ versus α prepared using Equation (52) for $\Delta P/P = .01$ for the five orifice locations of Figures 17-21. It was found, however, that when $\Delta f(P)$ was large, Equation (52) gave poor estimates of $\pm\Delta\alpha$. This resulted because the equation assumes a straight line variation in $f(P)$ over the corresponding $\Delta\alpha$ interval, which was not always the case. Therefore, for large $\Delta P/P$, values of $\Delta f(P)$ from Equation (49a) were calculated and graphical values of $\Delta\alpha$ were obtained directly from Figures 17-21. These values are also shown in Figures 22-26.

The optimization of Equation (47) can now be obtained through examination of Figures 17-26. The results of these plots are given in Table I, which comprises a summary of the investigation listing cases, accuracy uncertainty due to 1% pressure uncertainties at $\alpha = 0$ and range of use. The purpose of examining the five different cases is, of course, an attempt to achieve for Equation (47) a calibration which will produce a maximum attitude angle range of use and a minimum sensitivity to pressure error. These requirements are somewhat conflicting, however, as can be seen in Table I.

Table I

ANGLE-OF-ATTACK CALIBRATIONS
FOR LOGARITHMIC RELATION

FIGURE	CASE	ϕ_1	ϕ_3	POSSIBLE INACCURACY AT $\alpha = 0°$ $\Delta P/P = 1\%$	LIMITS IN RANGE OF α: UPPER MIN. IN CURVE	UPPER $\lvert\alpha-\phi_3\rvert=65°$	LOWER $2\alpha-\phi_3=0$	LOWER $\lvert\alpha-\phi_1\rvert=65°$
17	1	45°	-15°	14°, -3.0°	62°	60°	- 7.5	-20
18	2	45°	-30°	1.9°, -1.6°	45°	35°	-15	-20
19	3	45°	-45°	0.5°, -1.0°	38°	20°	-22.5	-20
20	4	60°	-30°	2.1°, -1.7°	49.5°	35°	-15	- 5
21	5	30°	-30°	1.7°, -1.4°	42.5°	35°	-15	-35

An explanation of the limits in attitude angle range shown in Table I are given as follows:

1) Minimum in Curve - Causes an upper limit in attitude range because an attempt to use the calibration above this minimum would result in a double value attitude solution for a given set of pressure inputs. A cross plot of the maximum positive range in α limited by a minimum in the calibration curve is shown in Figure 27.

2) $|\alpha - \phi_1| = 65°$ or $|\alpha - \phi_3| = 65°$ - The calibration equation was derived from an assumed pressure distribution of $P = P_s \cos^n \theta$ which is considered to be valid only up to an angle between the orifice and the stagnation point of approximately 65°.

3) $(2\alpha - \phi_3) = 0$ - The functions become discontinuous if this occurs, see Equation (47).

The range in orifice location was selected in view of these limits and desired range of angle of attack $(-20° \leq \alpha \leq 50°)$ as follows:

1) Upper limit in ϕ_1 was set by condition 2 above (for $\cos\theta$ distribution to hold to -20°, ϕ_1 should be no greater than about 45°).

2) Upper limit in $|\phi_3|$ was set by condition 1 (upper α limit in calibration curve due to minimum decreases as $|\phi_3|$ increases) or, condition 2 (for $\cos\theta$ distribution to hold to 50°, $|\phi_3|$ should be no greater than 15°).

3) Lower limit in $|\phi_3|$ was set in consideration of the fact that the inaccuracy in α near $\alpha = 0$ increases as $|\phi_3|$ decreases, and by condition 3 (for α range to -20°, $|\phi_3|$ should be no less than 40°).

Considering the possible α inaccuracies at $\alpha = 0$ listed in Table I, it can be seen that ϕ_3 must have a large negative value, perhaps 45°, to make the calibration of any practical use. This requirement, however, restricts the upper limit in useful α range to about +20°. Thus, in terms of accuracy and range of use, Equation (47) is not as acceptable as Equation (32) in the hypersonic range.

In addition, it was previously felt that, even though the required α range was -20° to +50°, it would be most desirable to have the calibration operable at large limits in α (see Section II. 2. d.). Such is not the case for Equation (47), since discontinuities in the calibration occur at negative α values (within the required range for all but $\phi_3 = -45°$, case 3) and multiple values occur in the positive α range.

One possible solution or compromise would be to use one equation as a back up for the other. At high altitude, high Mach numbers when the attitude angles could conceivably be quite large, Equation (32) would be most valuable. A switch over to Equation (47) at supersonic-transonic Mach numbers, where the attitude angles would not be too great (say $\leq 20°$) could then be made.

Orifice locations $\phi_1 = 45°$, $\phi_2 = 0°$ are compatible for both solutions and the additional orifice input ϕ_3 could be made available as needed.

The required attitude range in β is far less demanding than for α, being from -15° to +15°. Thus, there is no requirement to make δ_1 or δ_3, the orifice locations in the x-y plane (see sketch) small. The δ angles should be greater than 30° to eliminate any discontinuity in the calibration and could perhaps reach 40° or 45°; they are limited, however, by the $\cos\theta$ distribution at large α.* Actually, $\delta_1 = 45°$, $\delta_3 = -45°$ provide good accuracy near $\beta = 0$, do not exceed the acceptable $\cos\theta$ range, except at very large angle of attack, and allow the simplified calibration

$$\beta = \tan^{-1}\left[\sqrt{2}\left(\frac{P_4}{P_2}\right)^{1/n} - 1\right] \tag{41}$$

for the hypersonic case.

Selection of the logarithmic equation for β

$$\frac{\log\left(\frac{P_4}{P_2}\right)}{\log\left(\frac{P_5}{P_2}\right)} = \frac{\log\left(\frac{\cos(\beta-\delta_1)}{\cos\beta}\right)}{\log\left(\frac{\cos(\beta-\delta_3)}{\cos\beta}\right)} \tag{54}$$

in place of Equation (41) in the hypersonic case is dependent upon the same question of accuracy and convenience as was just discussed for angle of attack. For the case of $\delta_1 = 45°$, $\delta_3 = -45°$, Equation (54) reduces to

$$\frac{\log\left(\frac{P_4}{P_2}\right)}{\log\left(\frac{P_5}{P_2}\right)} = \frac{\log\frac{\sqrt{2}}{2}\left(1 + \tan\beta\right)}{\log\frac{\sqrt{2}}{2}\left(1 - \tan\beta\right)} \tag{54a}$$

* At $\alpha = 45°$, $\beta = 15°$, the total angle between the stagnation point and the orifice at $-\delta_3$ is about 65° for $\delta_3 = 40°$.

SECTION III

TRUE AIR SPEED AND INDICATED AIR SPEED

1. CALCULATION PROCEDURE

In Section II, it was shown that pressure distributions in the x-z and x-y planes are sufficient inputs to determine the hemispherical probe attitude angles, α and β. Using α and β, the centerline orifice pressure measurement and an assumed pressure distribution, the probe stagnation pressure can be determined. For a given free stream density, the stagnation pressure can then be used to obtain free stream velocity (true air speed) through a stagnation pressure, dynamic pressure relation.

2. CALCULATION OF STAGNATION PRESSURE

The pressure distribution on the hemispherical probe surface is assumed to be of the form

$$P = P_s \cos^n \theta \tag{10}$$

where θ is the angle between the stagnation point and some orifice at which pressure P is measured, see Section II. It was also seen in Section II that if the orifice is located on the probe axis of symmetry

$$\cos\theta = \cos\delta \cos\alpha \tag{15}$$

where angles δ and α are also defined in Section II. 1. Substituting this relationship into Equation (10) and solving for P_s results in

$$P_s = P_2 / \cos^n \delta \cos^n \alpha \tag{55}$$

where P_2 is the pressure measured at orifice 2.

Next, consider the relations between angles α, β and δ as given in Section II. 1.

$$\sin\delta = \frac{v}{V} \quad (56a) \qquad \sin\alpha = \frac{w}{(u^2+w^2)^{1/2}} \quad (57a) \qquad \sin\beta = \frac{v}{(w^2+v^2)^{1/2}} \quad (58a)$$

$$\cos\delta = \frac{(u^2+w^2)^{1/2}}{V} \quad (56b) \qquad \cos\alpha = \frac{u}{(u^2+w^2)^{1/2}} \quad (57b) \qquad \cos\beta = \frac{u}{(w^2+v^2)^{1/2}} \quad (58b)$$

$$\tan\delta = \frac{v}{(u^2+w^2)^{1/2}} \quad (56c) \qquad \tan\alpha = \frac{w}{u} \quad (57c) \qquad \tan\beta = \frac{v}{u} \quad (58c)$$

By inspection Equations (56c), (57b) and (58c) combine to give

$$\tan\delta = \cos\alpha \tan\beta \tag{59}$$

$$\delta = \tan^{-1}\left[\cos\alpha \tan\beta\right] \tag{59a}$$

Combining Equations (55) and (59a) results in

$$P_s = \frac{P_2}{\left[(\cos\alpha)\cos\left(\tan^{-1}(\cos\alpha\tan\beta)\right)\right]^n} \tag{60}$$

This equation then presents a closed form solution for the pitot pressure in terms of the pressure measured on the centerline orifice, the attitude angles α and β and the cosine exponent n. For Mach numbers greater than 6, it was shown in Section II that $n = 2.24$; that is, Equation (60) can be written

$$P_s = \frac{P_2}{\left[(\cos\alpha)\cos\left(\tan^{-1}(\cos\alpha\tan\beta)\right)\right]^{2.24}} \tag{60a}$$

for the hypersonic case.

For transonic-supersonic Mach numbers, Equation (60) can be solved only after obtaining n through the method described in Section II. 3. Equation (60a) can be written entirely in terms of measured pressures for the case where the attitude angles are expressed as a function of two orifice pressures and n is known. For hypersonic Mach numbers then:

$$\alpha = \tan^{-1}\left[\sqrt{2}\left(\frac{P_1}{P_2}\right)^{\frac{1}{2.24}} - 1\right] \tag{32}$$

$$\beta = \tan^{-1}\left[\sqrt{2}\left(\frac{P_4}{P_2}\right)^{\frac{1}{2.24}} - 1\right] \tag{41}$$

Substitution of Equation (32) and (41) into (60a) results in

$$P_s = \frac{P_2}{\left\{\cos\left[\tan^{-1}\left(\sqrt{2}\left(\frac{P_1}{P_2}\right)^{\frac{1}{2.24}}-1\right)\right]\cos\left[\tan^{-1}\left[\cos\left[\tan^{-1}\left(\sqrt{2}\left(\frac{P_1}{P_2}\right)^{\frac{1}{2.24}}-1\right)\right]\left(\sqrt{2}\left(\frac{P_4}{P_2}\right)^{\frac{1}{2.24}}-1\right)\right]\right]\right\}^{2.24}} \tag{60b}$$

Because of the complexity of this expression, several simplifying small angle assumptions were considered. First, for the assumption

$$\tan\delta = \delta \tag{61}$$

Equation (60b) reduces to

$$P_s = \frac{P_2}{\left[\cos\left[\tan^{-1}\left(\sqrt{2}\left(\frac{P_1}{P_2}\right)^{\frac{1}{2.24}}-1\right)\right]\ \cos\left[\left(\sqrt{2}\left(\frac{P_1}{P_2}\right)^{\frac{1}{2.24}}-1\right)\left(\sqrt{2}\left(\frac{P_4}{P_2}\right)^{\frac{1}{2.24}}-1\right)\right]\right]^{2.24}} \tag{62}$$

which offers a significant reduction in complexity over (60b).

The error in P_s using (62) is shown in Figure 28 for β 's of 0°, 5° and 10°. As can be seen, the error introduced in the worst case is only .07%. Thus, Equation (62) introduces negligible error in the pitot pressure calculation. It is possible to simplify the stagnation pressure relation, Equation (62), further by the additional assumption

$$\tan\beta = 0 \tag{63}$$

Therefore, $\tan\delta = 0$ and Equation (62) reduces to

$$P_s = \frac{P_2}{\cos\left[\tan^{-1}\left(\sqrt{2}\left(\frac{P_1}{P_2}\right)^{\frac{1}{2.24}}-1\right)\right]^{2.24}} \tag{64}$$

The error in P_s using Equation (64) is shown in Figure 29, again for β 's of 0°, 5° and 10°. Errors for this case can be as large as 3.5%. In view of these errors, Equation (62) would appear to be the best choice of the expression for P_s, however, the value of the trade in accuracy for simplicity can only be ultimately judged in the case of a specific application.

3. RELATION BETWEEN STAGNATION AND DYNAMIC PRESSURE

a. Imperfect or Real Gas Solution for Supersonic-Hypersonic Stagnation Streamline

For an imperfect gas, the following flow conservation equations are valid for the flow in a streamtube which goes through a normal shock and comes to rest at the stagnation point of a blunt body (velocities are given with respect to a body fixed coordinate system).

First, because the process is one-dimensional through the shock, the mass flow rate entering the shock surface per unit area must exactly equal the mass flow rate leaving the shock. The mass continuity equation for this process is therefore

$$\rho_\infty U_\infty = \rho_r U_r \tag{65}$$

where the subscripts are noted in the sketch below

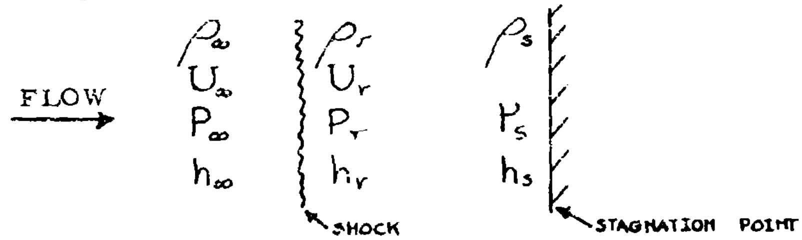

Secondly, since the shock wave is stationary, the net force on the shock surface must be zero. The force balance or the conservation of momentum equation is

$$P_\infty + \rho_\infty U_\infty^2 = P_r + \rho_r U_r^2 \tag{66}$$

Finally, for an adiabatic process, the energy equation between the shocked gas at station r and the stagnation point s is

$$h_r + \frac{1}{2} U_r^2 = h_s \tag{67}$$

These three conservation equations form the basis of the stagnation streamline pressure calculation. Note that at this point, no gas restrictions (i.e., perfect, incompressible, etc.) have been assumed. Rewriting Equation (66) and substituting for U_r using Equation (65) results in:

$$P_r = P_\infty + \rho_\infty U_\infty^2 - \rho_r \left(\frac{\rho_\infty}{\rho_r} U_\infty\right)^2 \tag{68}$$

$$P_r = P_\infty + \rho_\infty U_\infty^2 \left(1 - \frac{\rho_\infty}{\rho_r}\right) \tag{68a}$$

The thermodynamic equations

$$P = Z \rho R T \qquad \text{imperfect gas law} \tag{69}$$

$$h = C_p T \qquad \text{definition of specific heat at constant pressure*} \tag{70}$$

are next substituted in Equation (67) resulting in

$$\left(\frac{C_p}{ZR}\right)_r \frac{P_r}{\rho_r} + \frac{1}{2} U_r^2 = \left(\frac{C_p}{ZR}\right)_s \frac{P_s}{\rho_s} \tag{71}$$

Equation (71) is next solved for P_s, the stagnation pressure:

$$P_s = \left(\frac{ZR}{C_p}\right)_s \left(\frac{C_p}{ZR}\right)_r \frac{\rho_s}{\rho_r} P_r + \left(\frac{ZR}{C_p}\right)_s \frac{1}{2} \rho_s U_r^2 \tag{71a}$$

* Equation (70) merely constitutes a definition of C_p, it is not meant to imply that this value is insensitive to imperfect gas properties (i.e., a constant).

$$P_s = \frac{\rho_s}{\rho_r}\left[\left(\frac{ZR}{C_p}\right)_s\left(\frac{C_p}{ZR}\right)_r P_r + \left(\frac{ZR}{C_p}\right)_s \frac{\rho_\infty}{\rho_r}\frac{\rho_\infty U_\infty^2}{2}\right] \tag{71b}$$

Next, using Equation (68) to eliminate P_r, and defining dynamic pressure,

$$q = \frac{1}{2}\rho_\infty U_\infty^2 \tag{72}$$

$$P_s/q = \frac{\rho_s}{\rho_r}\left[\left(\frac{ZR}{C_p}\right)_s\left(\frac{C_p}{ZR}\right)_r \frac{P_\infty}{q} + \left(\frac{ZR}{C_p}\right)_s\left(\frac{C_p}{ZR}\right)_s 2\left(1-\frac{\rho_\infty}{\rho_r}\right) + \left(\frac{ZR}{C_p}\right)_s \frac{\rho_\infty}{\rho_r}\right] \tag{73}$$

$$P_s/q = \frac{\rho_s}{\rho_r}\left(\frac{ZR}{C_p}\right)_s\left(\frac{C_p}{ZR}\right)_r \left[2 + \frac{P_\infty}{q} - \frac{\rho_\infty}{\rho_r}\left(2-\left(\frac{ZR}{C_p}\right)_r\right)\right] \tag{73a}$$

b. Approximations to Stagnation-Dynamic Pressure Relation for Hypersonic Flow

Equation (73a) is the imperfect gas result for the relation of stagnation to dynamic pressure, P_s/q. However, analytical relations for $\left(\frac{ZR}{C_p}\right)_s$, $\left(\frac{C_p}{ZR}\right)_r$ must be formulated to solve the equation, resulting in a relation for P_s/q too difficult and unwieldy for air data usage. Fortunately, numerical solutions from which P_s/q can be calculated exist in the literature so that P_s/q can be found for the flight envelope in question. This has been done using Reference (16) and these real gas results are shown in Figure 30.

Given numerical solutions to Equation (73a), a logical method of attack to formulate a usable P_s/q relation is to simplify (73a) with perfect gas assumptions, compare the results to the exact solutions, and try to represent the variation between exact and simplified solutions with simple correlation functions. This is the method of attack used here. The simplifications were performed progressively in a step wise fashion and although it would suffice to show only the end product, it was, nevertheless, deemed worthwhile to include the whole process.

First, assume that the fluid behaves as a perfect gas allowing

$$P = \rho R T, \qquad Z_r = Z_s = 1 \tag{74}$$

$$\frac{C_p}{R} = \frac{C_p}{C_p - C_v} = \frac{\gamma}{\gamma - 1} \tag{75}$$

Substitute Equations (74) and (75) into (73a) which gives

$$P_s/q = \frac{\rho_s}{\rho_r}\left[2 + \frac{P_\infty}{q} - \frac{\rho_\infty}{\rho_r}\left(2 - \frac{\gamma}{\gamma-1}\right)\right] \tag{76}$$

which reduces to

$$P_s/q = \frac{\rho_s}{\rho_r}\left[2 + \frac{P_\infty}{q} - \frac{\rho_\infty}{\rho_r}\left(\frac{\gamma+1}{\gamma}\right)\right] \qquad (76a)$$

Next, assume the gas between stations ∞ and r is incompressible, in which case

$$\rho_s = \rho_r \qquad (77)$$

and

$$\frac{\gamma + 1}{\gamma} \longrightarrow 1 \qquad \text{see Reference (17)} \qquad (78)$$

By substituting Equation (77) and (78) into (76a)

$$P_s/q = 2 + \frac{P_\infty}{q} - \frac{\rho_\infty}{\rho_r} \qquad (79)$$

For hypersonic conditions

$$P_\infty/q \approx 0 \qquad (80)$$

Thus, Equation (79) can be written

$$P_s/q = 2 - \frac{\rho_\infty}{\rho_r} \qquad (81)$$

Equation (81) becomes recognizable now as the most commonly derived solution for the stagnation pressure.

The next and final approximation requires taking an average or constant value for $\frac{\rho_\infty}{\rho_r}$ over the range of usage and thus simply assuming a constant ratio of P_s/q,

$$P_s/q = K \qquad (82)$$

The results of the solutions are now shown for the velocity envelope of interest in Figure 30. It is interesting to note, that the assumptions of $P_\infty/q = 0$ and incompressible flow have had little effect on Equation (76a); thus, Equation (81) suffers very little from these assumptions. Logical candidates for an approximation to Eq. (73a) thus become Equation (81) or (82).

A correction to Equation (81) or (82) could include velocity and altitude or velocity and density, e.g.

$$P_s/q = 2 - \frac{\rho_\infty}{\rho_r} + f(\rho_\infty, U_\infty) \qquad (83)$$

However, P_s/q is quite insensitive to ρ_∞ and the correction can be written simply in terms of U_∞,

$$P_s/q = 1.84 + f(U_\infty) \qquad (83a)$$

Finally, from a curve fit of Eq. (83a) to Eq. (73a) for the range of interest (Fig. 30), the results are

$$P_s/q = 1.84 + \frac{U_\infty^{1/2}}{1400} \qquad (83b)$$

Equation (83b) is plotted in Figure 30 and is seen to hold to within ±1/2%.

4. TRUE AIR SPEED, HYPERSONIC

Equation (60a) can be substituted into Equation (83b) to express true air speed in terms of the measured quantities α, β, P_2 and density. This velocity relation would still need to be solved for U_∞, however, which can not be done directly. An iterative procedure whereby values of U_∞ would be assumed is needed to obtain a solution in U_∞. Rather than resort to this procedure, it was decided to first investigate the necessity of the complexity of this expression for P_s/q. This was done by investigating the error introduced by the use of Equation (82).

$$P_s/q = K \tag{82}$$

where K = 1.92 ±.03 since $1.89 < P_s/q < 1.96$ over the range of interest, see Figure 30. Then from Equation (72), we can write

$$U_\infty^2 = \frac{2 P_s}{\rho_\infty K} \tag{84}$$

Differentiating this expression results in

$$2 U_\infty dU_\infty = -\frac{2 P_s}{\rho_\infty}\frac{dK}{K^2} + \frac{2K}{\rho_\infty} dP_s - \frac{2KP_s}{\rho_\infty^2} d\rho_\infty \tag{85}$$

Next, divide Equation (85) by Equation (84), assume $dU/U = \pm \Delta U/U$ etc. and again assume all errors are accumulative; the result is

$$\frac{\Delta U_\infty}{U_\infty} = \frac{1}{2}\left[\frac{\Delta K}{K} + \frac{\Delta P_s}{P_s} + \frac{\Delta\rho_\infty}{\rho_\infty}\right] \tag{86}$$

From Equation (82) $\frac{\Delta K}{K} = \frac{.03}{1.92}$ = ±.015. Assume density is known to within 5%, $\Delta\rho_\infty/\rho_\infty$ = ±.05.

In order to get $\Delta P_s/P_s$, we must differentiate Equation (60), which would be difficult and unwieldy, but it can be done for the simple case of $\beta = 0$, Equation (64), which will still serve the purpose of illustrating the validity of the $P_s/q = K$ assumption. Equation (64) in terms of α is simply:

$$P_s = P_2/\cos^n \alpha \tag{87}$$

and

$$dP_s = P_2\, n \cos\alpha \sin\alpha\, d\alpha + \cos^n\alpha\, dP_2 + P_2 \cos^n\alpha \log_e \cos\alpha\, dn \tag{88}$$

Again assume $dP_s = \Delta P_s$, etc. giving

$$\frac{\Delta P_s}{P_s} = n\frac{\sin\alpha}{\cos^{n-1}\alpha}\Delta\alpha + \frac{\Delta P_2}{P_2} + \log_e \cos\alpha\, \Delta n \tag{89}$$

Substituting this expression back into Equation (86), the result obtained is:

$$\frac{\Delta U_\infty}{U_\infty} = \frac{1}{2}\left[\frac{\Delta K}{K} + \frac{\Delta\rho_\infty}{\rho_\infty} + n\frac{\sin\alpha}{\cos^{n-1}\alpha}\Delta\alpha + \frac{\Delta P_2}{P_2} + \log_e \cos\alpha\, \Delta n\right] \tag{86a}$$

Note that from Section II, for $\phi_2 = 45°$

$$\Delta\alpha = \frac{1}{\sqrt{2}}(1+\tan\alpha)\frac{\cos^2\alpha}{n}\left[2C + \left(\log_e\left(\frac{1+\tan\alpha}{\sqrt{2}}\right)\right)\right] \tag{36a}$$

Therefore,

$$\frac{\Delta U_\infty}{U_\infty} = \frac{1}{2}\left[\frac{\Delta K}{K} + \frac{\Delta\rho_\infty}{\rho_\infty} + \frac{\Delta P_2}{P_2} + (\log_e(\cos\alpha))\Delta n + \frac{\sin\alpha}{\cos^{(1.3)}\alpha}\frac{(1+\tan\alpha)}{\sqrt{2}}\left[2C + \log_e\left(\frac{1+\tan\alpha}{\sqrt{2}}\right)\Delta n\right]\right] \tag{86b}$$

If this expression is evaluated at $\alpha = 0$ for illustration purposes

$$\frac{\Delta U_\infty}{U_\infty} = \frac{1}{2}\left[\frac{\Delta K}{K} + \frac{\Delta\rho_\infty}{\rho_\infty} + C\right] \tag{86c}$$

$$\frac{\Delta U_\infty}{U_\infty} = 1/2\,(.015 + .05 + .01) = .0375$$

or $\frac{\Delta U_\infty}{U_\infty} = 3\text{-}3/4\%$

From this result, we can see that the error in U_∞ due to the uncertainty in K contributes only 3/4% to the total 3-3/4% uncertainty. Therefore, the error in U_∞ introduced by the assumption of the simple relationship $P_s/q = K$ is small and we are justified in using $P_s/q = 1.92$ for the velocity, density, stagnation pressure relation.

Solving Equation (84) for U_∞ gives

$$U_\infty = 1.021\left(\frac{P_s}{\rho_\infty}\right)^{1/2} \tag{90}$$

Substitution of Equation (60b) into Equation (90) produces

$$U_\infty = \frac{1.021\left(\frac{P_2}{\rho_\infty}\right)^{1/2}}{\left\{\cos\left[\tan^{-1}\left(\sqrt{2}\left(\frac{P_1}{P_2}\right)^{1/n}-1\right)\right]\cos\left[\tan^{-1}\left[\cos\left[\tan^{-1}\left(\sqrt{2}\left(\frac{P_1}{P_2}\right)^{1/n}-1\right)\right]\left(\sqrt{2}\left(\frac{P_4}{P_2}\right)^{1/n}-1\right)\right]\right]\right\}^{n/2}} \tag{91}$$

which gives true air speed in terms of P_1, P_2, P_4 and ρ_∞.

Since, however, it was shown in Section III. 2 that the assumptior

$$\tan\delta = \delta \tag{61}$$

introduced negligible error in P_s, Equation (91) can be rewritten for $n = 2.24$, including this approximation, as

$$U_\infty = \frac{1.021\left(\frac{P_2}{\rho_\infty}\right)^{\frac{1}{2}}}{\left[\cos\left[\tan^{-1}\left(\sqrt{2}\left(\frac{P_1}{P_2}\right)^{\frac{1}{2.24}}-1\right)\right]\cos\left[\left(\sqrt{2}\left(\frac{P_1}{P_2}\right)^{\frac{1}{2.24}}-1\right)\left(\sqrt{2}\left(\frac{P_4}{P_2}\right)^{\frac{1}{2.24}}-1\right)\right]\right]^{\frac{2.24}{2}}} \tag{92}$$

The error in U_∞ using Equation (92) instead of Equation (91) is shown in Figure 31. For β up to 10°, Equation (92) gives very good results over the entire α range; and, therefore, represents a satisfactory approximation to the air-data velocity equation.

Finally, for the sake of completeness, the assumption of

$$\tan\beta = 0 \tag{63}$$

can be introduced into Equation (92) resulting in the simplification

$$U_\infty = \frac{1.021\left(P_2/\rho_\infty\right)^{1/2}}{\cos\left[\tan^{-1}\left(\sqrt{2}\left(\frac{P_1}{P_2}\right)^{\frac{1}{2.24}} - 1\right)\right]^{\frac{2.24}{2}}} \tag{93}$$

The error introduced in U_∞ by this assumption is shown in Figure 32.

5. INDICATED AIR SPEED, HYPERSONIC

Indicated air speed U_i is the air speed obtained using sea level ambient density reference conditions. For the methods used in this study, U_i can be expressed simply as

$$U_i = U_\infty\left(\frac{\rho_\infty}{\rho_o}\right)^{1/2} \tag{94}$$

where ρ_o = .002377 slugs/ft^3. The value of U_i can be obtained once U_∞ is known, or by direct substitution of Equation (92) into Equation (94) which gives

$$U_i = \frac{1.021\left(\frac{P_2}{\rho_o}\right)^{1/2}}{\left[\cos\left[\tan^{-1}\left(\sqrt{2}\left(\frac{P_1}{P_2}\right)^{\frac{1}{2.24}}-1\right)\right]\cos\left[\left(\sqrt{2}\left(\frac{P_1}{P_2}\right)^{\frac{1}{2.24}}-1\right)\left(\sqrt{2}\left(\frac{P_4}{P_2}\right)^{\frac{1}{2.24}}-1\right)\right]\right]^{\frac{2.24}{2}}} \tag{95}$$

Equation (95) avoids introducing the uncertainty of ρ_∞ into the U_i expression. The simplifying assumption, Equation (61), that was made for U_∞ is, of course, also applicable to the indicated air speed expression, Equation (95).

6. AIR SPEED, SUPERSONIC

Determination of the air data outputs U_∞ and U_i for the hemisphere pressure probe is dependent upon determination of stagnation pressure and upon the relationship between the stagnation pressure behind the normal shock P_s and the free stream dynamic pressure q. For Mach numbers less than 6, it is possible to determine P_s once M is found as discussed in Section II.

For $M_\infty > 6$, it was found that

$$\frac{P_s}{q} = K \tag{82}$$

where K = 1.92 ±.03 over the hypersonic range (see Section III.4.). The assumption of a value of K of 1.92 resulted in maximum errors in U_∞ of 3/4%.

For $M_\infty \leq 6$, values of P_s/q were computed for Mach numbers as low as M_∞ = 1, and the results are shown in Figure 33. At Mach numbers up to about M_∞ = 4, P_s/q decreases with increasing M_∞. This decrease is true Mach number dependence existing even for an ideal gas. The variation in P_s/q in the hypersonic regime, however, (i.e. the slight increase in P_s/q with M_∞) is a real gas effect for the free stream velocities and densities of the re-entry trajectories considered in this study. Errors in U_∞ resulting from the assumption

$$\frac{P_s}{q} = 1.92 \tag{82}$$

are shown as a function of free stream Mach number in Figure 34. For Mach numbers as low as $M_\infty = 2$, the true air speed errors resulting from the use of Equation (82) are 2% or less. Therefore, in view of velocity uncertainties of ±2-1/2% and ±1/2% resulting from assumed uncertainties of ±5% in density and ±1% in pressure, respectively, Equation (82) appears to have practical use in the supersonic range.

For Mach numbers less than $M_\infty = 2$, Equation (82) rapidly becomes unusable; for example, at $M_\infty = 1$, $\frac{\Delta U_\infty \times 100}{U_\infty} = 20\%$. Thus it appears that the hemisphere pressure inputs, along with free stream density and speed of sound, are inadequate for accurate determination of true air speed, indicated air speed and Mach number at M_∞ less than 2. Considerable effort, however, can be found in the literature related to the use of a hemisphere cylinder pitot-static air data probe at subsonic, transonic and low supersonic Mach number; for example, References (18) and (19). Therefore, based on these references and the above statement, it is felt that the pitot static tube, that is, the additional input of static pressure, is needed in order to determine Mach number for $M_\infty < 2$.

With density given, true air speed (free stream velocity) can be obtained for $M_\infty > 2$ using Equation (82). The indicated air speed calculation merely requires substitution of the sea level density ρ_o for ρ_∞ in Equation (82) (see Section III. 5.). Therefore

$$U_i = 1.021\left(\frac{P_s}{\rho_o}\right)^{1/2} \tag{96}$$

SECTION IV

DETERMINATION OF ALTITUDE AND MACH NUMBER

1. ALTITUDE DETERMINATION

An altitude, or more properly a pressure altitude, cannot be obtained from the pressures measured on a hemisphere in high supersonic-hypersonic flow. This conclusion is a direct result of the insensitivity of the local flow field pressure distribution to free stream Mach number and hence the inability to determine M_∞ and subsequently static pressure from the input of surface pressure (see Reference 14 for a further explanation of this conclusion). Thus, the only altitude output one can get from the air data inputs must come from the input of density, i.e. simply a density altitude (when given). Using the information on density altitude variations available in the 1962 U.S. Standard Atmosphere, Reference (19), it is possible to estimate how accurately one can determine altitude when density is known.

A detailed investigation, or detailed results of investigations of atmospheric variations and uncertainties in pressure, density, etc. will not be attempted in this report. This information is adequately covered in Reference (19) and references cited in that work. Rather, we will look at the conclusions of Reference (19) only to the point where we may formulate the ability to obtain altitude when density is given as an air data input.

Figure 35, taken from Reference (19), presents the U.S. Standard Density Altitude. The dotted lines in this figure are fairings through density extremes (symbols) observed at given altitudes. From these extremes, altitude uncertainties at a given density can be found as lying horizontally between the density uncertainty band. Since these extremes in density are on the order of ±50%, an additional measured density uncertainty of ±5%, which is to be assumed, becomes of little practical significance in determining altitude from density. One finds that the density is very sensitive to altitude. Conversely, altitude is a weak function of density; thus, the large uncertainties in density produce much smaller uncertainties in h. Values of $\Delta h/h$ in percent are given in Figure 36 as a function of altitude.

One can see from this analysis that an altitude based on density gives nominally about ±8% uncertainty in h. Furthermore, the extreme density uncertainty that was assumed to exist is all inclusive for latitudinal and seasonal variations. For an actual flight case with latitude and season specified, Reference (19) points out that the uncertainty in density would be much smaller. Using appropriate density-altitude charts, therefore, altitude could be determined to much better than ±8% from a density input.

2. MACH NUMBER DETERMINATION

As stated previously, the pressure distribution on the hemisphere and the pitot pressure are insufficient inputs to obtain M_∞ in the hypersonic regime. When density is given, however, velocity (true air speed) is calculable, and Mach number can then be obtained through

$$M_\infty = \frac{U_\infty}{a_\infty} \tag{97}$$

The free stream speed of sound, however, must be obtained from the density-altitude. Thus, we must look at the uncertainty in a_∞ as a function of altitude. From Figure 37, also taken from Reference (19), it can be seen that at a given altitude the uncertainty in temperature (symbols) is on the order of ±10%. The variation of temperature with altitude is not strong enough to add much additional uncertainty in temperature. Thus, the total uncertainty in T_∞ is still on the order of ±10%. Since

$$a_\infty \propto T_\infty^{1/2} \tag{98}$$

$$\frac{\Delta a_\infty}{a_\infty} = \frac{1}{2}\,\frac{\Delta T_\infty}{T_\infty} \tag{98a}$$

a ±10% uncertainty in T_∞ results in a ±5% uncertainty in a_∞.

Now, since

$$M_\infty = \frac{U_\infty}{a_\infty} \tag{97}$$

$$\frac{\Delta M_\infty}{M_\infty} = \frac{\Delta U_\infty}{U_\infty} + \frac{\Delta a_\infty}{a_\infty} \tag{97a}$$

In Section III, it was shown that $\frac{\Delta U_\infty}{U_\infty} \sim \pm 4\%$ so that the uncertainty in M_∞ is ±10% or less. Again, as with altitude for a given flight case, the temperature as a function of altitude would be known to much better than ±10% and the resultant uncertainty in M_∞ would correspondingly be much less.

For Mach numbers between $.5 < M_\infty < 6$, it was seen in Section II that the cosine exponent n in the basic relation for the pressure distribution was Mach number dependent (see Figure 16). In addition, it was shown that the value of n could be calculated once α and β were obtained. Therefore, using Figure 16 as a calibration, it would be possible to obtain an estimate of M_∞ in this transonic-supersonic range. It is felt, however, that a calibration better defined through further experiments would be required to make this Mach number determination scheme valuable.

SECTION V

ABLATION AND RESULTANT UNCERTAINTIES ON AIR DATA ATTITUDE ANGLE OUTPUTS

1. ABLATION PERTURBATIONS

Thus far, the air data equations have been derived for a hemispherical probe. However, ablation of the nose can result in a change in nose shape and therefore perturb the equations. Given the re-entry trajectory, and the nose material and diameter, the amount of nose recession can be calculated. The perturbation on the equations, due to ablation, is then treated as an uncertainty in the pressure equation exponent, $n \pm \Delta n$, where $P = P_s \cos^n \theta$. The resultant uncertainty in α or β for the two orifice per plane calibration, Equations (32) and (41), is then determined from error Equations (36) or (42). While by no means rigorous, this analysis was performed in order to obtain an order of magnitude indication of the possible effects caused by ablation.

2. ABLATION

A re-entry trajectory chosen for ablation analysis is the DODCO trajectory presented in Reference (20). The trajectory was extrapolated down to 60,000 ft. to extend the ablation calculations over a greater range of interest (see Figure 38). In addition to the trajectory, other assumed inputs were:

1) nose diameter; $D = 6.0$ inches
(felt to be a lower limit on size)

2) nose material; "Graphitite G"
(a material for which experimental ablation data taken in the CAL Wave Superheater Supersonic Tunnel are available)

3) zero angle of attack and sideslip over the entire trajectory.

The results of the ablation calculations are presented in Figures 39 to 41. In Figure 39, the nose temperature time history is given. In Figure 40, the stagnation point heat transfer rate is presented. Both of these curves are fairings through point by point integrations (symbols) that were hand calculated for the trajectory. The nose recession $\Delta \ell$ (see sketch) as a function of altitude is presented in Figure 41. The maximum ablation is seen to be approximately .825 inches, or $\Delta \ell / r = .275$.

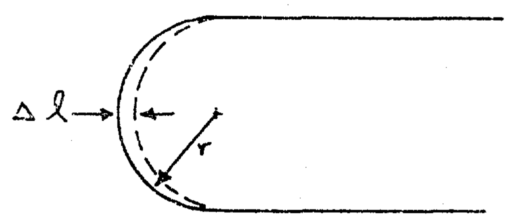

3. ABLATION EFFECTS

For the conditions presented in Section V. 2., it was seen that the maximum value of stagnation point nose recession was $\Delta \ell / r = .275$. The following assumptions and methods were used to interpret this recession distance as a perturbation to the air data equations. First, as previously stated, only the case at zero attitude angle was considered. Second, it was assumed that as the stagnation point recedes, no ablation occurs at the probe shoulder and, further, that the nose shape can be approximated by an ellipse, see sketch.*

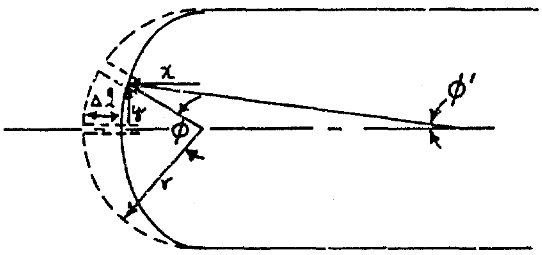

For an ellipse, the coordinates of the orifice can be found from

$$\frac{x^2}{a^2} + \frac{y^2}{b^2} = 1 \tag{99}$$

where

$$a = r - \Delta \ell$$
$$b = r$$

Solving Equation (99) for x and taking the first derivative results in,

$$\frac{dx}{dy} = -\frac{y}{x}\left[1 - \frac{2\Delta \ell}{r} - \left(\frac{\Delta \ell}{r}\right)^2\right] \tag{100}$$

Next, it is necessary to assume that the pressure ratio P/P_s at x, y can be approximated by a cosine function even though the surface is elliptical rather than circular.

Thus,

$$P/P_s = \cos^n \phi = \cos^{n'} \phi' \tag{101}$$

where ϕ' is the angle between the axis and a line normal to the body surface. Therefore,

$$\frac{dx}{dy} = \tan \phi' \tag{102}$$

---

* Alternatively, a model in which the nose shape remains spherical but increases in radius of curvature due to ablation was also considered, however, the resultant perturbation to the air data equations is nearly the same as the above analysis, therefore, it is not included herein.

and further $$\frac{y}{x} = \tan \phi \qquad (103)$$

Substituting Equations (102) and (103) into Equation (100) for port location, $\phi = 45°$ results in $\phi' = 27° 45'$.

From Equation (101)

$$n' = \frac{n \log (\cos \phi')}{\log (\cos \phi)} \qquad (104)$$

and since the n value used in the assumed distribution is $n = 2.24$ (for the hypersonic case), we get an error in n of:

$$\Delta n = n - n' = 1.44$$

From Section II, the resulting error in α for the two orifice configuration is,

$$\Delta \alpha = (\cot \phi_1 + \tan \alpha) \frac{\cos^2 \alpha}{n} \left[2C + \left[\log_e (\cos \phi_1 + \sin \phi_1 \tan \alpha) \right] \Delta n \right] \qquad (36)$$

Values of $\Delta\alpha$ versus α for $\Delta n = 1.44$ are given in Figure 42. Here, values at $\alpha \neq 0$ are considered. To arrive at these conditions physically, it would be necessary to fly at $\alpha = 0$ while the nose ablates symmetrically, and then go to some angle of attack while the nose is still symmetrically ablated. The curve for $\Delta n = 1.44$ shows that large errors exist in α due to ablation. However, this perhaps is the largest possible ablation case in consideration, since the stagnation point was kept fixed and because the nose diameter considered was the lower limit in size. The ablation equations (not presented here) show an ablation dependence on nose radius of the form

$$\frac{\Delta l}{r} \propto \frac{1}{r^{3/2}} \qquad (105)$$

Thus, for example, for a 12-inch diameter probe

$$\frac{\Delta l}{r} \approx .097$$

and for this case, $\Delta n = .60$. The angle of attack error $\Delta \alpha$, for $D = 12$ inches is also shown in Figure 42. While a 12-inch diameter probe reduces $\Delta \alpha$ significantly, it can be seen that the perturbation is still large. Thus, it could be concluded that nose recession should be limited, either by cooling, or by large nose diameter to $\Delta l / r$ less than perhaps 5% if satisfactory attitude angle results are expected, using the two-orifice per plane model and equations.

Alternatively, the sensitivity of the attitude equations to the exponent n can be eliminated by using three pressure ports instead of two in each attitude plane. For the case of three orifices and a logarithmic pressure relation, Equations (45) and (52), it is possible to eliminate the pressure distribution exponent n and for this case the change in nose shape due to ablation will not cause an error in attitude determination. Pressure and attitude equations for this orifice configuration are described in Section II. It should be cautioned however, that for this scheme to be correct, the nose pressure distributions must obey a $\cos^n \theta$ relation even though the value of n is unknown.

SECTION VI

SUMMARY OF RESULTS AND RECOMMENDATIONS

1. SUMMARY OF RESULTS

Air data outputs obtainable from pressure measurements on a hemisphere probe have been investigated analytically for free stream Mach numbers which include and put emphasis on the hypersonic flow regime. Specifically, vehicle attitude can be obtained from the pressure inputs alone, whereas true air speed requires the additional input of free stream density. A simple flow chart of air data inputs and obtainable air data outputs at hypersonic and supersonic Mach numbers are shown in Tables IIa and IIb, respectively. A more detailed chart, Table III, lists air data inputs, outputs, equations, assumptions, etc., and provides in effect a summary of the study performed. At hypersonic Mach numbers, vehicle attitude or angle of attack α and sideslip β can be obtained using only pressure distributions measured on a hemispherical nose through the relations

$$\alpha = \tan^{-1}\left[\sqrt{2}\left(\frac{P_1}{P_2}\right)^{\frac{1}{2.24}} - 1\right] \tag{32}$$

$$\beta = \tan^{-1}\left[\sqrt{2}\left(\frac{P_4}{P_2}\right)^{\frac{1}{2.24}} - 1\right] \tag{41}$$

Attitude angle uncertainties in these expressions resulting from one percent individual pressure measurement uncertainties, and possible pressure distribution variations are on the order of $\pm 1/2$ degree for attitude angle variations from $-20°$ to $+50°$. The equations can be used for angles as high as $85°$ with no resultant discontinuities, but with uncertainties becoming as large as $\pm 6°$.

Over the lower Mach number regime (transonic, supersonic) the recommended Mach number independent attitude angle expressions are

$$\frac{\log\left(P_1/P_2\right)}{\log\left(P_3/P_2\right)} = \frac{\log\left(\cos(\alpha - \phi_1)/\cos\alpha\right)}{\log\left(\cos(\alpha - \phi_3)/\cos\alpha\right)} \tag{47}$$

$$\frac{\log\left(P_4/P_2\right)}{\log\left(P_5/P_2\right)} = \frac{\log\left(\cos(\beta - \gamma_1)/\cos\beta\right)}{\log\left(\cos(\beta - \gamma_3)/\cos\beta\right)} \tag{54}$$

Attitude angle uncertainties for these expressions are also on the order of $\pm 1/2°$; however, the useful attitude range for these expressions is approximately $\pm 20°$, the expressions becoming unusable at higher angles due either to discontinuities or multiple value solutions.

Velocity (true air speed) can be obtained for Mach numbers of approximately two or greater from the hemisphere pressures if free stream density is an additional input using the expression

$$U_\infty = \frac{1.021\left(P_2/\rho_\infty\right)^{1/2}}{\left[\cos\left[\tan^{-1}\left(\sqrt{2}\left(\frac{P_1}{P_2}\right)^{1/n} - 1\right)\right]\cos\left[\left(\sqrt{2}\left(\frac{P_1}{P_2}\right)^{1/n} - 1\right)\left(\sqrt{2}\left(\frac{P_4}{P_2}\right)^{1/n} - 1\right)\right]\right]^{n/2}} \tag{92}$$

Likewise, indicated air speed can be obtained from the hemisphere pressure inputs using

$$U_i = \frac{1.021\left(P_2/\rho_o\right)^{1/2}}{\left[\cos\left[\tan^{-1}\left(\sqrt{2}\left(\frac{P_1}{P_2}\right)^{\frac{1}{n}}-1\right)\right]\cos\left[\left(\sqrt{2}\left(\frac{P_1}{P_2}\right)^{\frac{1}{n}}-1\right)\left(\sqrt{2}\left(\frac{P_4}{P_2}\right)^{\frac{1}{n}}-1\right)\right]\right]^{\frac{n}{2}}} \qquad (95)$$

where ρ_o is sea level atmospheric density.

For Mach numbers ≥ 6, n equals 2.24 whereas n is Mach number dependent for $2 < M < 6$.

An altitude, or more properly, a pressure altitude cannot be obtained from the pressures measured on a hemisphere in hypersonic flow. Given free stream density, a density altitude can be obtained to within at least ±8%.

As with altitude, the pressures measured on the hemisphere are insufficient inputs to obtain hypersonic free stream Mach number. When density is given, however, and velocity is calculable, Mach number can be obtained to ±10% or better.

For the simple attitude expressions, Eq. (32), (41), large errors in attitude due to ablation could be expected. However, use of Eq. (47), (54) would allow attitude to be determined even with ablation if the nose pressure distribution still obeyed a $\cos^n \theta$ relation.

2. RECOMMENDATIONS

The present analysis of air data outputs obtainable at hypersonic Mach numbers using measurements of nose pressure has led to a simplified set of air data equations. These expressions, believed to hold with acceptable accuracy in the high Mach number flow regime, resulted from methods used to predict the hemispherical pressure distribution over a broad range of flight conditions. Since these equations allow easy utilization of the air data inputs, they appear to be very promising for hypersonic flight usage. It would seem worthwhile, therefore, to study the equations experimentally. That is not to say that considerable experimental data have not been used in the derived expressions; however, the equations have not been experimentally verified over the range of attitude angles (up to 50°) and flight velocities (to 20,000 feet per second) considered in this study.

Specifically, experimental verification of the two following expressions upon which the air data equations are constructed would be of primary interest.

$$P = P_s \cos^n \theta \qquad n = 2.24 \qquad (10)$$

$$P_s = K \frac{\rho_\infty U_\infty^2}{2} \qquad K = 1.92 \qquad (106)$$

These two expressions should be studied experimentally over the flight envelope of interest with variation in U_∞, ρ_∞ (altitude), α and β. In addition, insofar as possible, other test variables, e.g. Mach number, Reynolds number, model size, should be duplicated.

Flight duplication of velocity presents the most difficult requirement for ground test facilities. With regard to this problem, hypersonic shock tunnel facilities appear to be the most promising, the Cornell Aeronautical Laboratory Shock Tunnels for example having the capability of duplicating velocity-density flight conditions for a full-size probe up to true air speeds of about 15,000 feet per second (see Reference 21).

In conclusion, if the air data equations for α , β and U_∞ can be shown to hold satisfactorily over the flight regime predicted, then the use of the hemisphere probe in actual vehicle flights is recommended.

TABLE IIa

HYPERSONIC CONTINUUM OUTPUT FLOW CHART

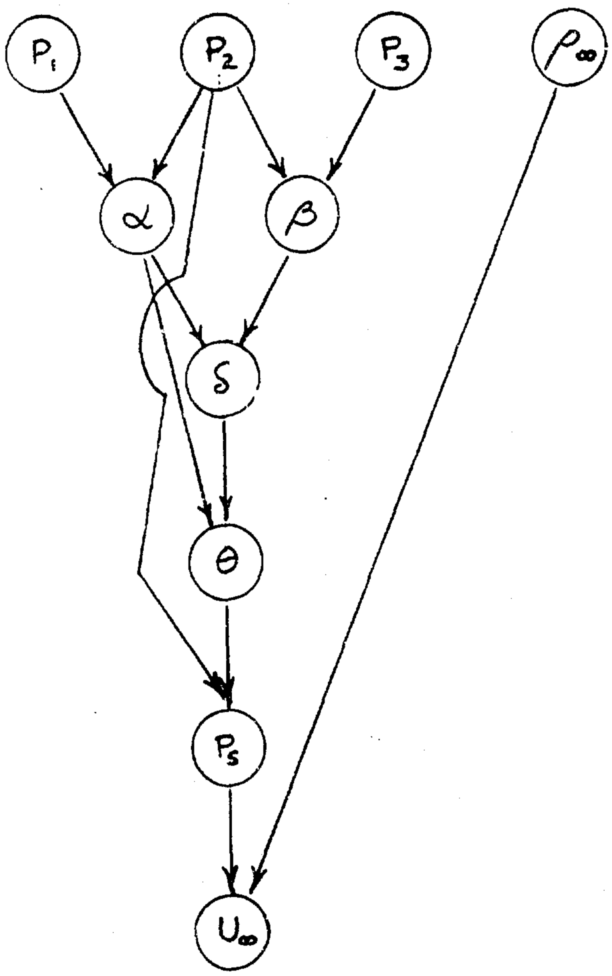

$$P = P_s \cos^n \theta \qquad n = 2.24$$

$$\alpha = \tan^{-1}\left[\csc \phi_1 \left(\frac{P_1}{P_2}\right)^{1/n} - \cot \phi_1\right]$$

$$\beta = \tan^{-1}\left[\csc \gamma_1 \left(\frac{P_4}{P_2}\right)^{1/n} - \cot \gamma_1\right]$$

$$\delta = \tan^{-1}(\cos\alpha \tan\beta)$$

$$\theta = \cos^{-1}(\cos\delta \cos\alpha)$$

$$P_s = P_2/\cos^n \theta$$

$$U_\infty = \left(\frac{2 P_s}{K \rho_\infty}\right)^{1/2}$$

TABLE II b

TRANSONIC - SUPERSONIC OUTPUT FLOW CHART

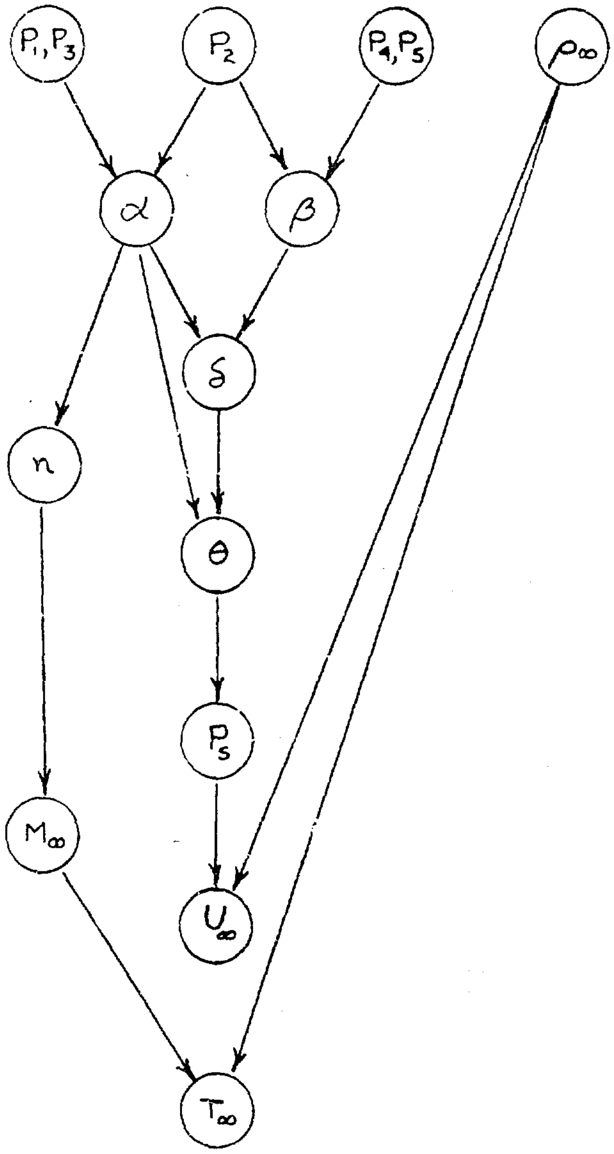

$$P = P_s \cos^n \theta$$

$$\frac{\log\left(\frac{P_1}{P_2}\right)}{\log\left(\frac{P_3}{P_2}\right)} = \frac{\log\left(\cos\phi_1 + \sin\phi_1 \tan\alpha\right)}{\log\left(\cos\phi_3 + \sin\phi_3 \tan\alpha\right)}$$

$$\frac{\log\left(\frac{P_4}{P_2}\right)}{\log\left(\frac{P_5}{P_2}\right)} = \frac{\log\left(\cos\gamma_1 + \sin\gamma_1 \tan\beta\right)}{\log\left(\cos\gamma_3 + \sin\gamma_3 \tan\beta\right)}$$

$$\delta = \tan^{-1}\left(\cos\alpha \tan\beta\right)$$

$$\theta = \cos^{-1}\left(\cos\delta \cos\alpha\right)$$

$$P_s = P_2 / \cos^n \theta$$

$$U_\infty = \left(\frac{2 P_s}{K \rho_\infty}\right)^{1/2}$$

TABLE III

SUMMARY OF AIR DATA F

① OUTPUT	② INPUT	③ EQUATIONS USED (GENERAL FORM)	④ ASSUMPTIONS MADE	⑤ EQUATIONS USED (SPECIFIC FORM)	⑥ EMPIRICAL CONSTANTS IN ⑤	RA (U
α	P_1, P_2	$\frac{P_1}{P_2} = \frac{\cos^n(\alpha-\phi_1)}{\cos^n(\alpha-\phi_3)}$	$P = P_s \cos^n \theta$	$\alpha = \tan^{-1}\left[\sqrt{2}\left(\frac{P_1}{P_2}\right)^{\frac{1}{2.24}} - 1\right]$	$n = 2.24$; P_1, P_2 LOCATED AT $\phi_1 = 45°, \phi_2 = 0°$ IN X–Z PLANE	$-20°$
α	P_1, P_2, P_3	$\frac{P_1-P_2}{P_2-P_3} = \frac{\cos^n(\alpha-\phi_1)-\cos^n(\alpha-\phi_2)}{\cos^n(\alpha-\phi_2)-\cos^n(\alpha-\phi_3)}$		$\frac{P_1-P_2}{P_2-P_3} = \frac{\left[\frac{\sqrt{2}}{2}(1+\tan\alpha)\right]^{2.24}-1}{1-(.966-.259\tan\alpha)^{2.24}}$	$\phi_1 = 45°$, $\phi_2 = 0°$, $\phi_3 = -15°$	$0°$ T
α	P_1, P_2, P_3	$\frac{\log\left(\frac{P_1}{P_2}\right)}{\log\left(\frac{P_3}{P_2}\right)} = \frac{\log\left[\frac{\cos(\alpha-\phi_1)}{\cos\alpha}\right]}{\log\left[\frac{\cos(\alpha-\phi_3)}{\cos\alpha}\right]}$		$\frac{\log\left(\frac{P_1}{P_2}\right)}{\log\left(\frac{P_3}{P_2}\right)} = \frac{\log\frac{\sqrt{2}}{2}(1+\tan\alpha)}{\log\frac{\sqrt{2}}{2}(1-\tan\alpha)}$	$\phi_1 = 45°$, $\phi_2 = 0°$, $\phi_3 = -45°$ IN X–Z PLANE	$\pm$
β	P_2, P_4	$\frac{P_4}{P_2} = \frac{\cos^n(\beta-\gamma_1)}{\cos^n(\beta-\gamma_3)}$		$\beta = \tan^{-1}\left[\sqrt{2}\left(\frac{P_4}{P_2}\right)^{\frac{1}{2.24}} - 1\right]$	$n = 2.24$; P_4, P_2 LOCATED AT $\gamma_1 = 45°, \gamma_2 = 0°$ IN X–Y PLANE	-20'
β	P_2, P_4, P_5	$\frac{P_4-P_2}{P_2-P_5} = \frac{\cos^n(\beta-\gamma_1)-\cos^n(\beta-\gamma_2)}{\cos^n(\beta-\gamma_2)-\cos^n(\beta-\gamma_3)}$		$\frac{P_4-P_2}{P_2-P_5} = \frac{\left[\frac{\sqrt{2}}{2}(1+\tan\beta)\right]^{2.24}-1}{1-(.966-.259\tan\beta)^{2.24}}$	$\gamma_1 = 45°$, $\gamma_2 = 0°$, $\gamma_3 = -15°$	$0°$
β	P_2, P_4, P_5	$\frac{\log\left(\frac{P_4}{P_2}\right)}{\log\left(\frac{P_5}{P_2}\right)} = \frac{\log\left[\frac{\cos(\beta-\gamma_1)}{\cos\beta}\right]}{\log\left[\frac{\cos(\beta-\gamma_3)}{\cos\beta}\right]}$	↓	$\frac{\log\left(\frac{P_4}{P_2}\right)}{\log\left(\frac{P_5}{P_2}\right)} = \frac{\log\frac{\sqrt{2}}{2}(1+\tan\alpha)}{\log\frac{\sqrt{2}}{2}(1-\tan\alpha)}$	$\gamma_1 = 45°$, $\gamma_2 = 0°$, $\gamma_3 = -45°$ IN X–Y PLANE	$\pm$
δ	α, β	$\delta = \tan^{-1}(\cos\alpha\tan\beta)$	NONE	$\delta = \tan^{-1}(\cos\alpha\tan\beta)$	NONE	DET BY
θ	α, δ	$\cos\theta = \cos\alpha\cos\delta$	NONE	$\theta = \tan^{-1}(\cos\alpha\tan\beta)$	NONE	O' α
P_s	P_2, θ	$P_s = \frac{P_2}{\cos^n\theta}$	VALIDITY OF EQ. IN ③	$P_s = \frac{P_2}{\cos^{2.24}\theta}$	$n = 2.24$	-20' ALL OF
U_∞	P_s, ρ_∞	$U_\infty = 1.021\left(\frac{P_s}{\rho_\infty}\right)^{1/2}$	VALIDITY OF EQ. IN ③; ρ_∞ GIVEN TO $\pm 5\%$	$U_\infty = 1.021\left(\frac{P_s}{\rho_\infty}\right)^{1/2}$	$P_s/q = 1.92$	4 TO
U_i	P_s, ρ_0	$U_i = 1.021\left(\frac{P_s}{\rho_0}\right)^{1/2}$	VALIDITY OF EQ. IN ③; ρ_0 GIVEN VERY ACCURATELY $\sim 1\%$	$U_i = 1.021\left(\frac{P_s}{\rho_0}\right)^{1/2}$	$\frac{P_s}{\left(\frac{\rho_0 U_i^2}{2}\right)} = 1.92$	4 TO
M_∞	U_∞, a_∞	$M_\infty = \frac{U_\infty}{a_\infty}$	a_∞ OBTAINED FROM DENSITY ALTITUDE	$M_\infty = \frac{U_\infty}{a_\infty}$		

III

DATA RELATIONS

⑥	⑦	⑧
1PIRICAL ONSTANTS IN ⑤	RANGE OF USE	ERROR EQUATIONS
2.24, P_1, P_2 ATED AT :45°, $\phi_2 = 0°$ X-Z PLANE	-20° TO 85°	$\Delta\alpha = (\cot\phi_1 + \tan\alpha)\frac{\cos^2\alpha}{n}\left[2C + \left[\log_e(\cos\phi_1 + \sin\phi_1\tan\alpha)\right]\Delta n\right]$
$_1 = 45°$, $_2 = 0°$, $_3 = -15°$	0° TO 50°	$\Delta\left(\frac{P_1 - P_2}{P_2 - P_3}\right) = C\left[\frac{P_1 + P_2}{P_1 - P_2} + \frac{P_2 + P_3}{P_2 - P_3}\right]\frac{P_1 - P_2}{P_2 - P_3}$
$_1 = 45°$, $_2 = 0°$, $_3 = -45°$ X-Z PLANE	±20°	$\Delta\alpha = \frac{\log(\cos\phi_3 + \sin\phi_3\tan\alpha)\left[\frac{\Delta P_1}{P_1} - \frac{\Delta P_2}{P_2}\right] + \log(\cos\phi_1 + \sin\phi_1\tan\alpha)\left[\frac{\Delta P_2}{P_2} - \frac{\Delta P_3}{P_3}\right]}{n\left[\log(\cos\phi_3 + \sin\phi_3\tan\alpha)(\tan\alpha - \tan(\alpha - \phi_1)) - \log(\cos\phi_1 + \sin\phi_1\tan\alpha)(\tan\alpha - \tan(\alpha - \phi_3))\right]}$
.24, P_4, P_2 ITED AT 45°, $\gamma_2 = 0°$ X-Y PLANE	-20° TO 85°	$\Delta\beta = (\cot\gamma_1 + \tan\beta)\frac{\cos^2\beta}{n}\left[2C + \left[\log_e(\cos\gamma_1 + \sin\gamma_1\tan\beta)\right]\Delta n\right]$
$_1 = 45°$, $_2 = 0°$, $_3 = -15°$	0° TO 50°	$\Delta\left(\frac{P_4 - P_2}{P_2 - P_5}\right) = C\left[\frac{P_4 + P_2}{P_4 - P_2} + \frac{P_2 + P_5}{P_2 - P_5}\right]\frac{P_4 - P_2}{P_2 - P_5}$
$\gamma_1 = 45°$, $\gamma_2 = 0°$, $\gamma_3 = -45°$ X-Y PLANE	±20°	$\Delta\beta = \frac{\log(\cos\gamma_3 + \sin\gamma_3\tan\beta)\left[\frac{\Delta P_4}{P_4} - \frac{\Delta P_2}{P_2}\right] + \log(\cos\gamma_1 + \sin\gamma_1\tan\beta)\left[\frac{\Delta P_2}{P_2} - \frac{\Delta P_5}{P_5}\right]}{n\left[\log(\cos\gamma_3 + \sin\gamma_3\tan\beta)(\tan\beta - \tan(\beta - \gamma_1)) - \log(\cos\gamma_1 + \sin\gamma_1\tan\beta)(\tan\beta - \tan(\beta - \gamma_3))\right]}$
IONE	DETERMINED BY α, β	NONE
IONE	OVER α, β RANGE	NONE
$= 2.24$	-20° TO 85° ALL VALUES OF $\lvert P_2 \rvert$	$\frac{\Delta P_s}{P_s} = n\frac{\sin\alpha}{\cos^{n-1}\alpha}\Delta\alpha + \frac{\Delta P_2}{P_2} + \log_e\cos\alpha\,\Delta n$
$= 1.92$	4 TO 26×10^3 FPS	$\frac{\Delta U_\infty}{U_\infty} = \frac{1}{2}\left[\frac{\Delta K}{K} + \frac{\Delta\rho_\infty}{\rho_\infty} + \frac{\Delta P_2}{P_2} + (\log_e(\cos\alpha))\Delta n + \frac{\sin\alpha}{\cos^{(n-3)}\alpha}\frac{(1 + \tan\alpha)}{\sqrt{2}}\left[2C + \log_e\left(\frac{1 + \tan\alpha}{\sqrt{2}}\right)\Delta n\right]\right]$
$= 1.92$	4 TO 24×10^3 FPS	$\frac{\Delta U_i}{U_i} = \frac{1}{2}\left[\frac{\Delta K}{K} + \frac{\Delta\rho_0}{\rho_0} + \frac{\Delta P_2}{P_2} + (\log_e(\cos\alpha))\Delta n + \frac{\sin\alpha}{\cos^{(n-3)}\alpha}\frac{(1 + \tan\alpha)}{\sqrt{2}}\left[2C + \log_e\left(\frac{1 + \tan\alpha}{\sqrt{2}}\right)\Delta n\right]\right]$
		$\frac{\Delta M_\infty}{M_\infty} = \frac{\Delta U_\infty}{U_\infty} + \frac{\Delta a_\infty}{a_\infty}$

2

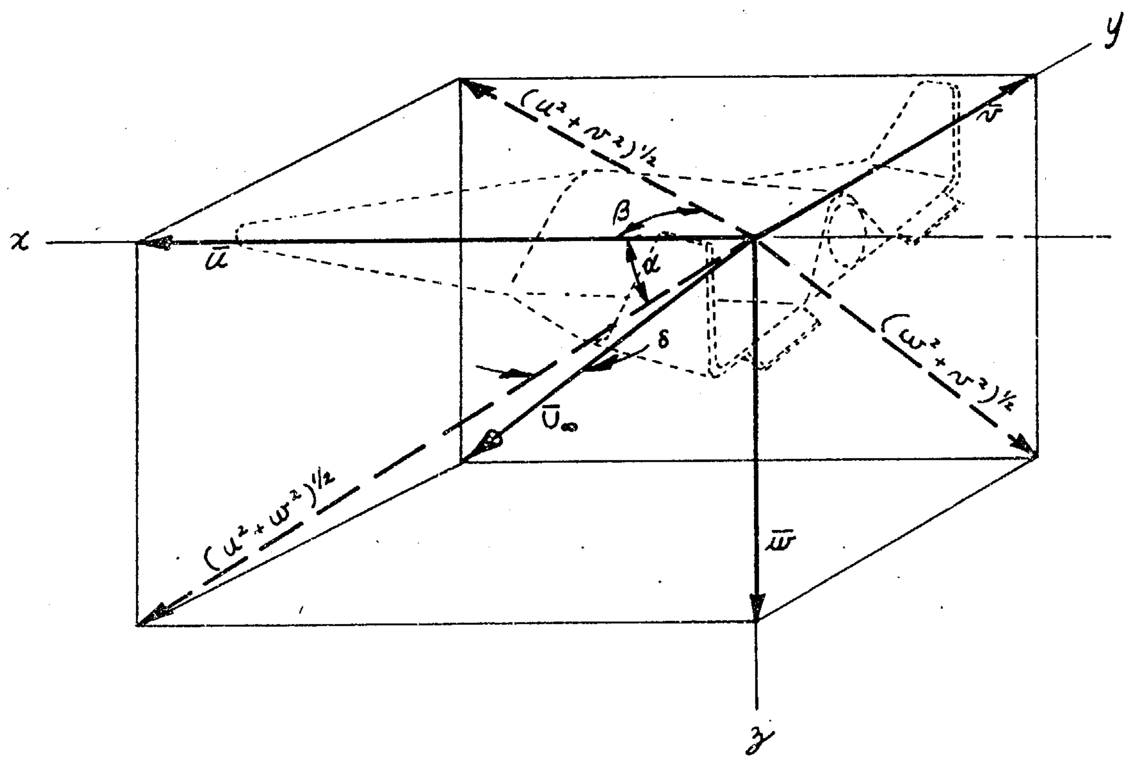

Figure I BODY AXES AND ATTITUDE ANGLES

FIG. 2

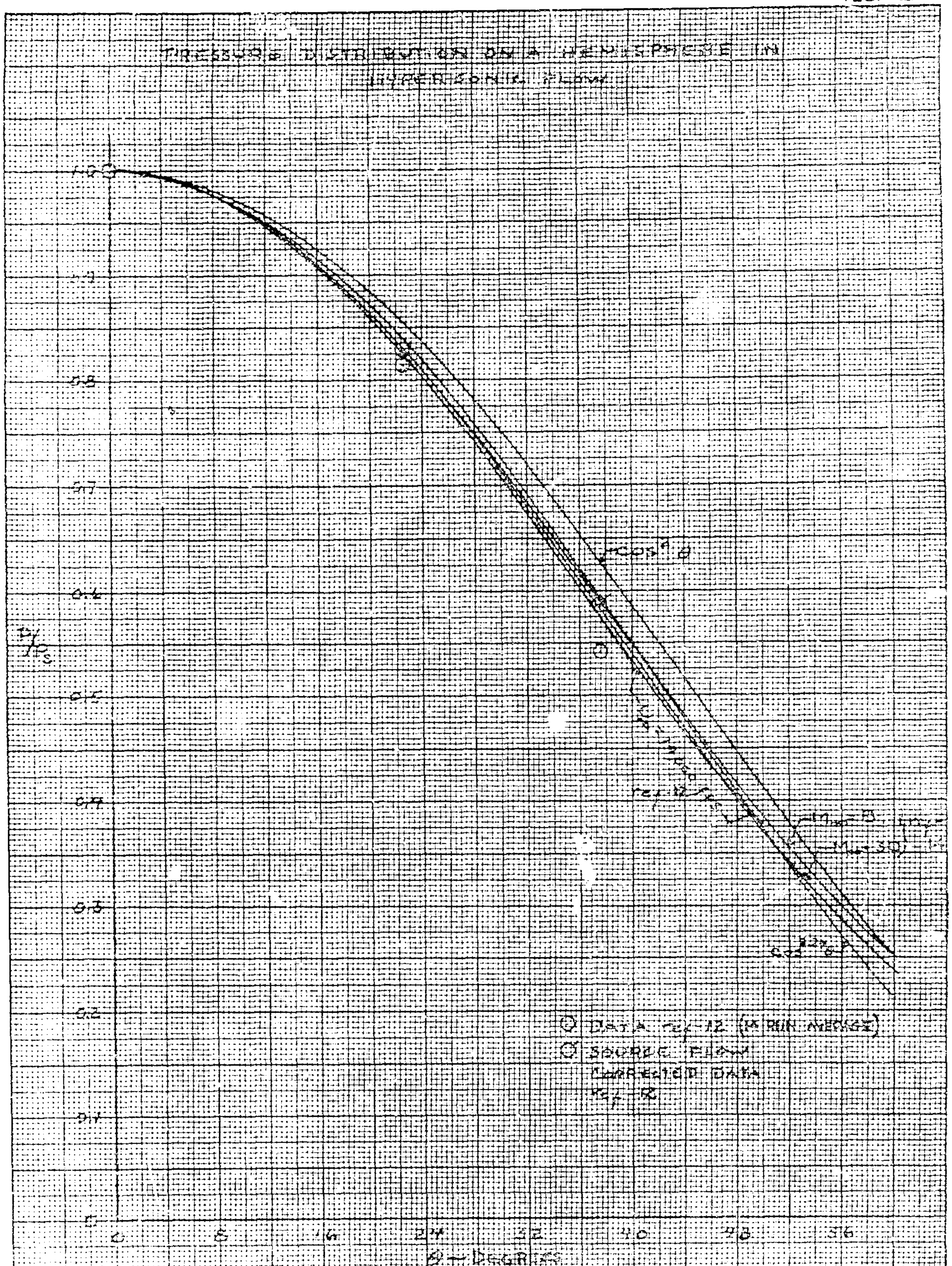
PRESSURE DISTRIBUTION ON A HEMISPHERE IN
HYPERSONIC FLOW
1.0
0.9
0.8
0.7
0.6
0.5
0.4
0.3
0.2
0.1
0
p/p_o
$\cos^2 \theta$
ref. 12
$M_\infty = 8$
$M_\infty = 30$
DATA REF 12 (4 RUN AVERAGE)
SOURCE FLOW
CORRECTED DATA
REF 12
0
8
16
24
32
40
48
56
θ — DEGREES

FIG. 3

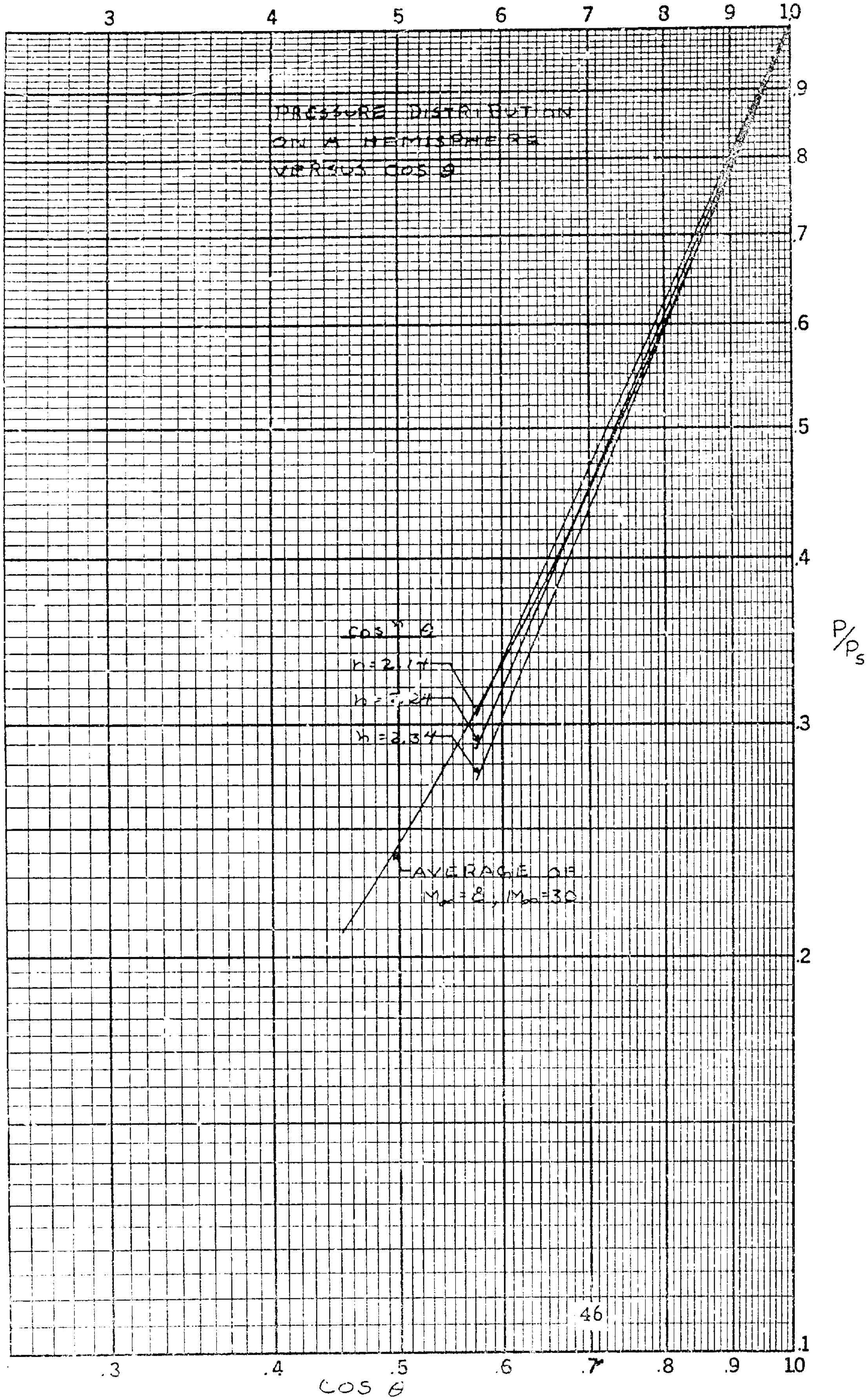
PRESSURE DISTRIBUTION
ON A HEMISPHERE
VERSUS COS θ
$\cos^n \theta$
n = 2.14
n = 2.24
n = 2.34
AVERAGE OF
$M_\infty = 8$, $M_\infty = 30$
P/P_s
COS θ
3
4
5
6
7
8
9
10
.9
.8
.7
.6
.5
.4
.3
.2
.1
.3
.4
.5
.6
.7
.8
.9
10

FIG. 4

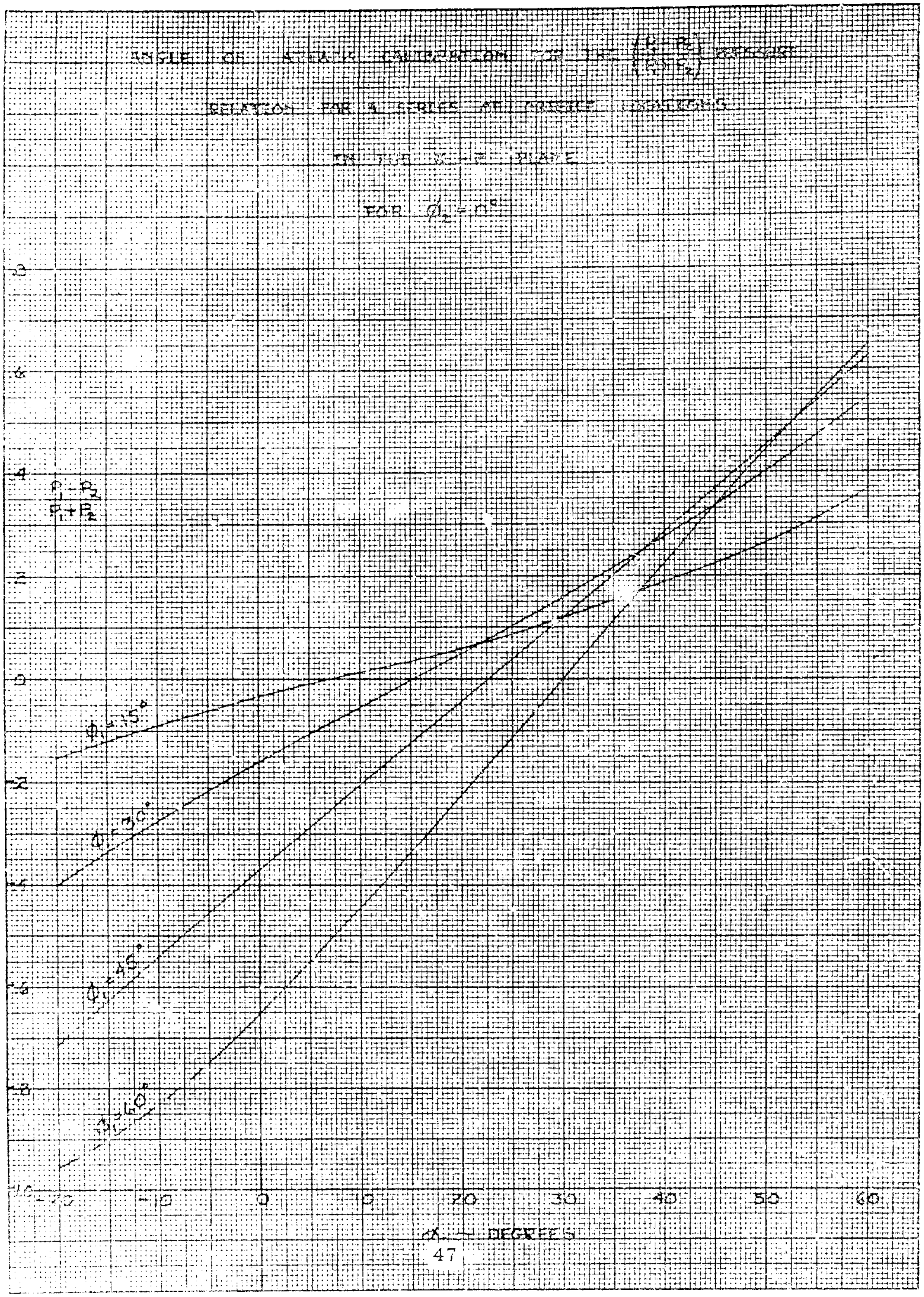

ANGLE OF ATTACK CALIBRATION
RELATION FOR A SERIES
FOR $\phi_2 = 0°$
$\frac{P_1 - P_2}{P_1 + P_2}$
$\phi_1 = 15°$
$\phi_1 = 30°$
$\phi_1 = 45°$
$\phi_1 = 60°$
.8
.6
.4
.2
0
-.2
-.4
-.6
-.8
-1.0
-20
-10
0
10
20
30
40
50
60
α — DEGREES

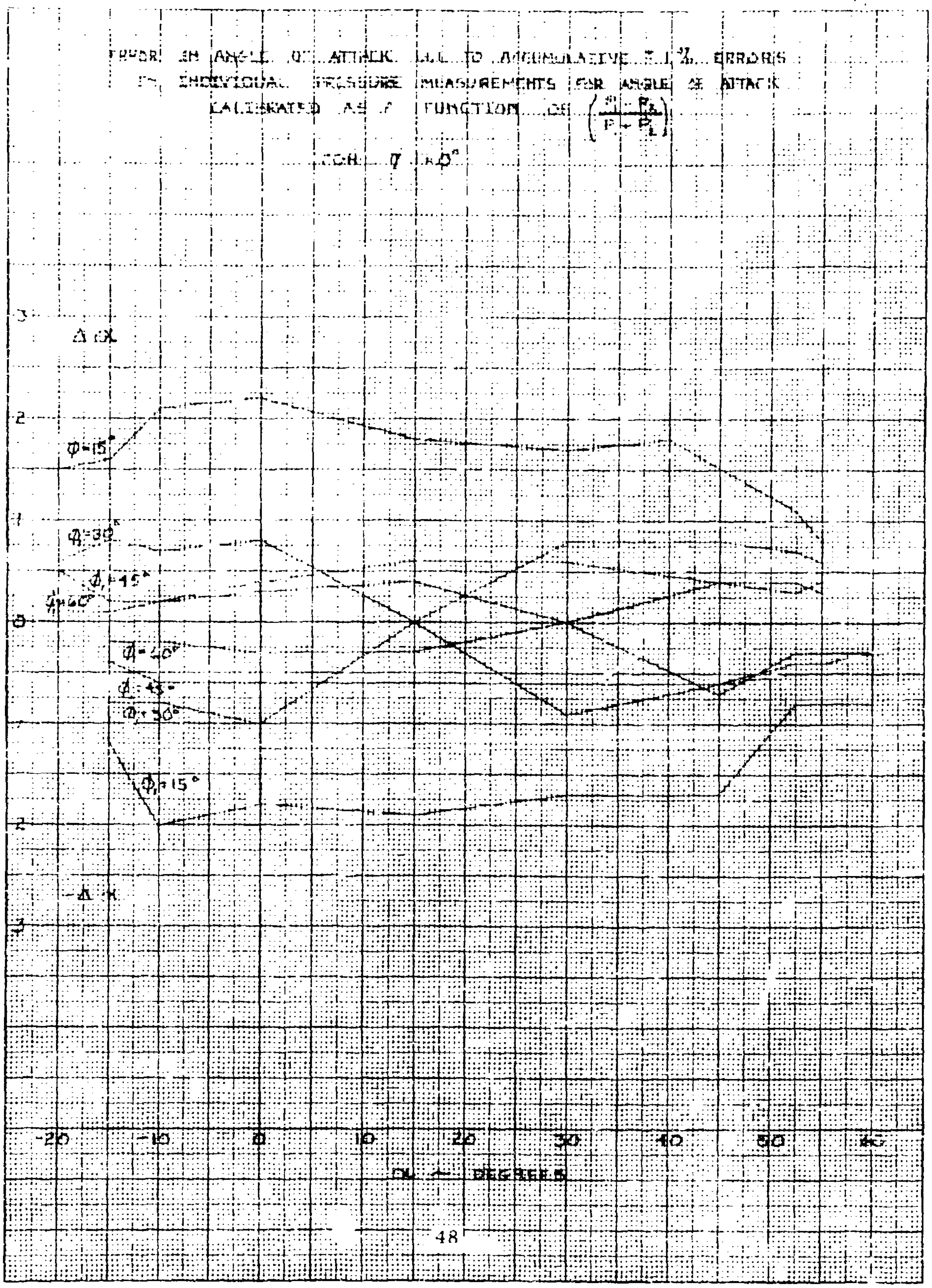

ATTACK
ERRORS
MEASUREMENTS
FUNCTION
Δα
φ=15°
φ=30°
φ=45°
φ=60°
-Δα
-20
-10
0
10
20
30
40
50
60
DEGREES

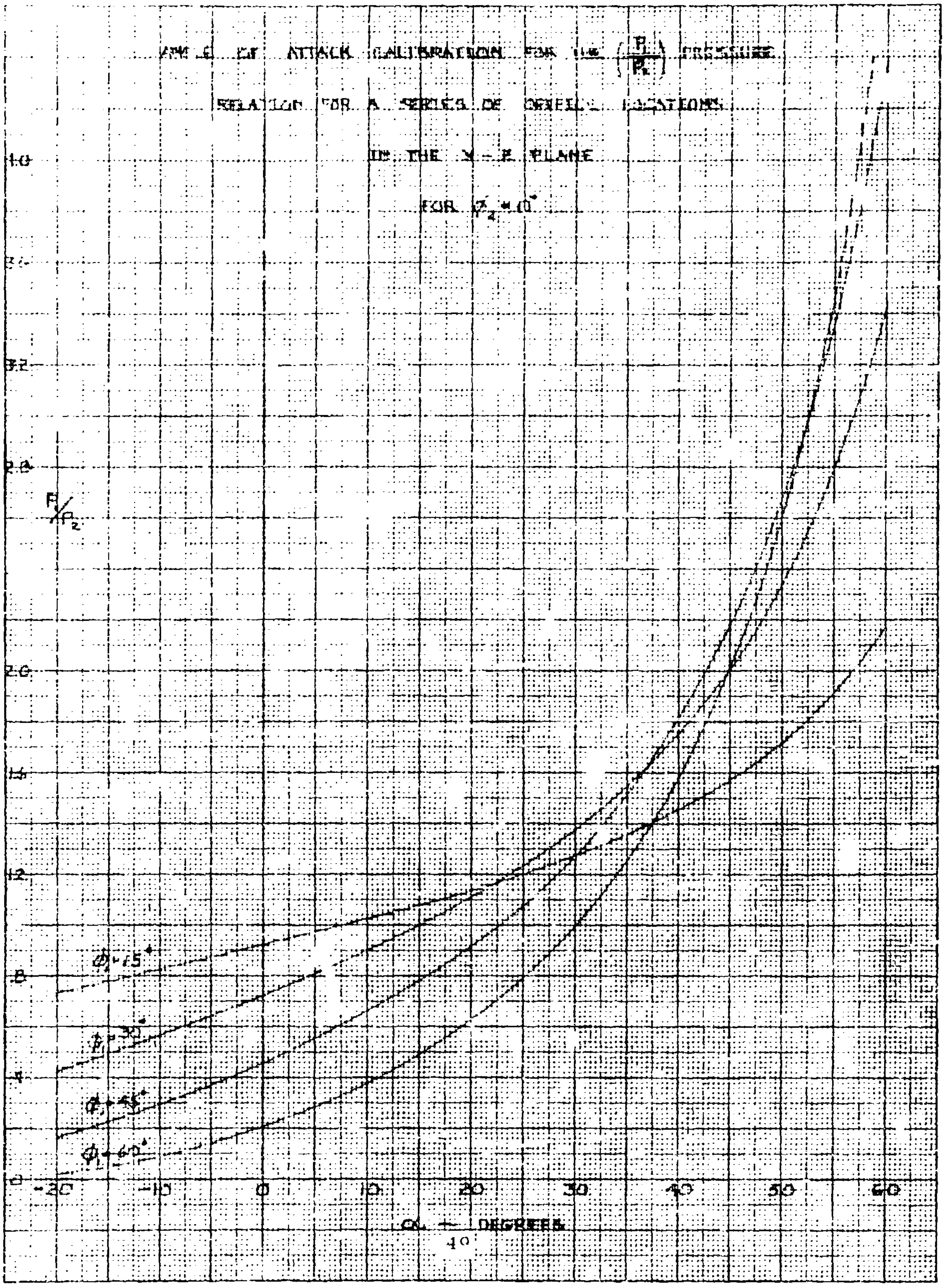
ATTACK CALIBRATION FOR THE (P_1/P_2) PRESSURE
RELATION FOR A SERIES OF ORIFICE LOCATIONS
IN THE Y - Z PLANE
FOR $\phi_2 = 0°$
P_1/P_2
2.8
2.0
1.6
1.2
.8
.4
0
$\phi_1 = 15°$
$\phi_1 = 30°$
$\phi_1 = 45°$
$\phi_1 = 60°$
-20
-10
0
10
20
30
40
50
60
α — DEGREES

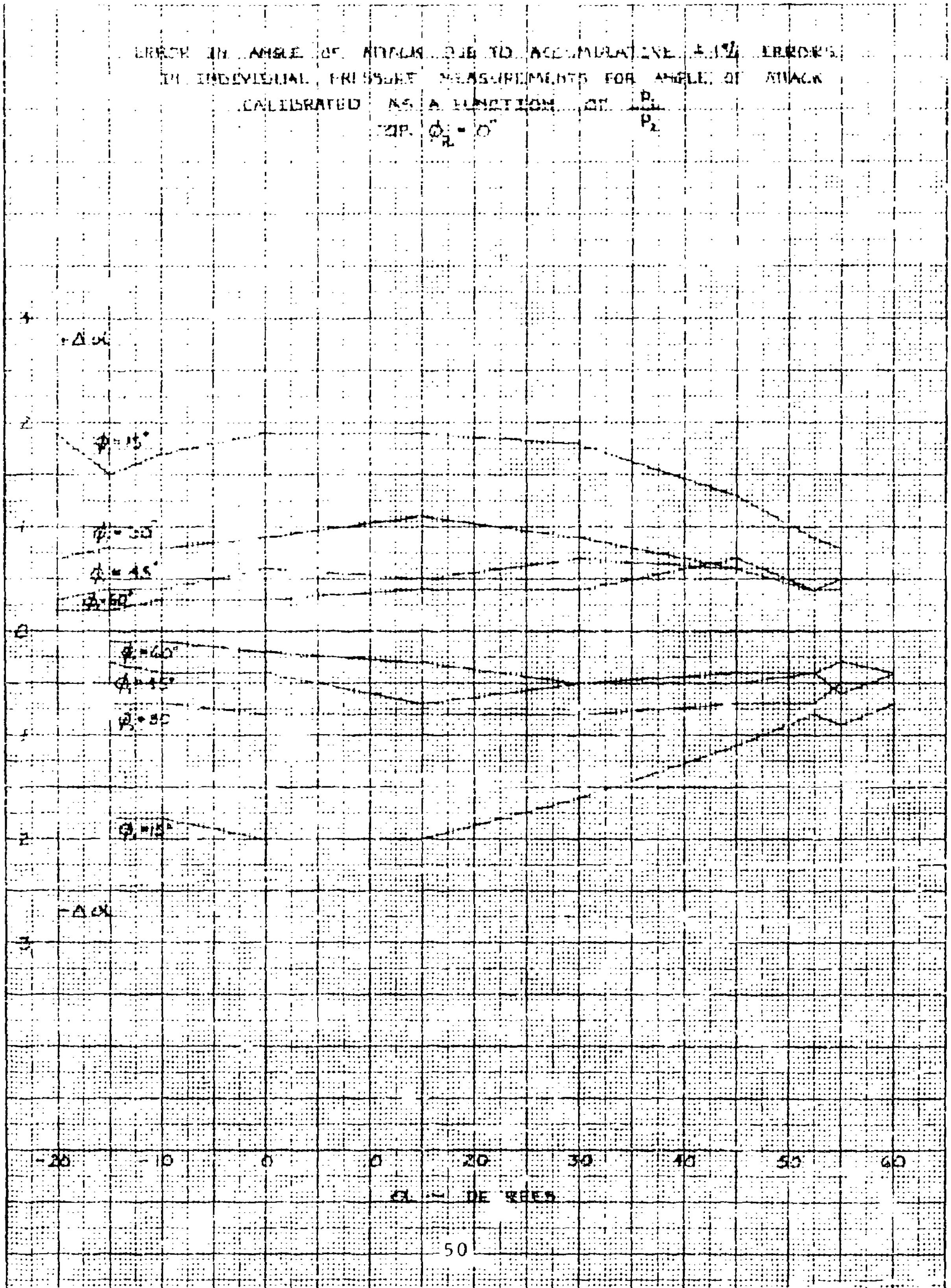
ERROR IN ANGLE OF ATTACK DUE TO ACCUMULATIVE ±1% ERRORS
IN INDIVIDUAL PRESSURE MEASUREMENTS FOR ANGLE OF ATTACK
CALIBRATED AS A FUNCTION OF $\frac{P_1}{P_2}$
FOR $\phi_R = 0°$
$+\Delta\alpha$
$-\Delta\alpha$
$\phi = 15°$
$\phi = 30°$
$\phi = 45°$
$\phi = 60°$
$\phi = 60°$
$\phi = 45°$
$\phi = 30°$
$\phi = 15°$
4
2
1
0
1
2
3
-20
-10
0
20
30
40
50
60
α — DEGREES

FIG. 8

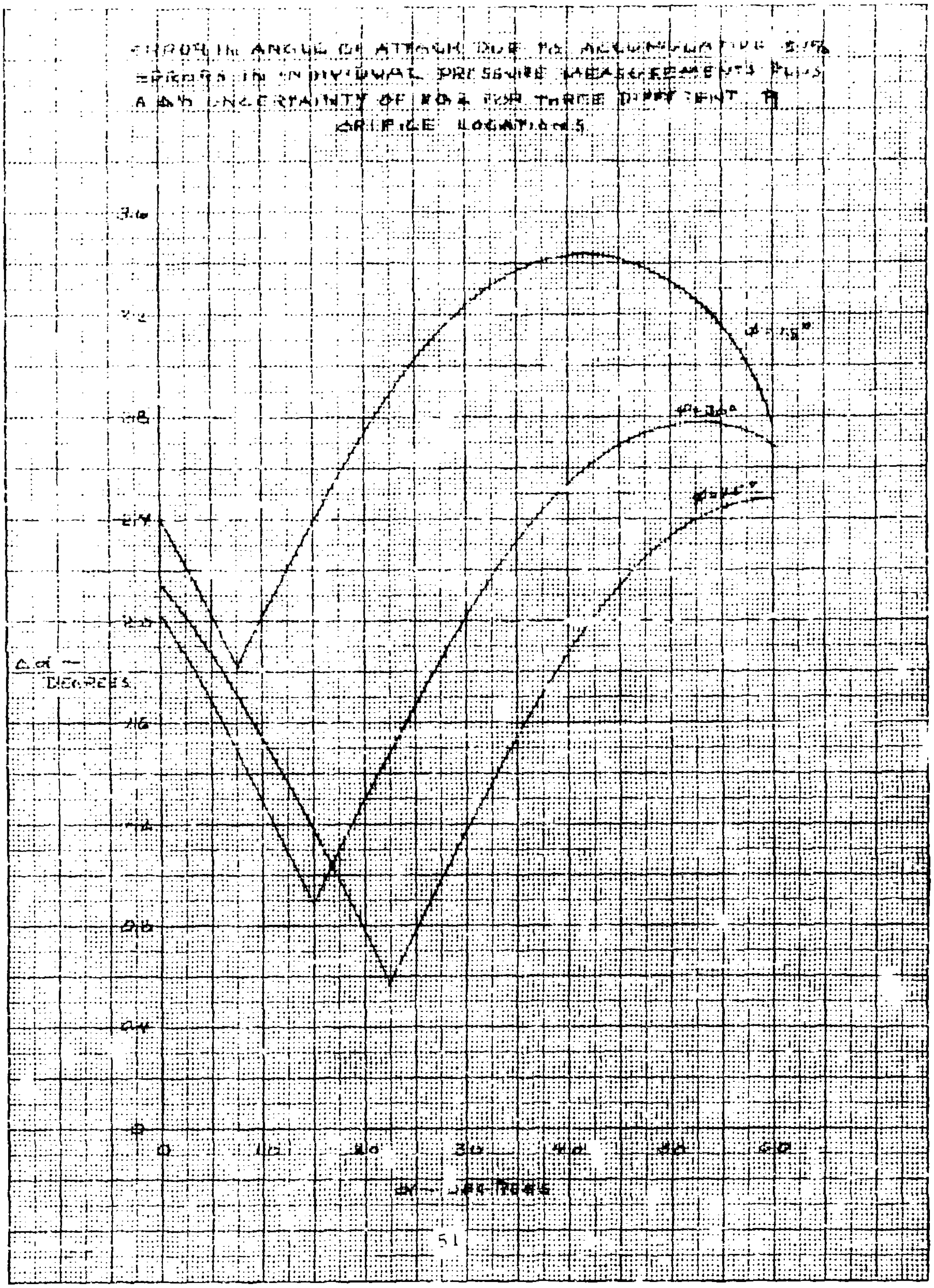
ERROR IN ANGLE OF ATTACK DUE TO ACCUMULATIVE .5% ERRORS IN INDIVIDUAL PRESSURE MEASUREMENTS PLUS A Δφ UNCERTAINTY OF ±0.2 FOR THREE DIFFERENT ORIFICE LOCATIONS
3.6
3.2
2.8
2.4
2.0
1.6
1.2
0.8
0.4
0
Δα —
DEGREES
0
10
20
30
40
50
60
α — DEGREES
φ = 15°
φ = 30°
φ = 45°

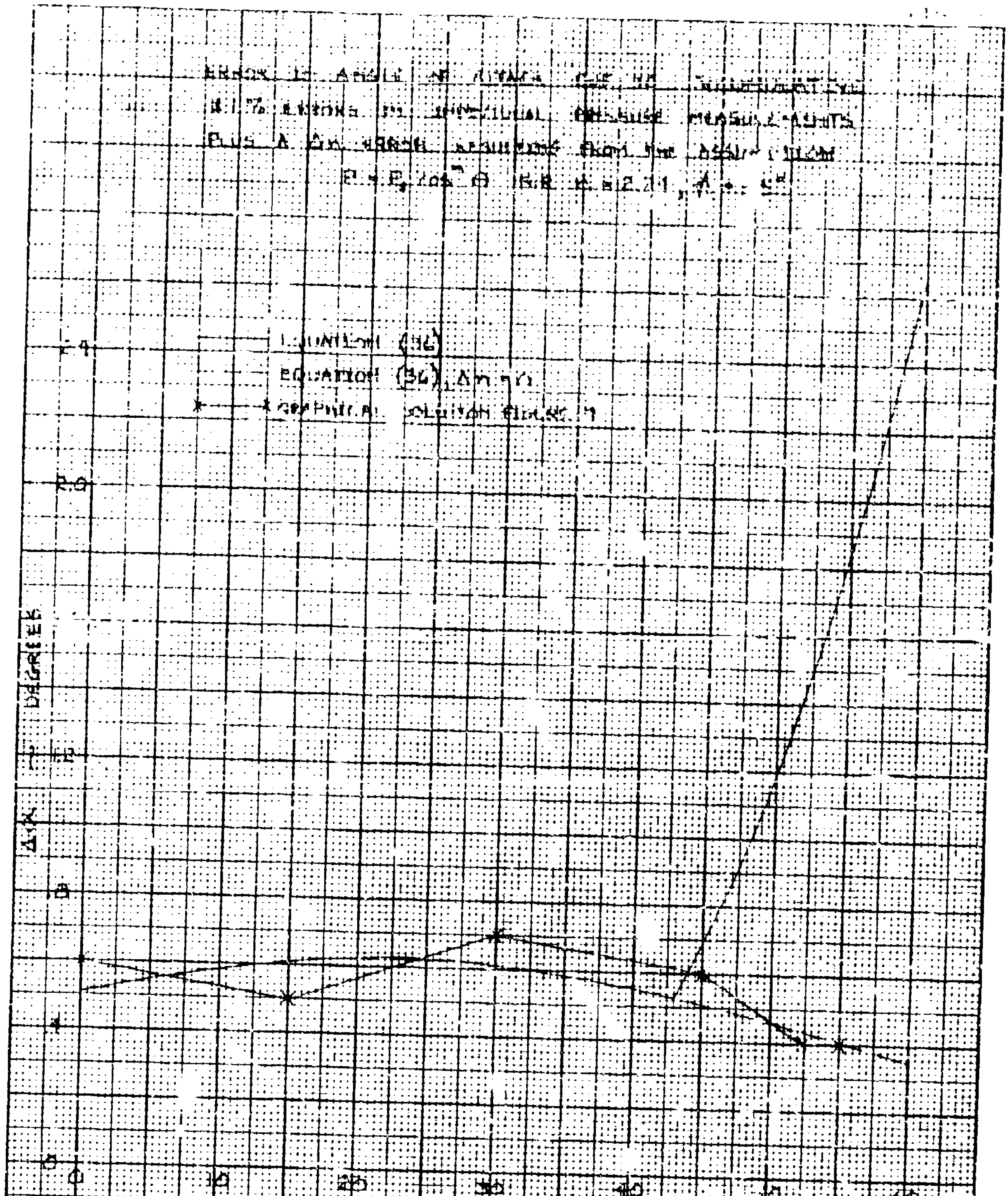
DEGREES
0
10
20
30
40
50
60

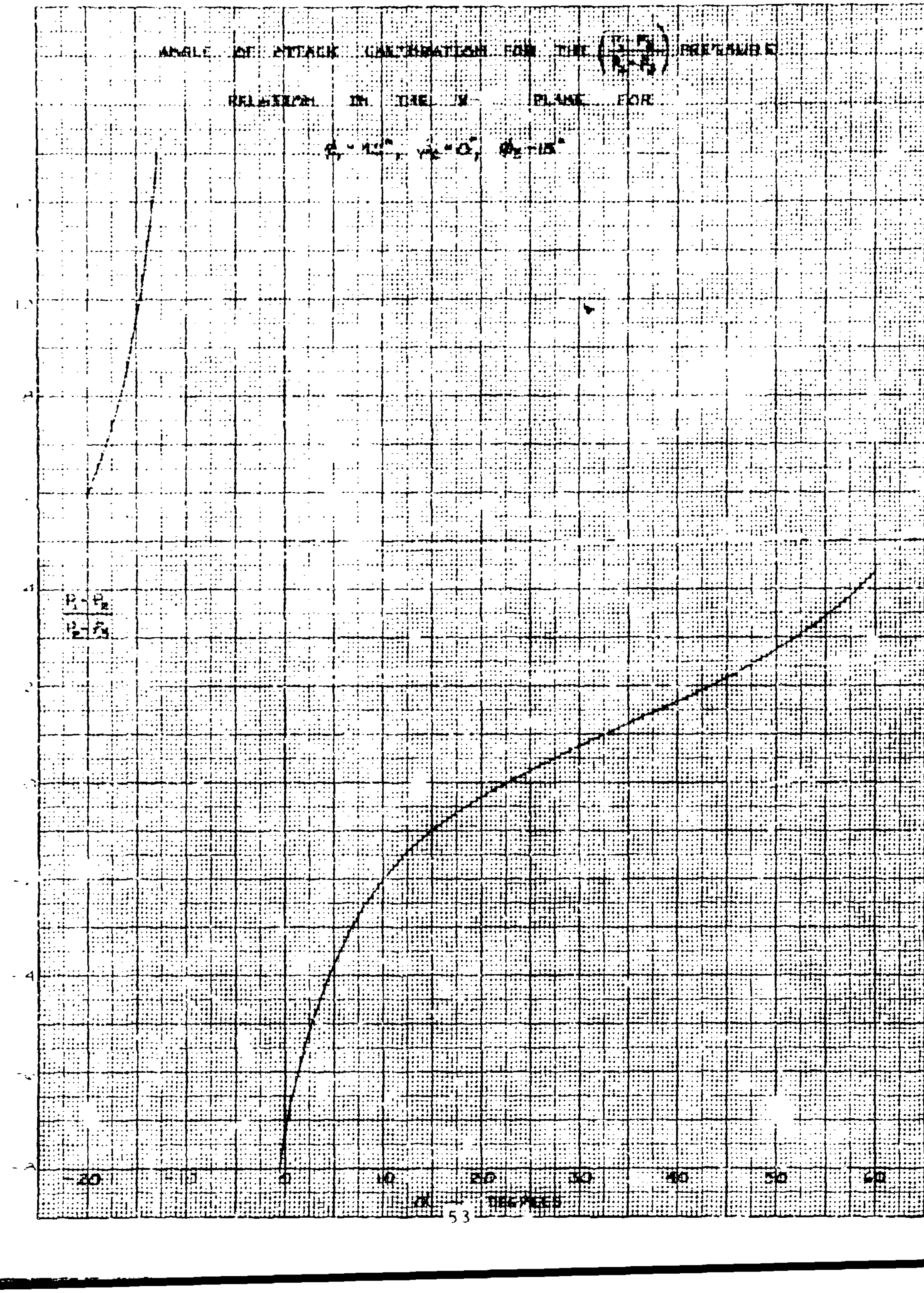
ANGLE OF ATTACK CALIBRATION FOR THE PRESSURE
RELATION IN THE PLANE FOR
$\frac{P_1 - P_2}{P_2 - P_3}$
-20
0
10
20
30
40
50
60
α — DEGREES

FIG. 11

ERROR IN ANGLE OF ATTACK DUE TO ACCUMULATIVE $\pm 1\%$ ERRORS IN INDIVIDUAL PRESSURE MEASUREMENTS FOR ANGLE OF ATTACK CALIBRATED AS A FUNCTION OF $\left(\frac{P_1 - P_3}{P_2 - P_3}\right)$

FOR $\phi_1 = 45°$, $\phi_2 = 0°$, $\phi_3 = -15°$

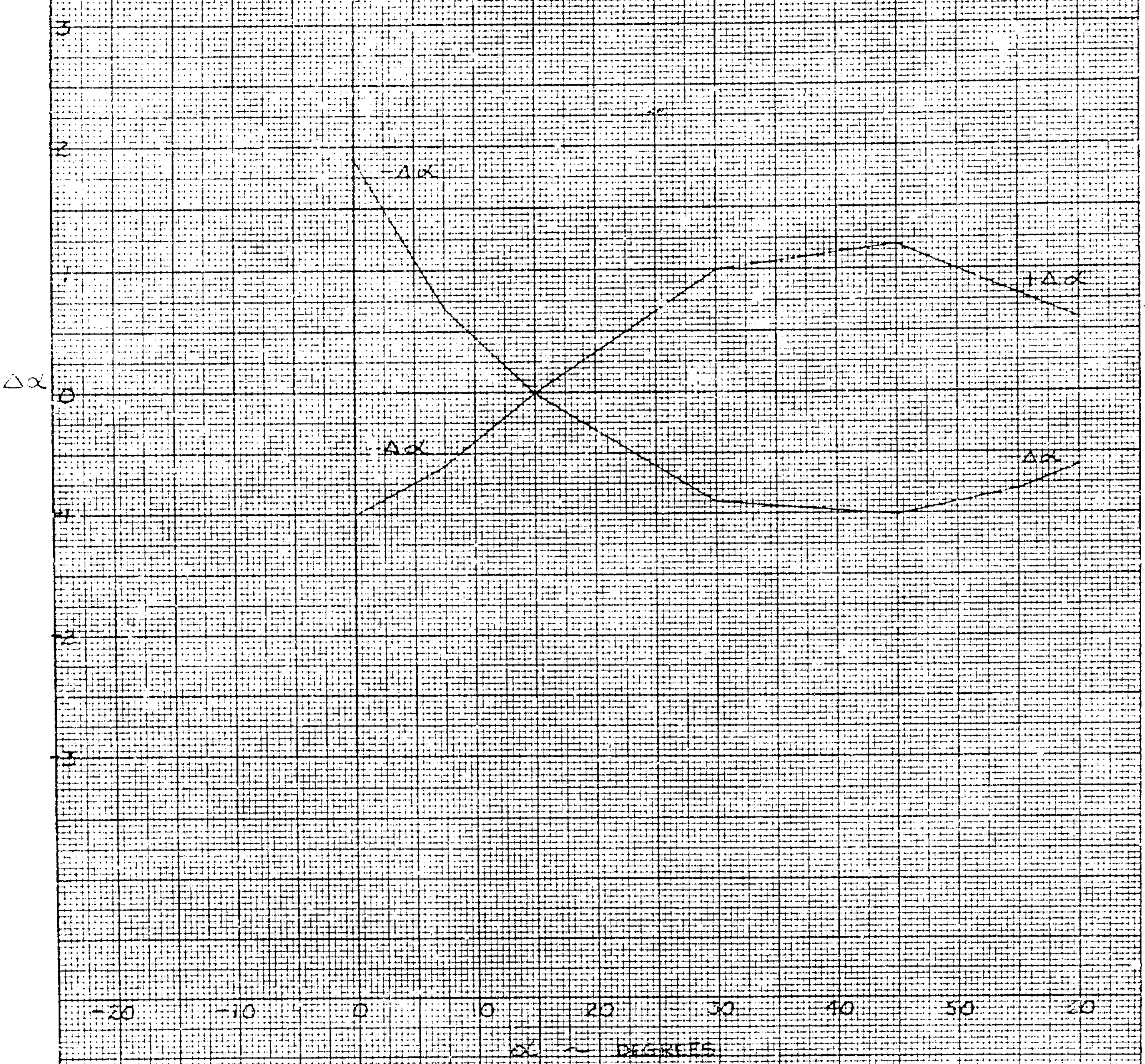

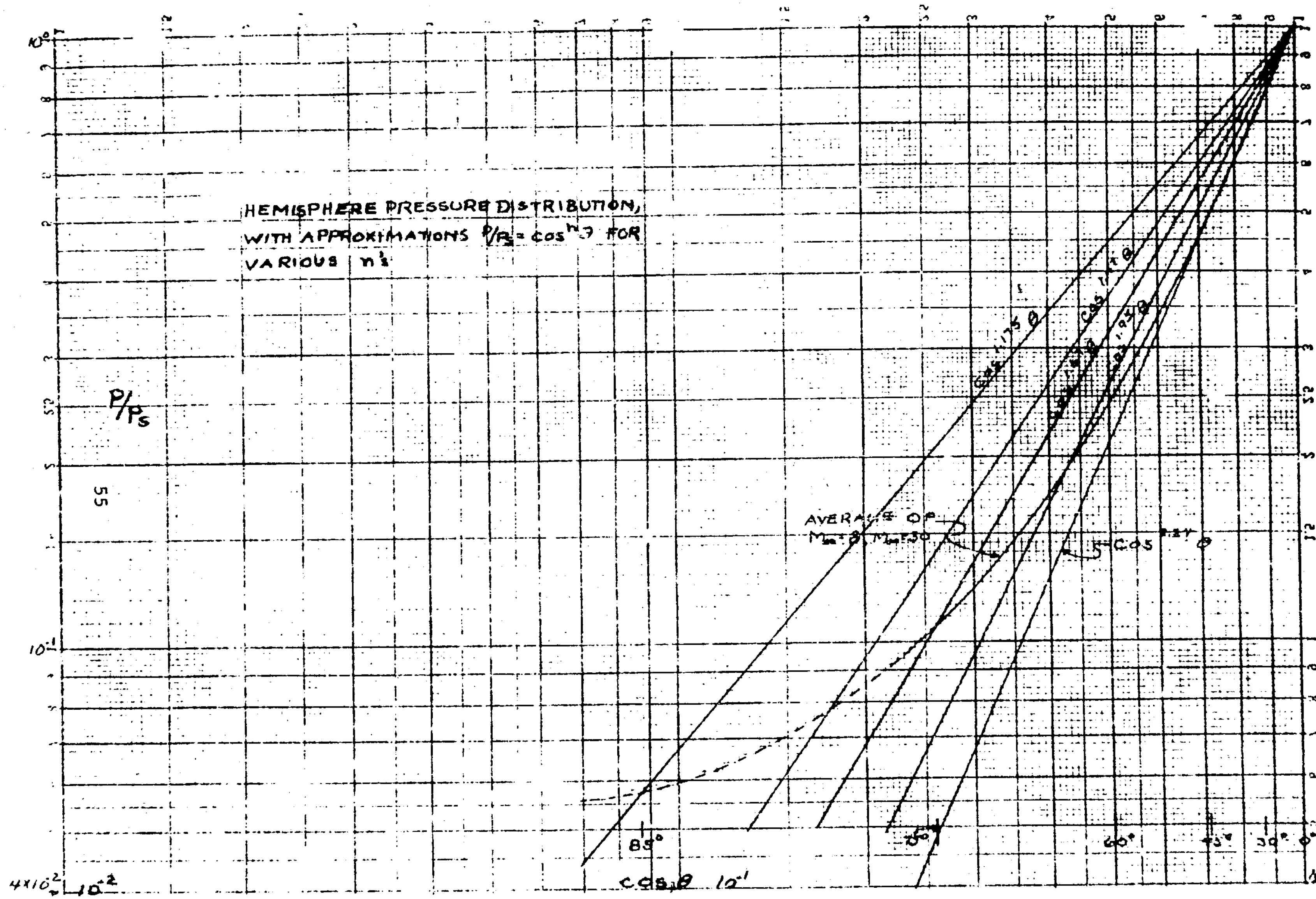
HEMISPHERE PRESSURE DISTRIBUTION,
WITH APPROXIMATIONS P/Ps = cos^n θ FOR
VARIOUS n's
P/Ps
AVERAGE OF
M∞=8, M∞=50
cos θ
10^0
10^-1
10^-2
4×10^-2
85°
60°
30°
0°

FIG. 12

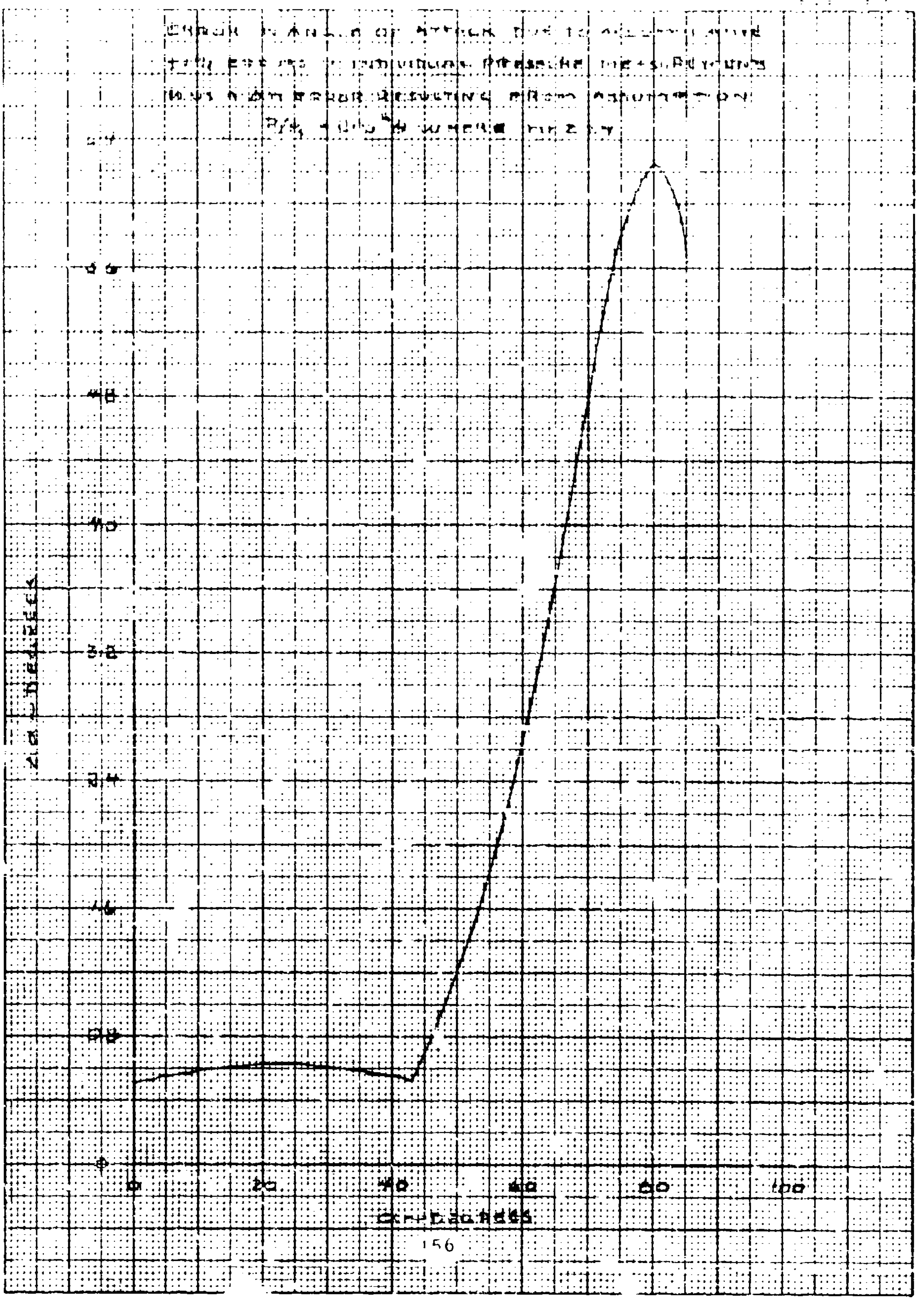
ERROR IN ANGLE OF ATTACK
INDIVIDUAL PRESSURE
ERROR RESULTING FROM
WHERE
4.8
4.0
3.2
.8
0
0
20
40
60
80
100

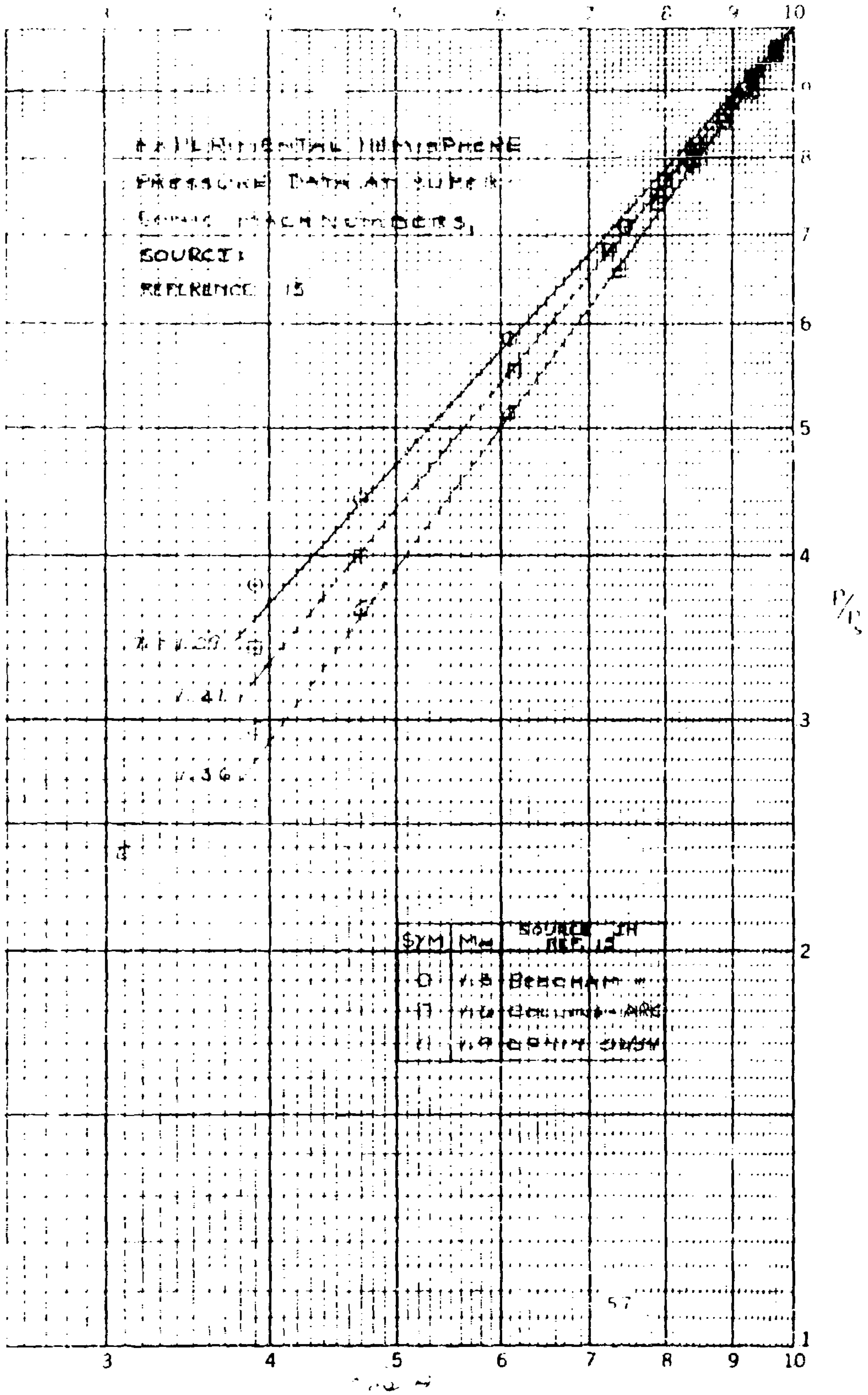
EXPERIMENTAL HEMISPHERE
PRESSURE DATA AT SUPER-
SONIC MACH NUMBERS,
SOURCE:
REFERENCE 15
SYM
M∞
SOURCE IN REF. 15
BEECHAM
57
P/P_s
3
4
5
6
7
8
9
10
1
2
3
4
5
6
7
8

FIG. 14 CONT.

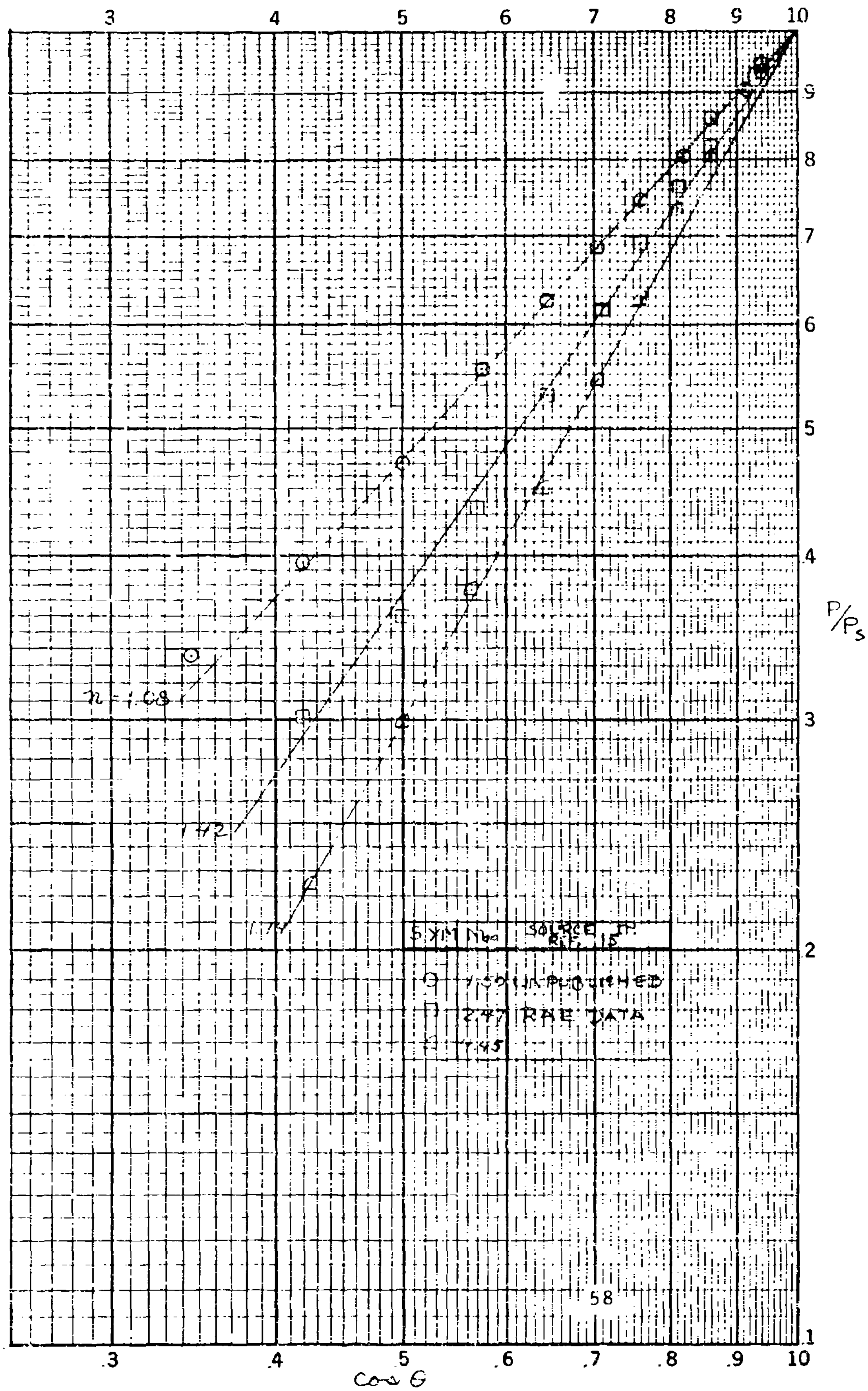

P/Ps
Cos θ
n = 1.68
1.42
1.77
SOURCE
REF. 15
UNPUBLISHED
2.47 RAE DATA
1.45

FIG. 14 CON'T.

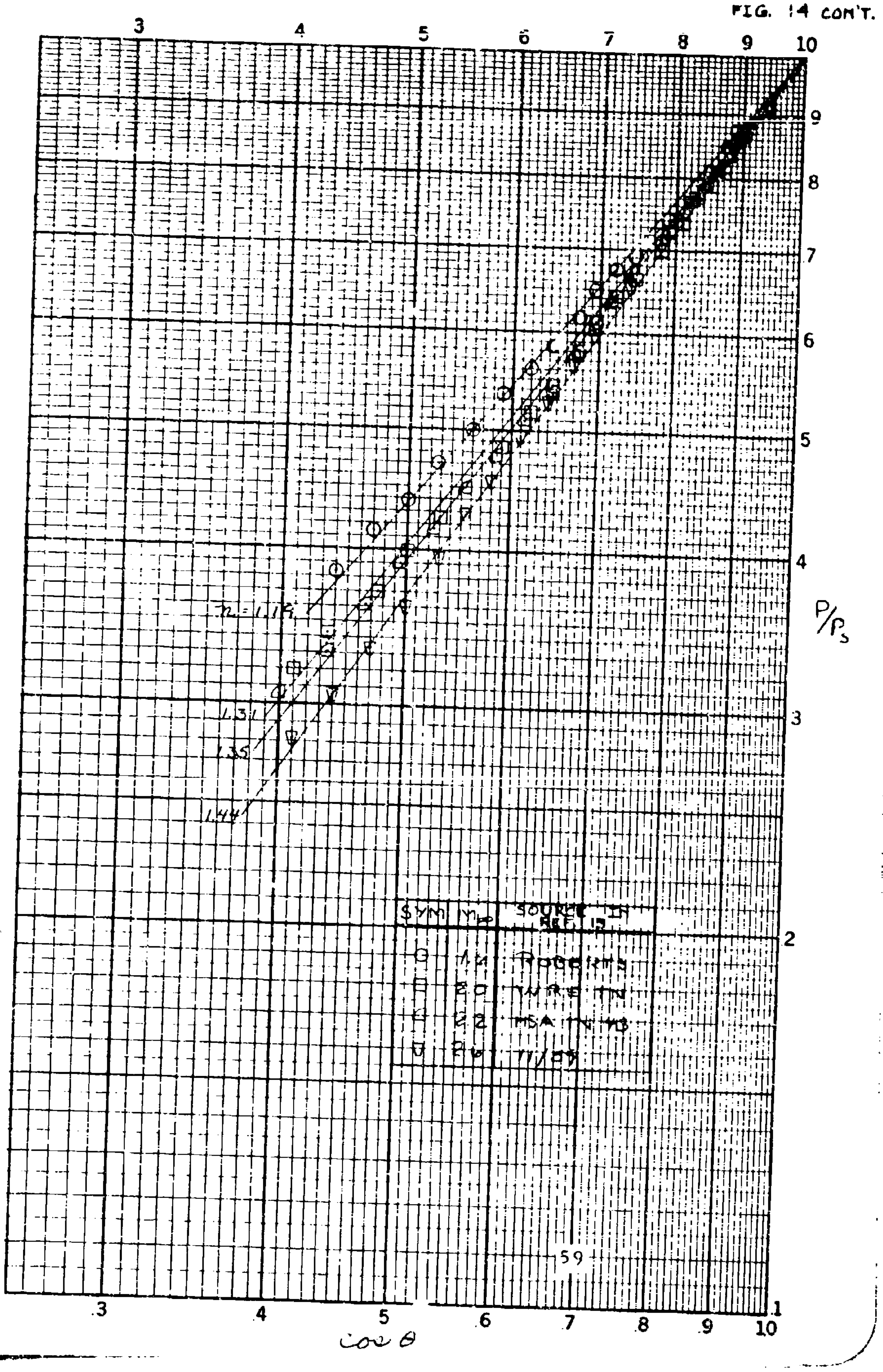

FIG. 14 CONT.

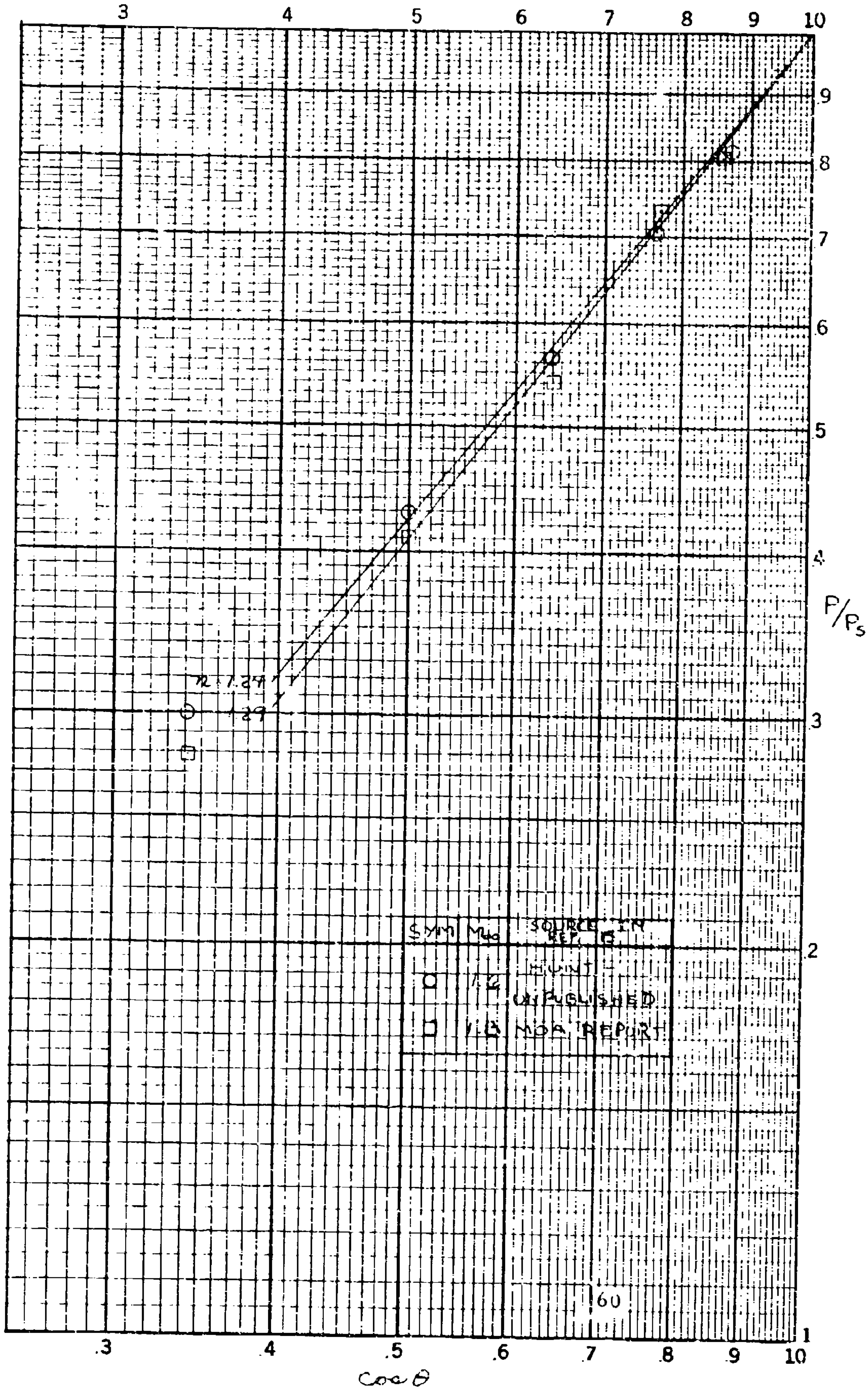

3
4
5
6
7
8
9
10
.9
.8
.7
.6
.5
.4
.3
.2
1
P/P_s
SYM
M_∞
SOURCE IN REF. 6
1.2
HUNT UNPUBLISHED
1.3
NOA REPORT
.3
.4
.5
.6
.7
.8
.9
10
Cos θ

FIG. 14 CON'T.

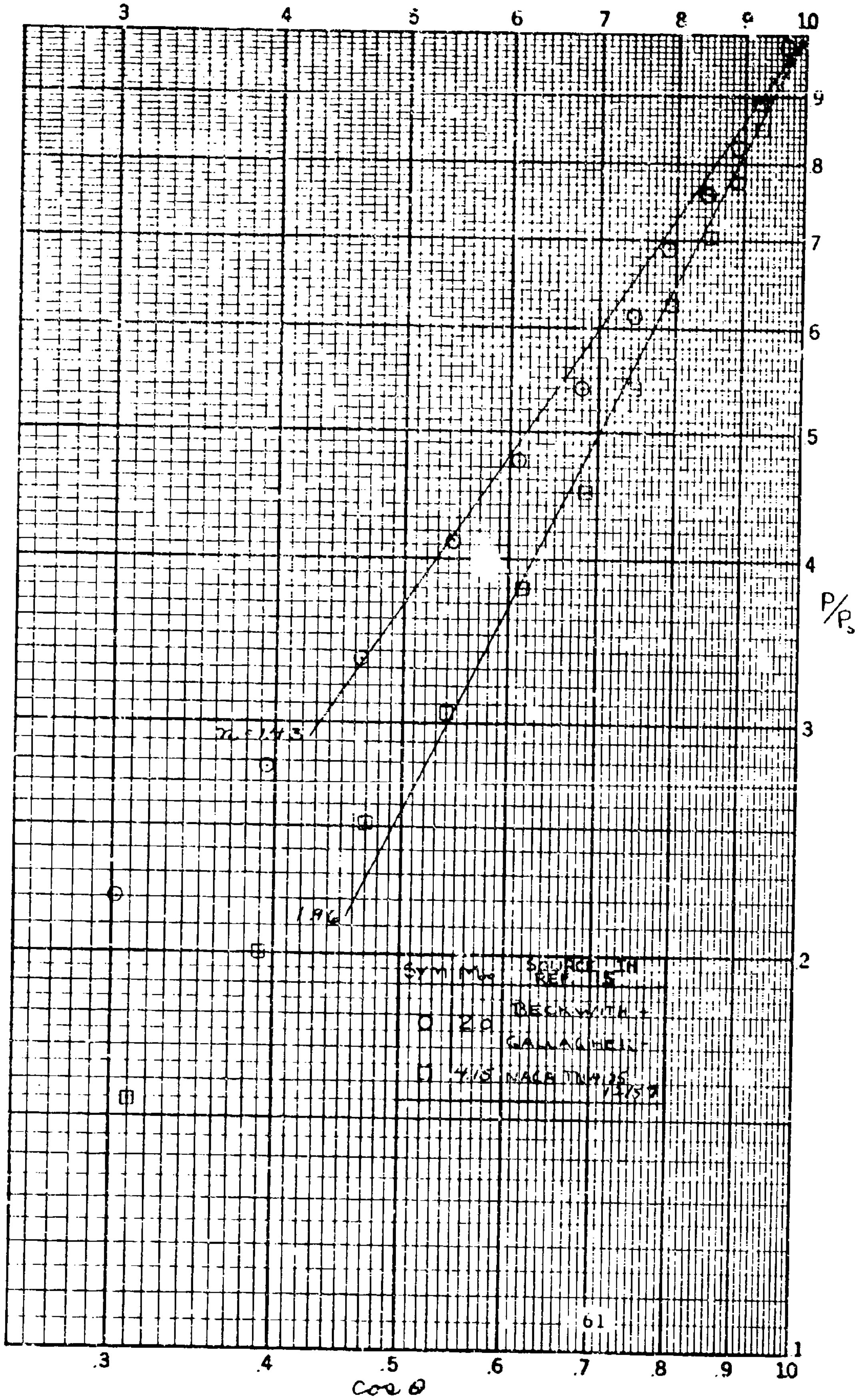

3
4
5
6
7
8
9
10
.9
.8
.7
.6
.5
.4
.3
.2
1
P/P_s
n = 1.43
1.96
SYM
M_∞
SOURCE TH REF 5
2.0
BECKWITH + GALLAGHER
4.15
NACA TN 4125 13757
.3
.4
.5
.6
.7
.8
.9
1.0
Cos θ

FIG. 14 CONCLUDED

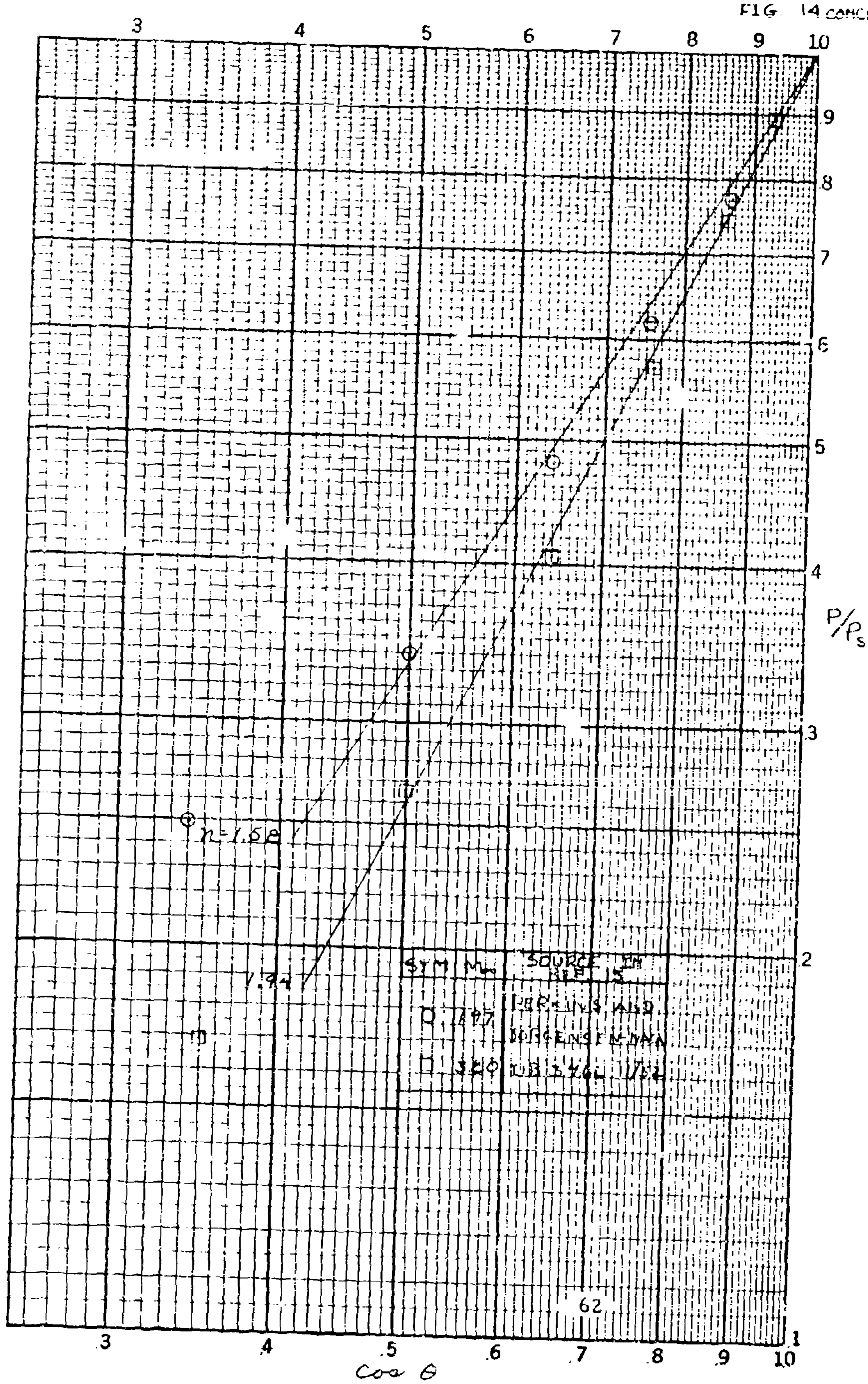

FIG. 15

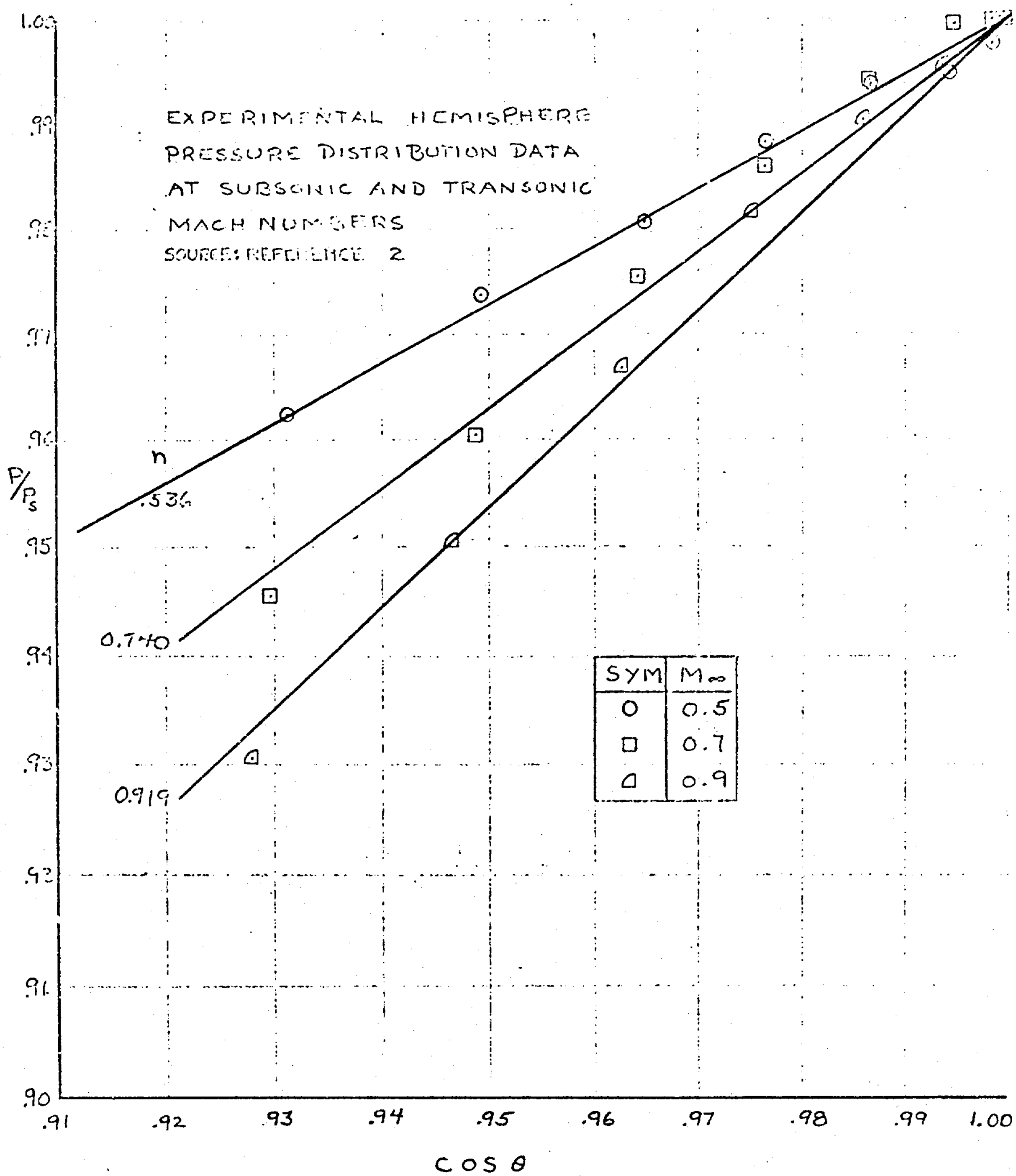

EXPERIMENTAL HEMISPHERE
PRESSURE DISTRIBUTION DATA
AT SUBSONIC AND TRANSONIC
MACH NUMBERS
SOURCE: REFERENCE 2
n
.536
0.740
0.919
SYM
M_∞
0.5
0.7
0.9
P/P_s
1.00
.99
.98
.97
.96
.95
.94
.93
.92
.91
.90
.91
.92
.93
.94
.95
.96
.97
.98
.99
1.00
cos θ

FIG. 15 CONCLUDED

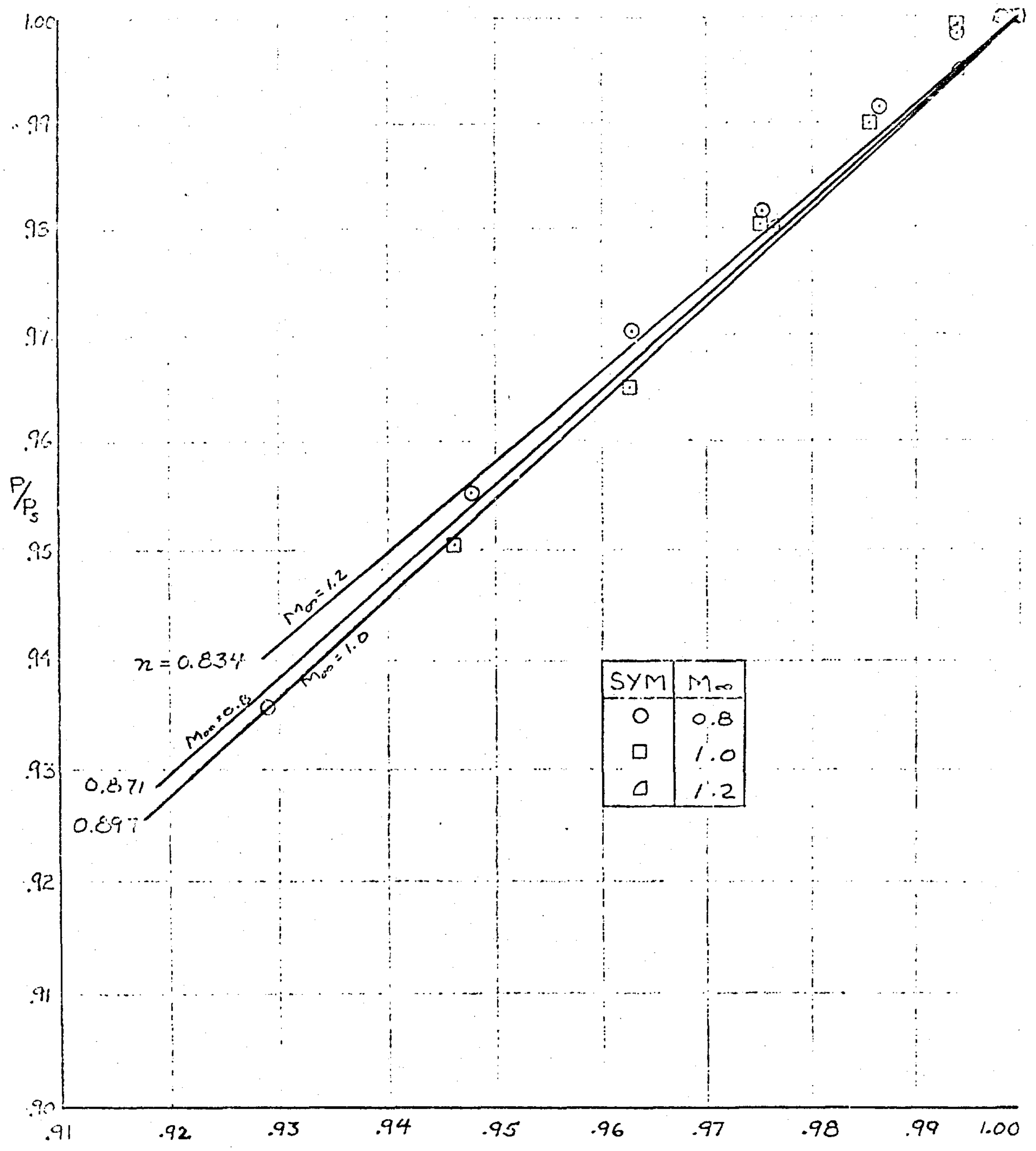

FIG. 16

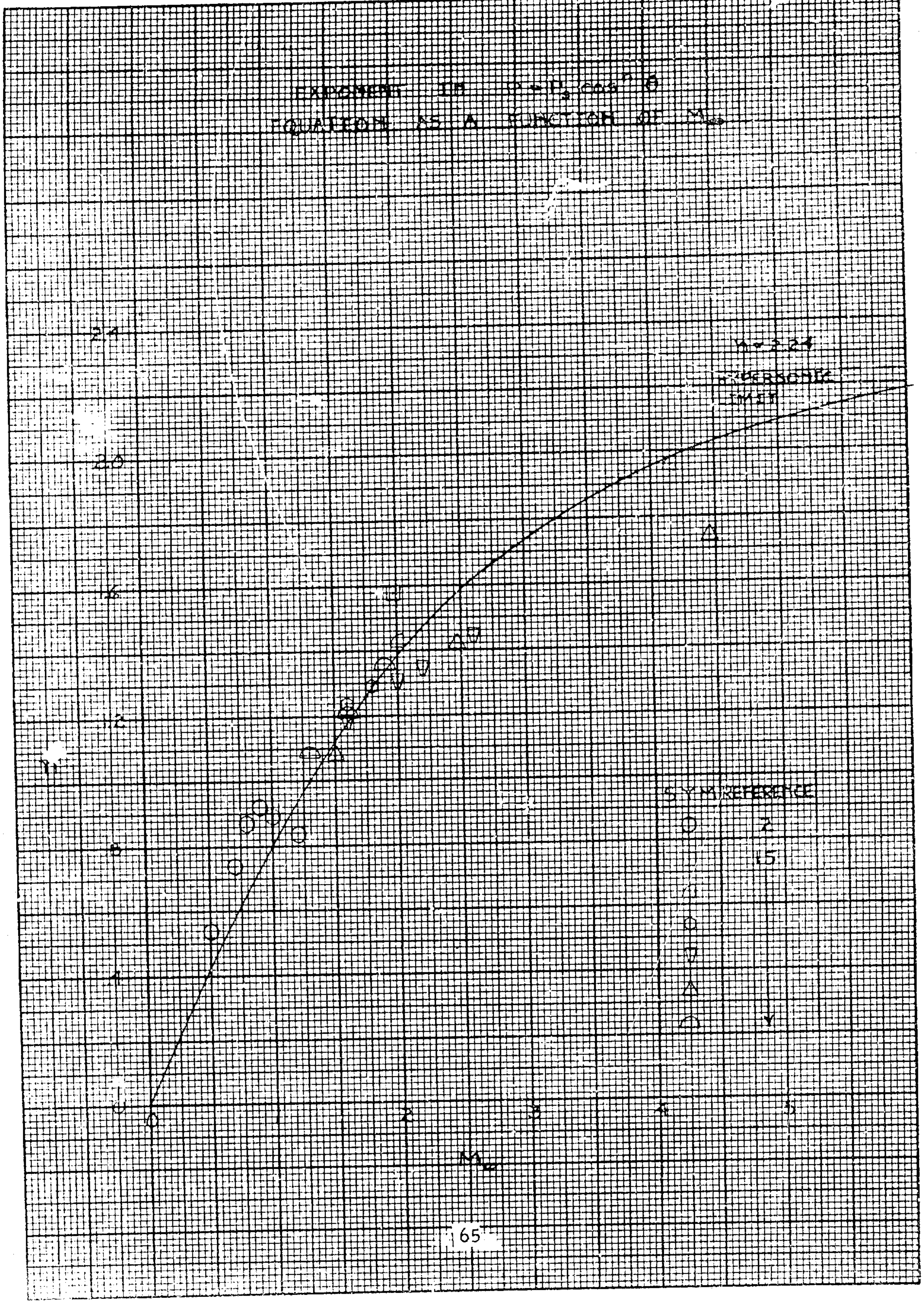
EXPONENT IN $p = p_s \cos^n \theta$
EQUATION AS A FUNCTION OF M_∞
HYPERSONIC
LIMIT
SYM REFERENCE
2
15
24
20
16
12
8
4
0
1
2
3
4
5
M_∞

FIG. 17

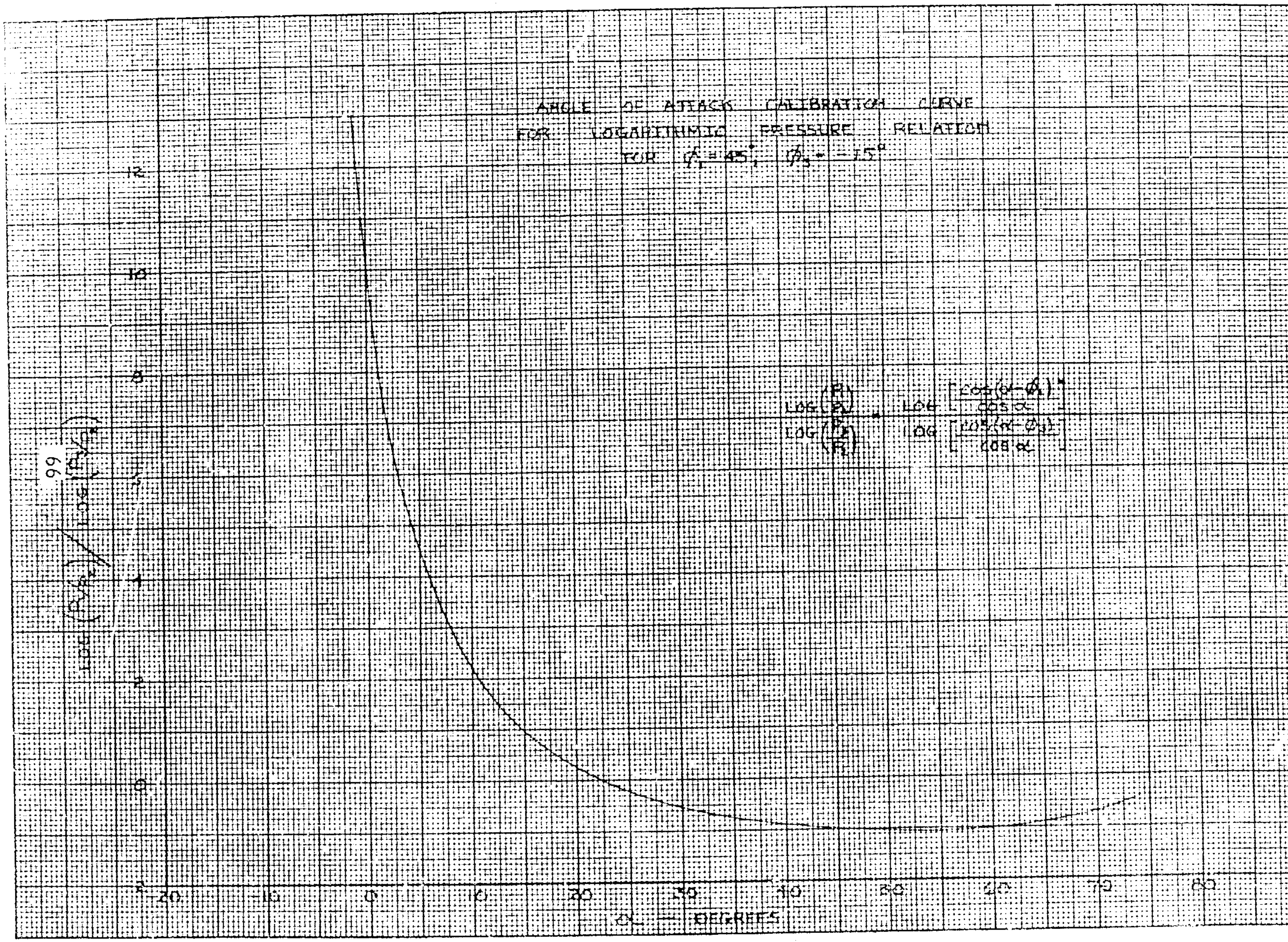
ANGLE OF ATTACK CALIBRATION CURVE
FOR LOGARITHMIC PRESSURE RELATION
FOR $\phi_1 = 45°$; $\phi_3 = -15°$
$\frac{LOG(P_1/P_2)}{LOG(P_3/P_2)} = \frac{LOG\left[\frac{\cos^2(\alpha-\phi_1)}{\cos\alpha}\right]}{LOG\left[\frac{\cos^2(\alpha-\phi_3)}{\cos\alpha}\right]}$
$LOG(P_1/P_2) / LOG(P_3/P_2)$
12
10
8
6
4
2
0
-2
-20
-10
0
10
20
30
40
50
60
70
80
α — DEGREES

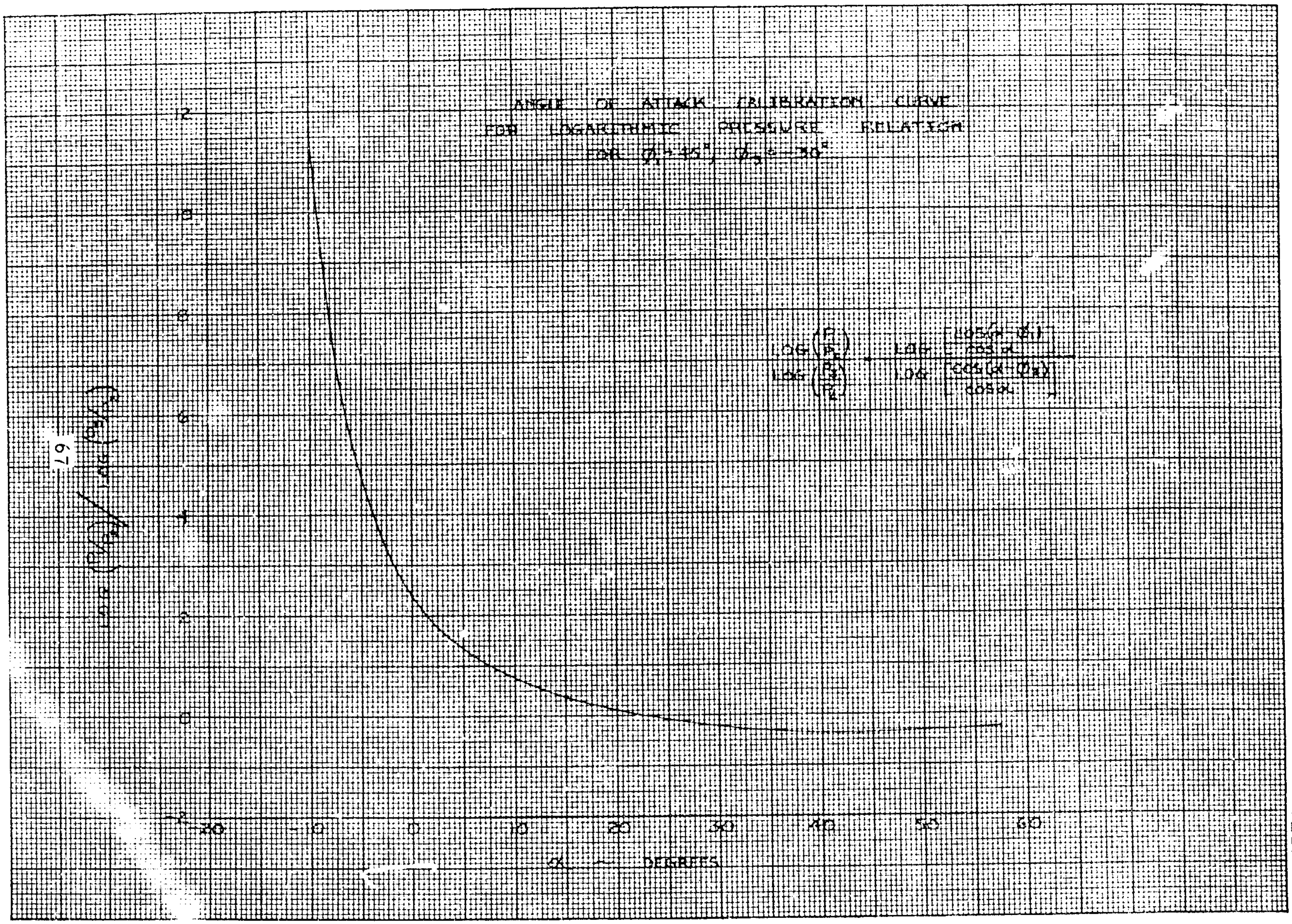
ANGLE OF ATTACK CALIBRATION CURVE
FOR LOGARITHMIC PRESSURE RELATION
FOR $\phi_1 = 45°$, $\phi_2 = -30°$
$\frac{\log(P_1/P_2)}{\log(P_3/P_2)} = \frac{\log\left[\frac{\cos(\alpha-\phi_1)}{\cos\alpha}\right]}{\log\left[\frac{\cos(\alpha-\phi_3)}{\cos\alpha}\right]}$
12
10
8
6
4
2
0
-2
-20
-10
0
10
20
30
40
50
60
α ~ DEGREES

FIG. 18

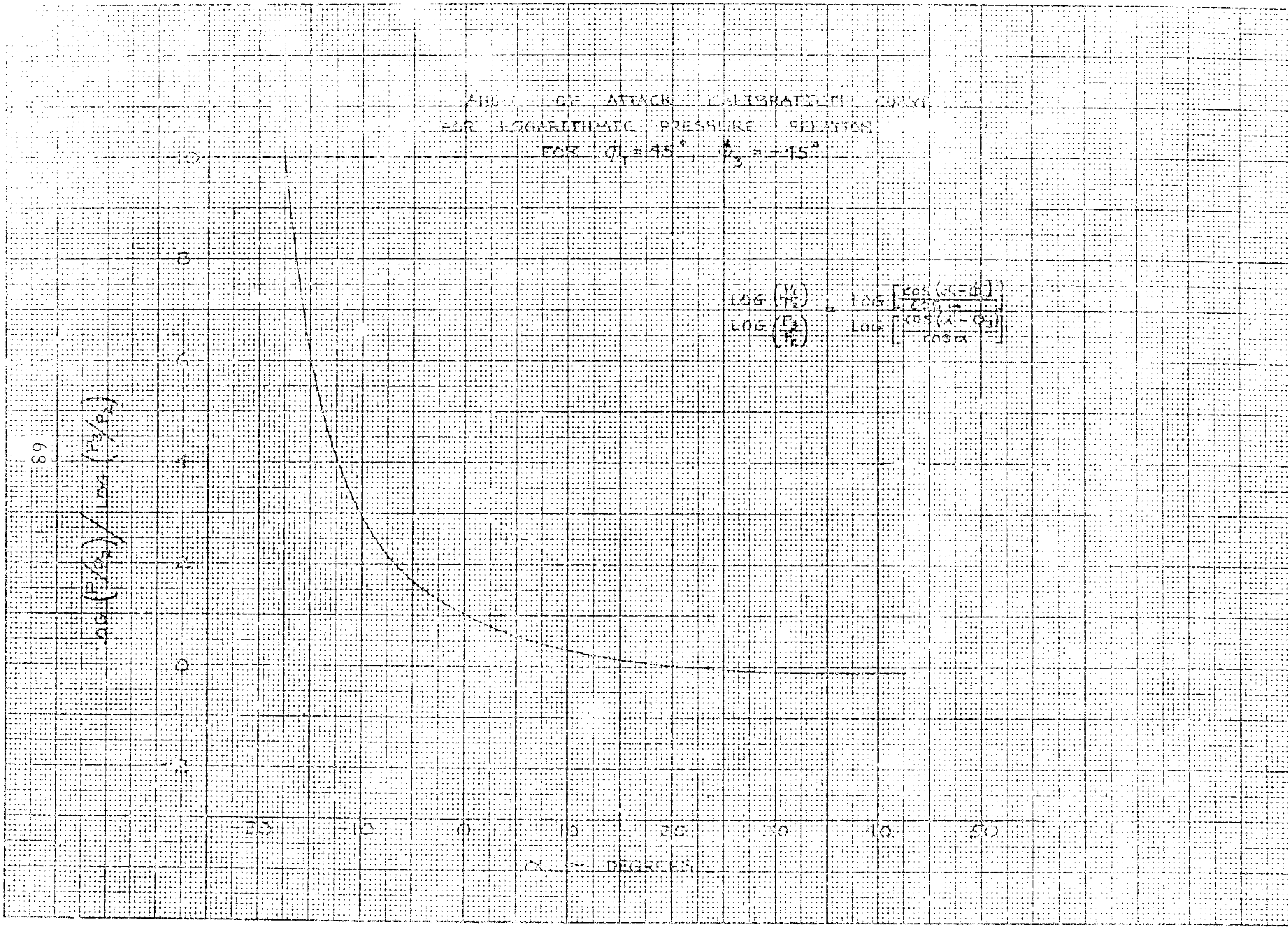
ANGLE OF ATTACK CALIBRATION CURVE
FOR LOGARITHMIC PRESSURE SOLUTION
FOR $\phi_1 = 45°$, $\phi_3 = -45°$
α — DEGREES
-20 -10 0 10 20 30 40 50
10 8 6 4 2 0 -2

FIG. 19

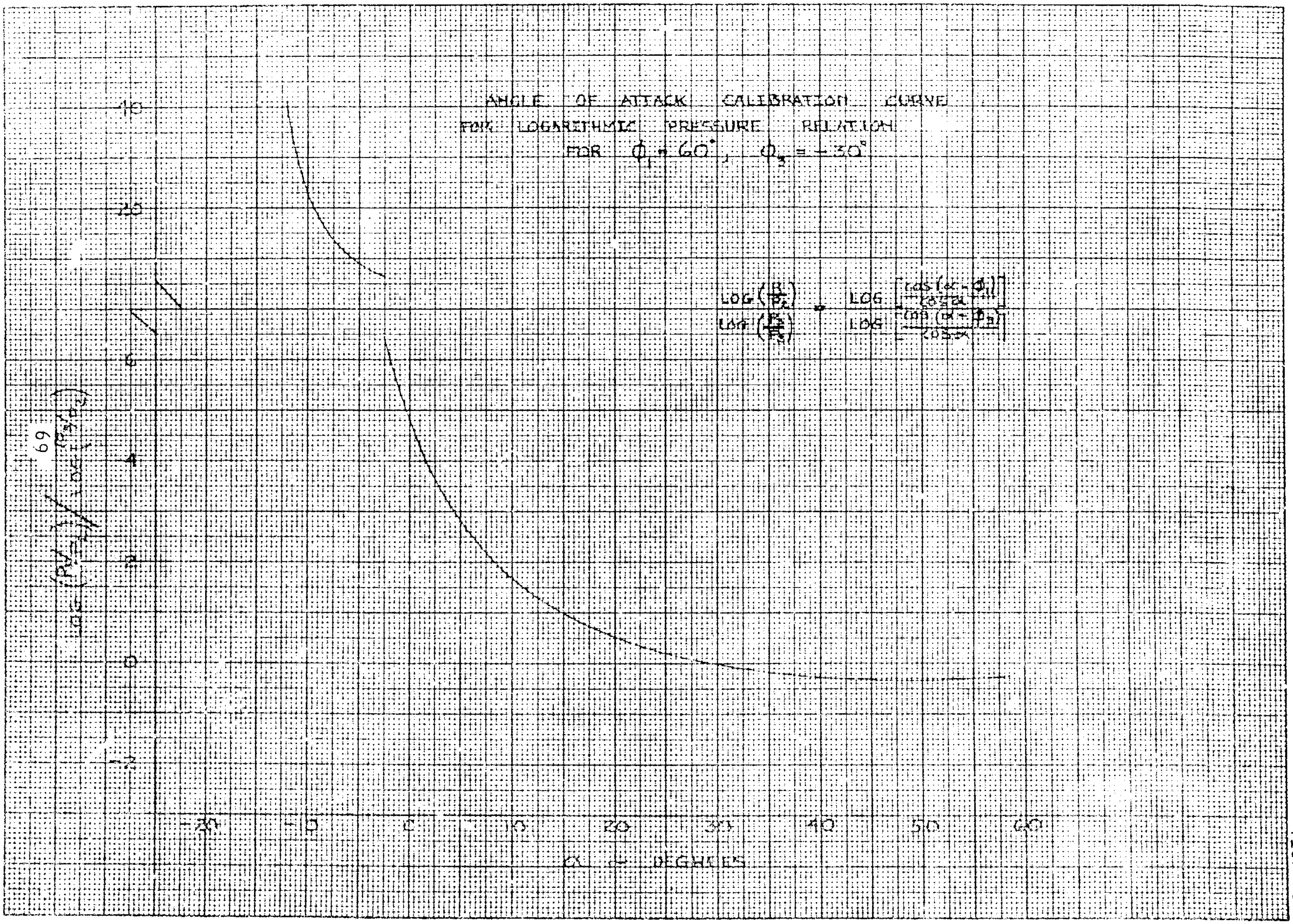
ANGLE OF ATTACK CALIBRATION CURVE
FOR LOGARITHMIC PRESSURE RELATION
FOR $\phi_1 = 60°$, $\phi_3 = -30°$
$\frac{\mathrm{LOG}\left(\frac{P_1}{P_2}\right)}{\mathrm{LOG}\left(\frac{P_3}{P_2}\right)} = \frac{\mathrm{LOG}\left[\frac{\cos(\alpha-\phi_1)}{\cos\alpha}\right]}{\mathrm{LOG}\left[\frac{\cos(\alpha-\phi_3)}{\cos\alpha}\right]}$
$\mathrm{LOG}\left(\frac{P_1}{P_2}\right) / \mathrm{LOG}\left(\frac{P_3}{P_2}\right)$
10
20
6
4
2
0
-2
-20
-10
0
10
20
30
40
50
60
α — DEGREES

FIG. 20

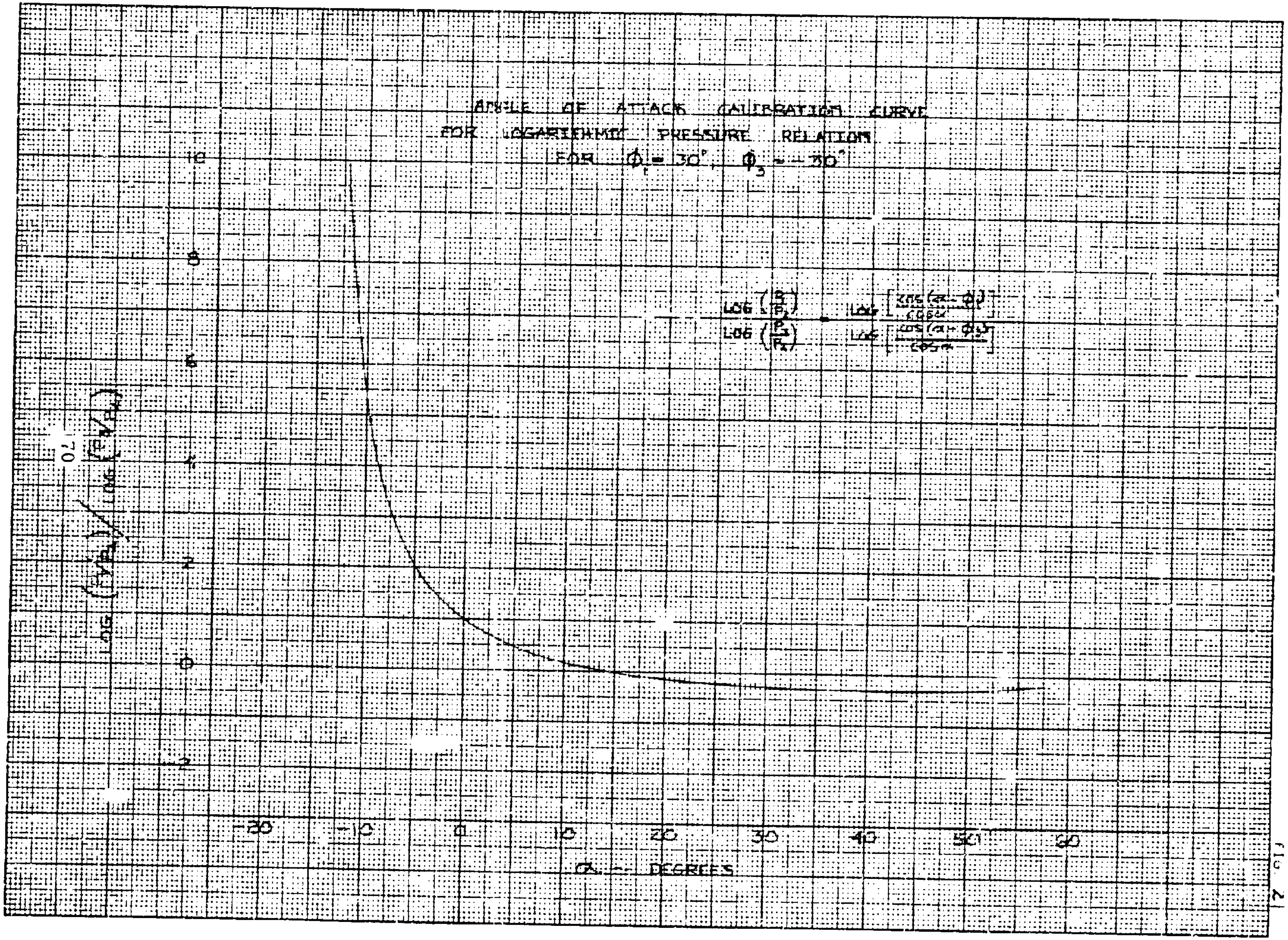
ANGLE OF ATTACK CALIBRATION CURVE
FOR LOGARITHMIC PRESSURE RELATION
FOR $\phi_1 = 30°$, $\phi_3 = -30°$
$\frac{\log(P_1/P_2)}{\log(P_3/P_4)} = \frac{\log\left[\frac{\cos(\alpha-\phi_1)}{\cos\alpha}\right]}{\log\left[\frac{\cos(\alpha-\phi_3)}{\cos\alpha}\right]}$
10
8
6
4
2
0
-2
$\log(P_1/P_2) / \log(P_3/P_4)$
-20
-10
0
10
20
30
40
50
60
α — DEGREES

FIG. 2

FIG 22

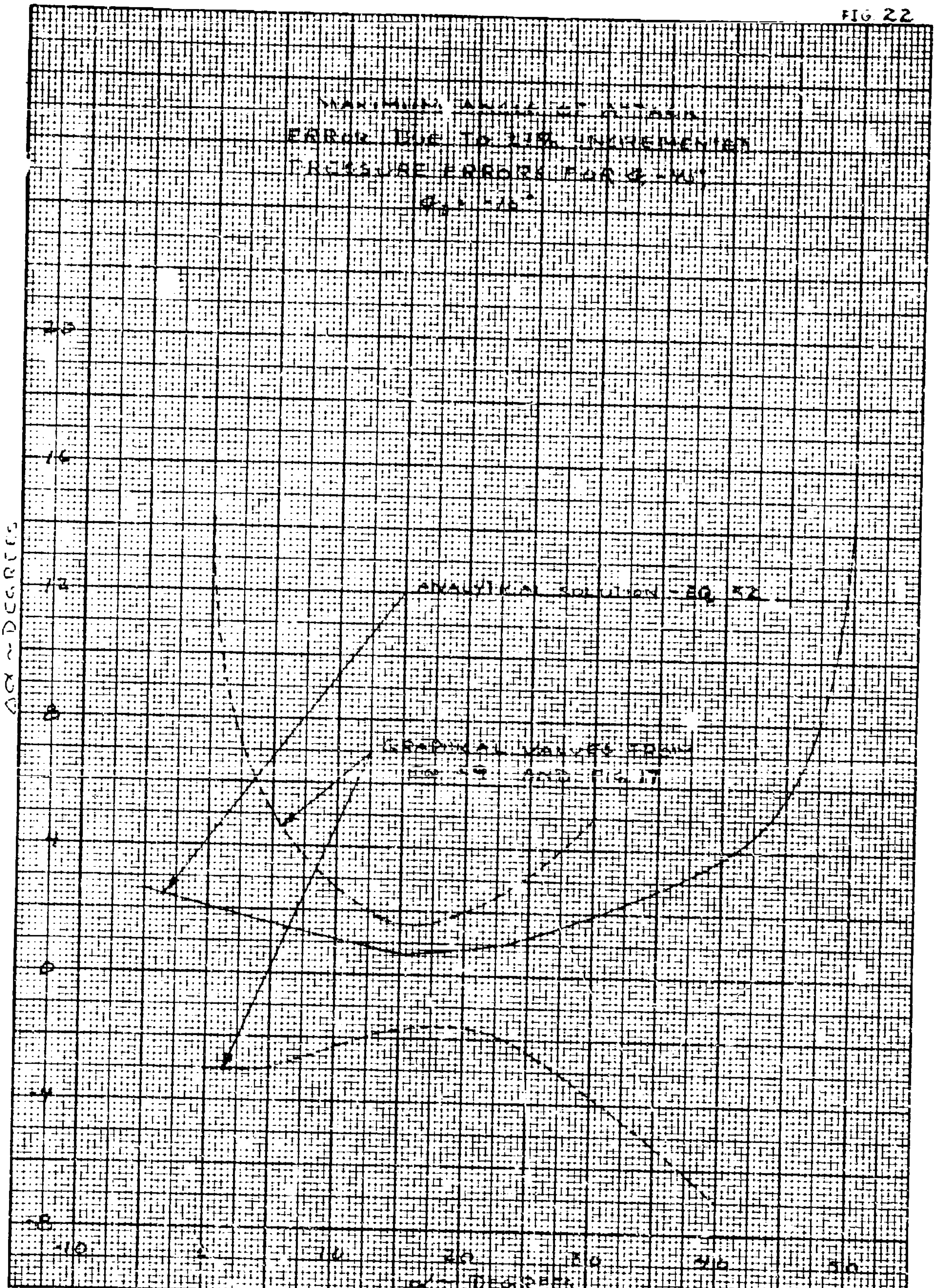

ANALYTICAL SOLUTION - EQ 52
GRAPHICAL VALUES FROM
20
16
12
8
4
0
-4
-8
-10
0
10
20
30
40
50

FIG. 23

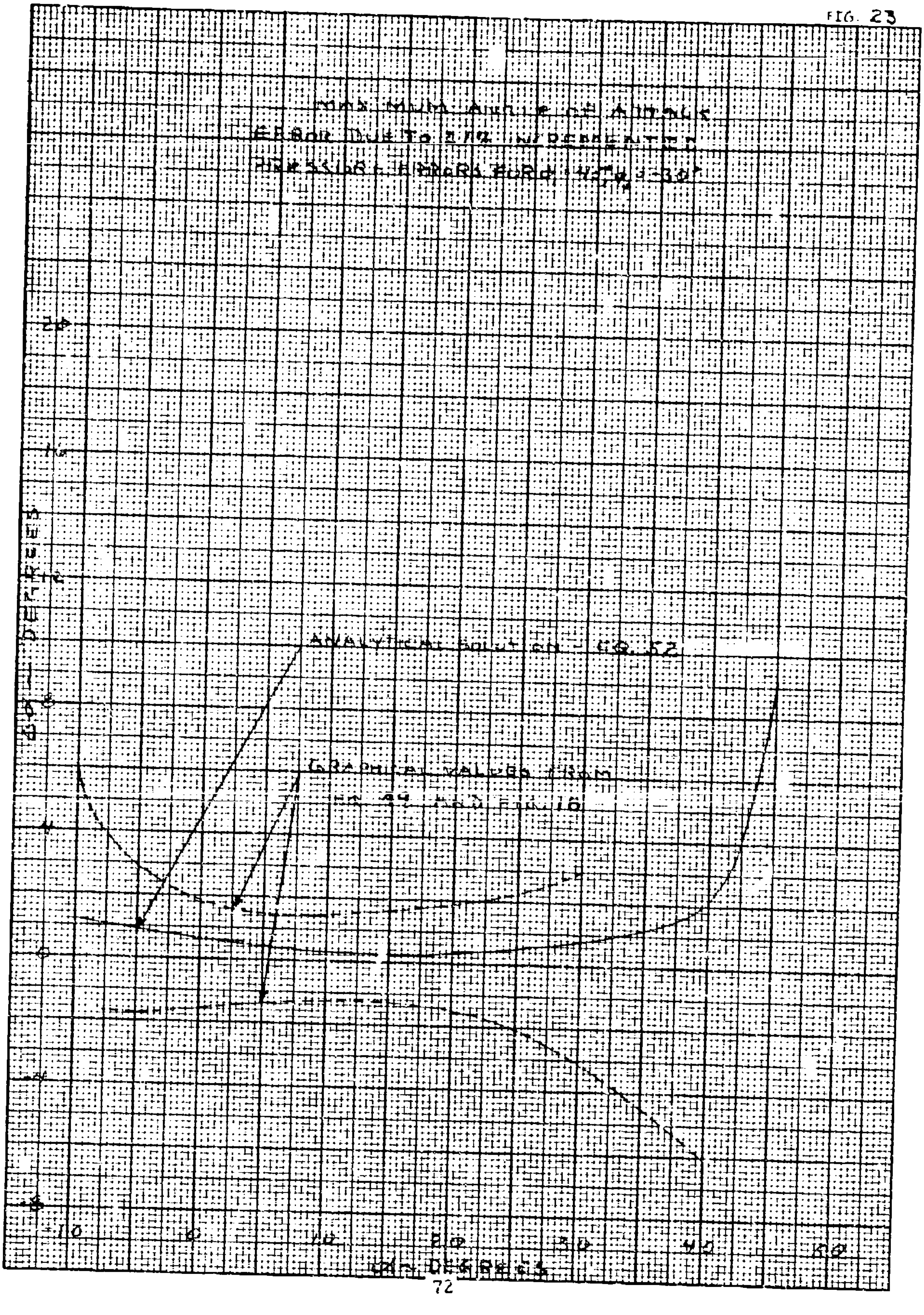

FIG 24

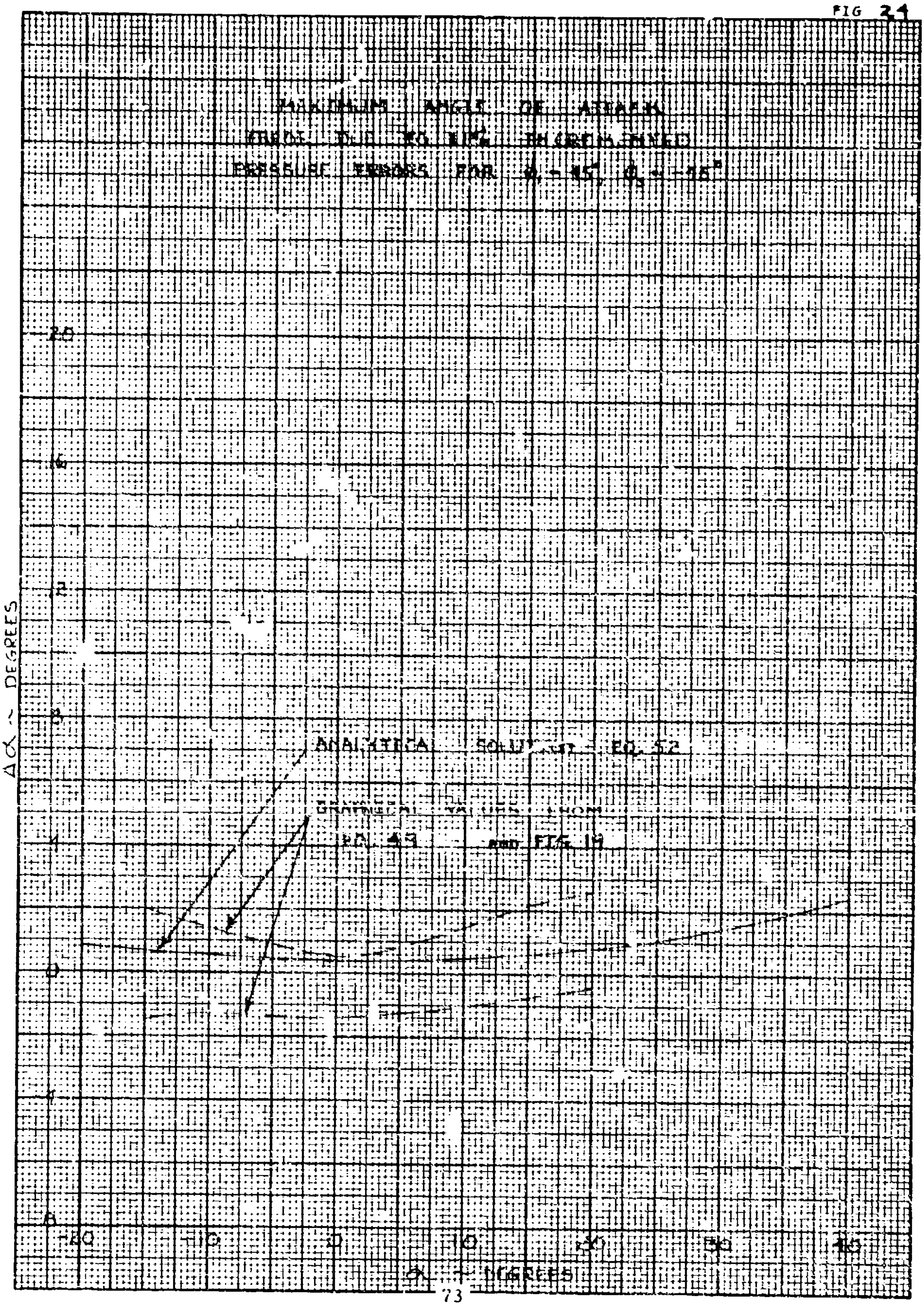

Δα ~ DEGREES
α ~ DEGREES
20
16
12
8
4
0
-20
-10
0
10
20
30
40
ANALYTICAL
EQ. 52
FIG. 19

FIG. 25

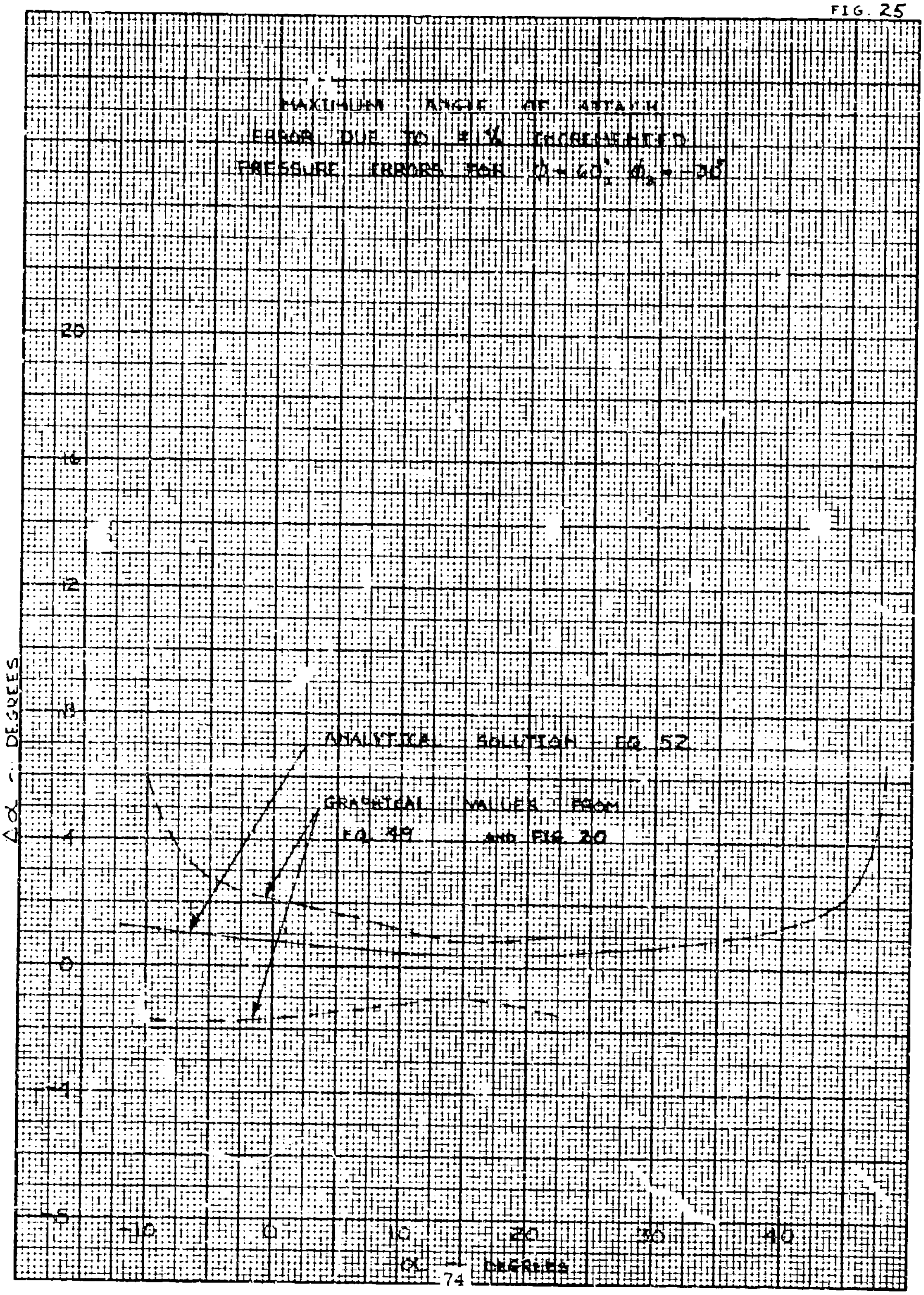
MAXIMUM ANGLE OF ATTACK
ERROR DUE TO
PRESSURE ERRORS FOR
ANALYTICAL SOLUTION EQ. 52
GRAPHICAL VALUES FROM
Δα — DEGREES
α — DEGREES
20
16
12
8
4
0
-10
10
20
30
40

FIG 26

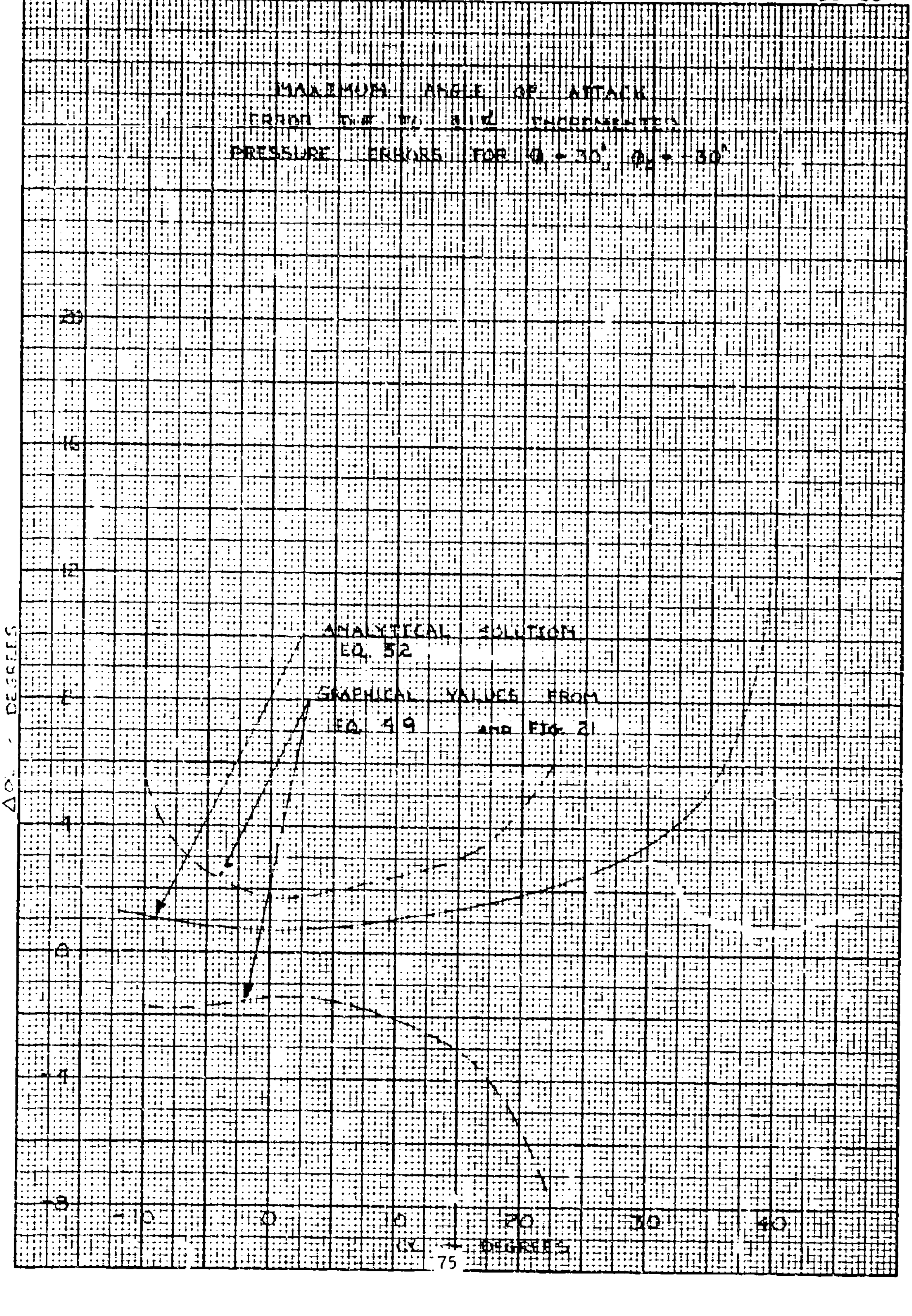
MAXIMUM ANGLE OF ATTACK
PRESSURE ERRORS FOR
ANALYTICAL SOLUTION
EQ. 52
GRAPHICAL VALUES FROM
EQ. 49 AND FIG. 21
20
16
12
8
4
0
-4
-8
-10
0
10
20
30
40
α - DEGREES

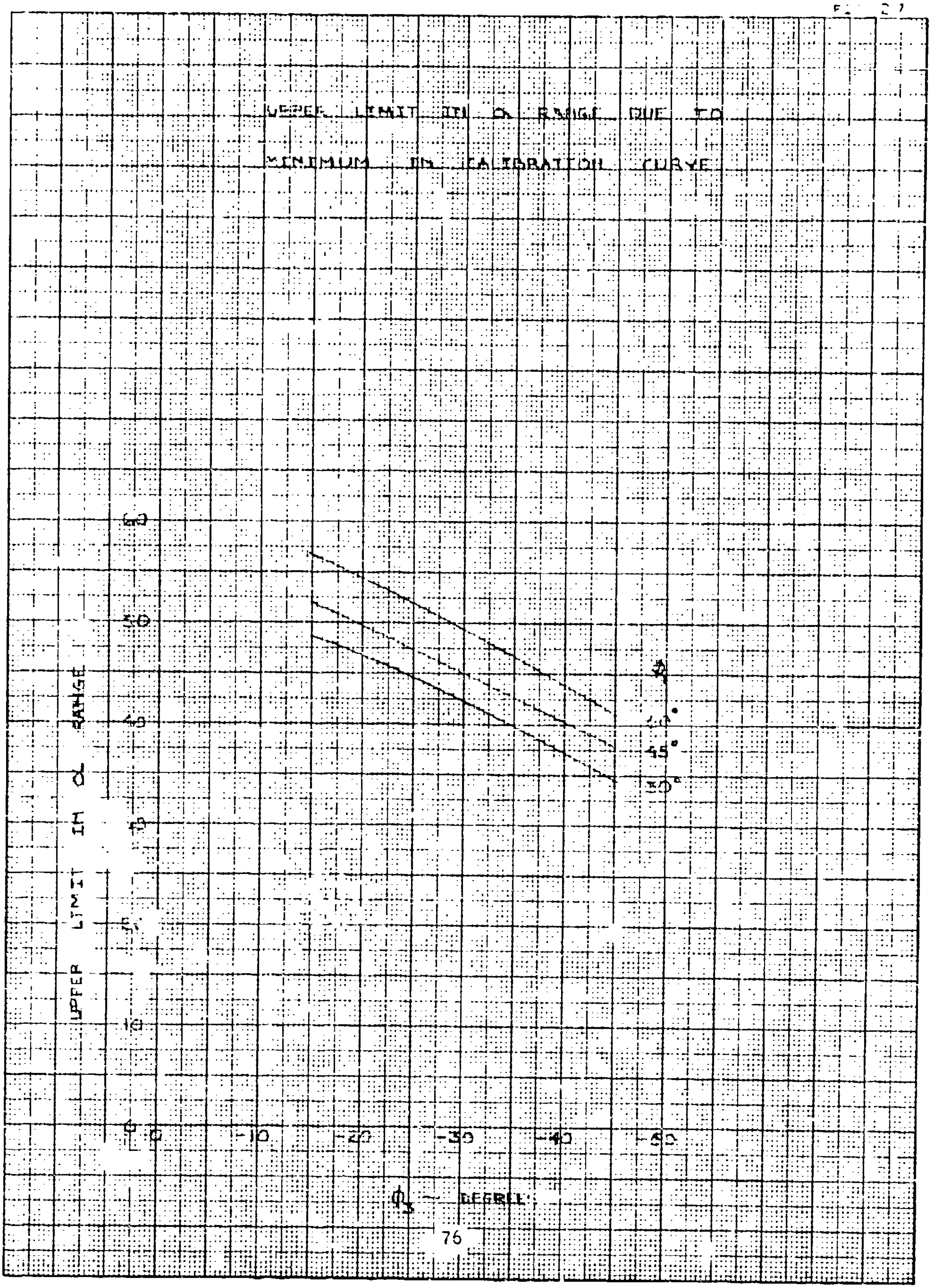
UPPER LIMIT IN α RANGE DUE TO
MINIMUM IN CALIBRATION CURVE
UPPER LIMIT IN α RANGE
60
50
40
10
0
0
-10
-20
-30
-40
-50
45°
30°
φs ~ DEGREE

FIG. 28

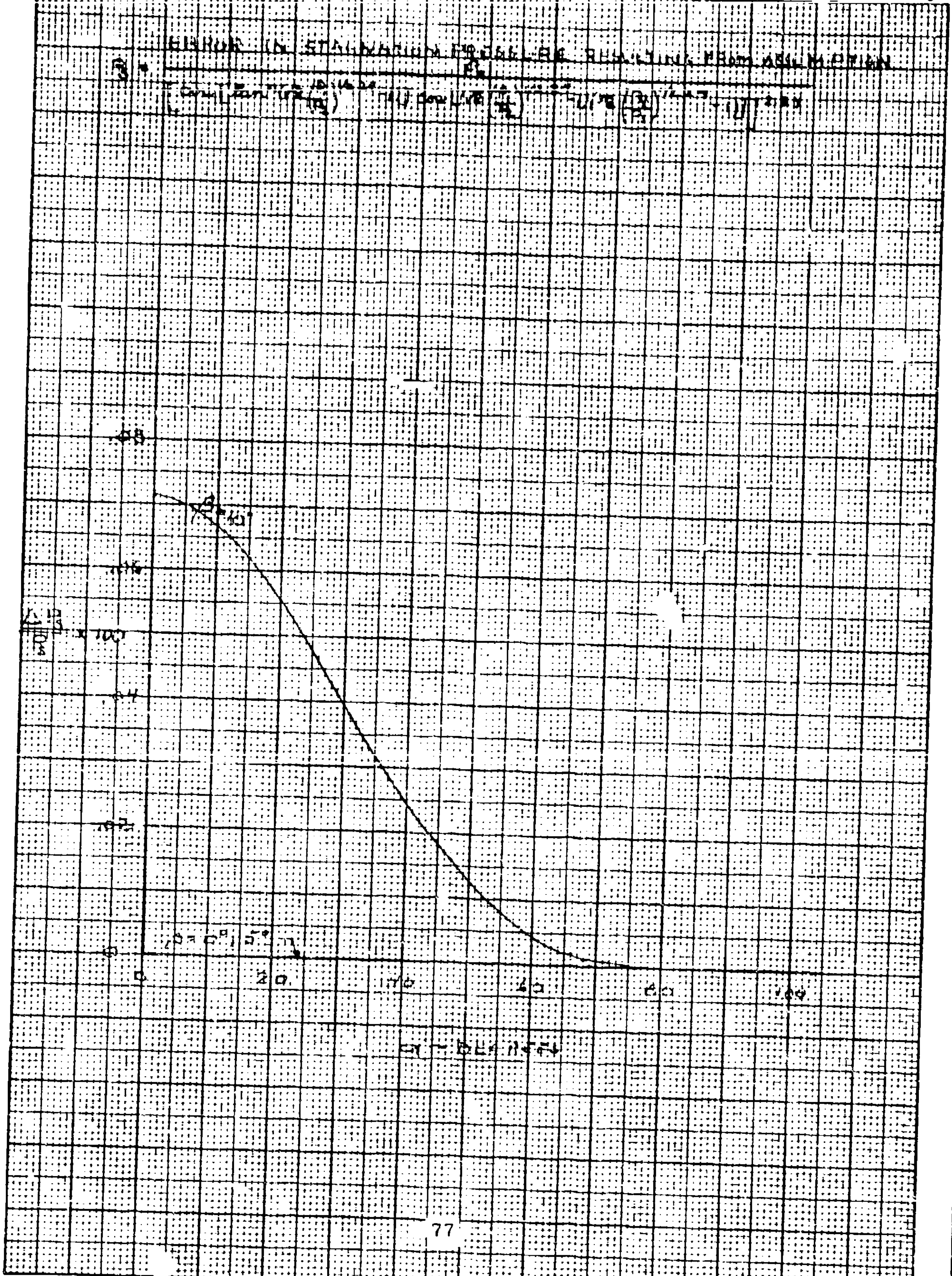

FIG. 29

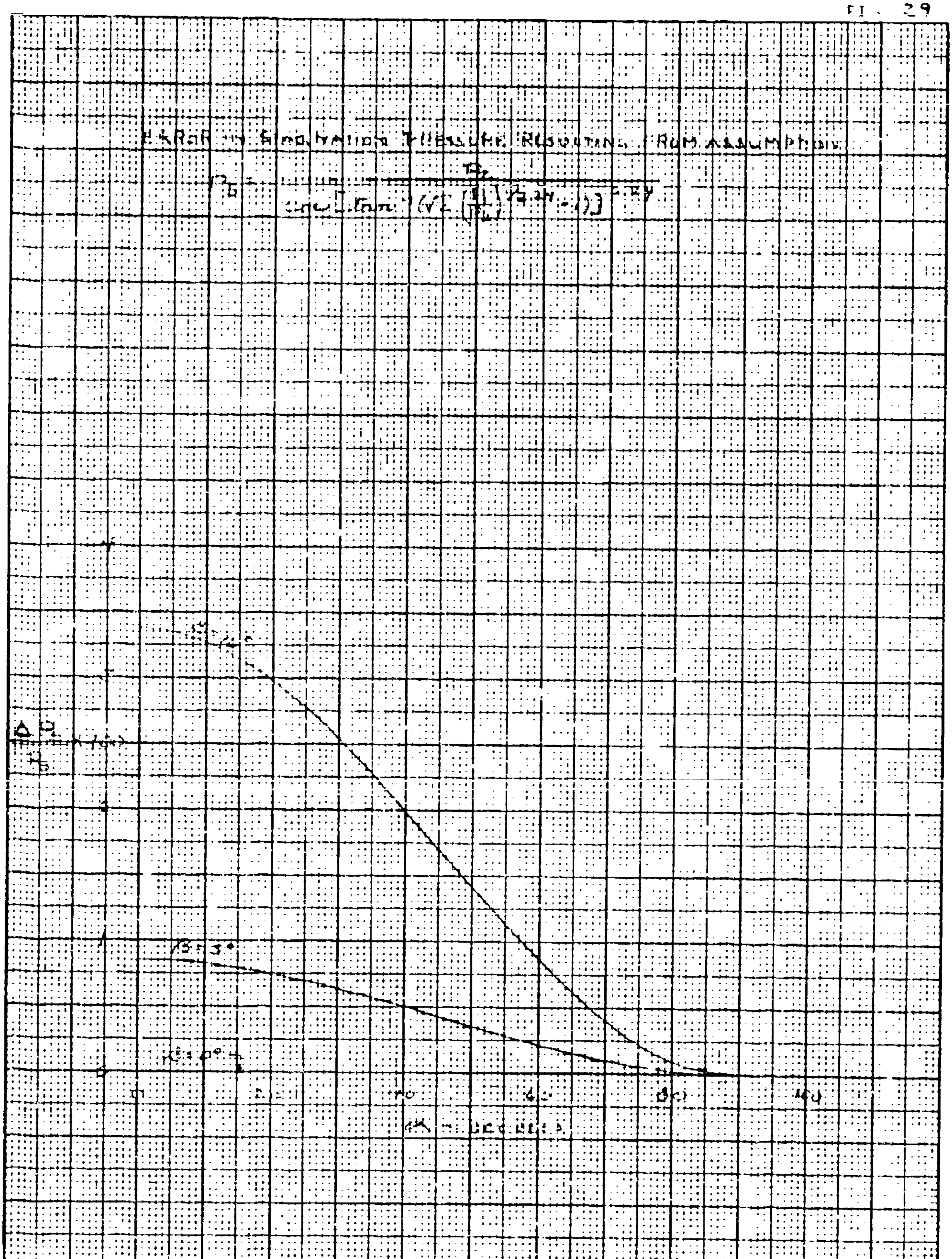

FIG. 30

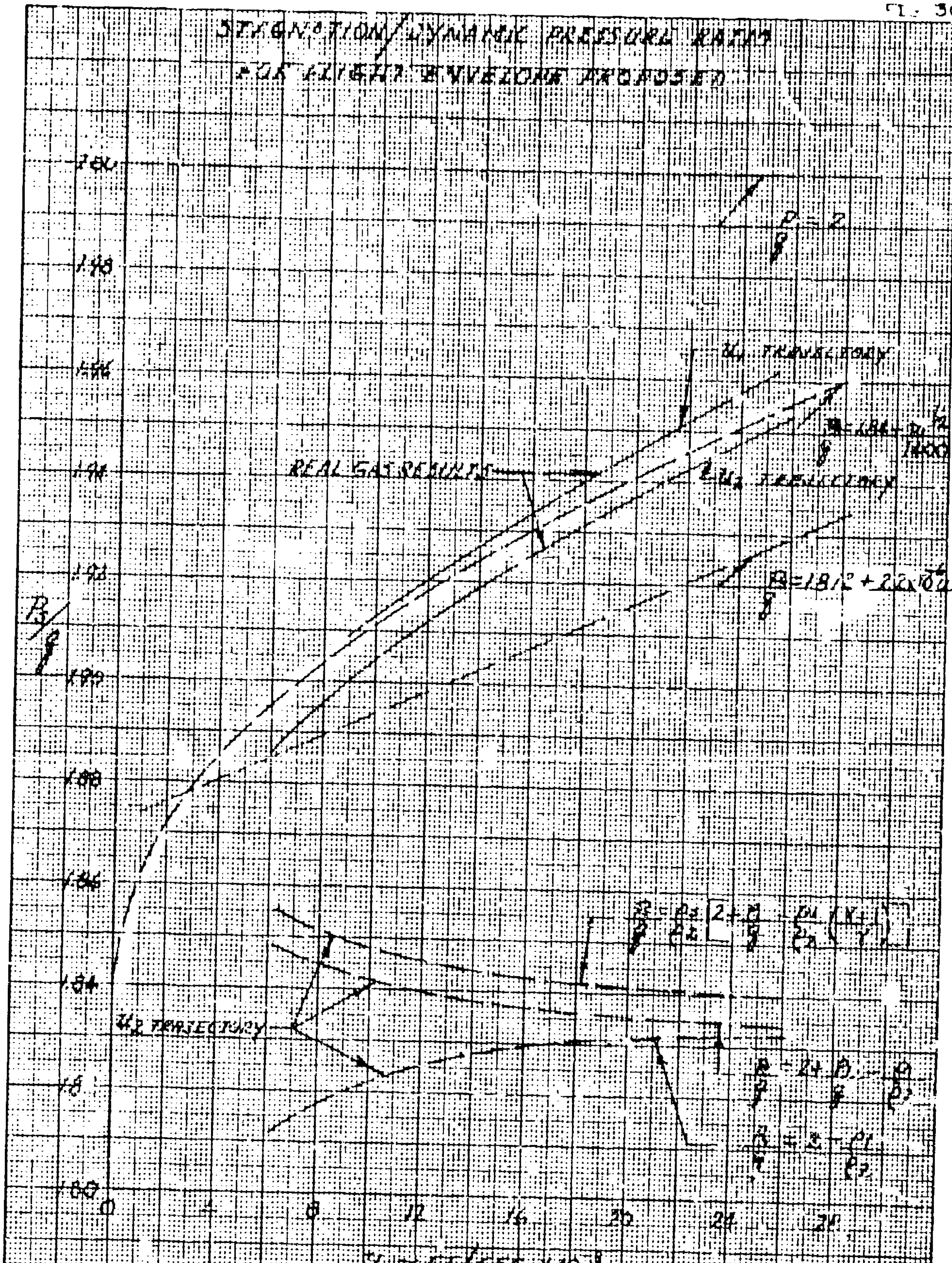
STAGNATION/DYNAMIC PRESSURE RATIO
FOR FLIGHT ENVELOPE PROPOSED
REAL GAS RESULTS
U_1 TRAJECTORY
$2U_1$ TRAJECTORY
U_2 TRAJECTORY
0
4
8
12
16
20
24
28
U - FT/SEC X 10^3

FIG 31

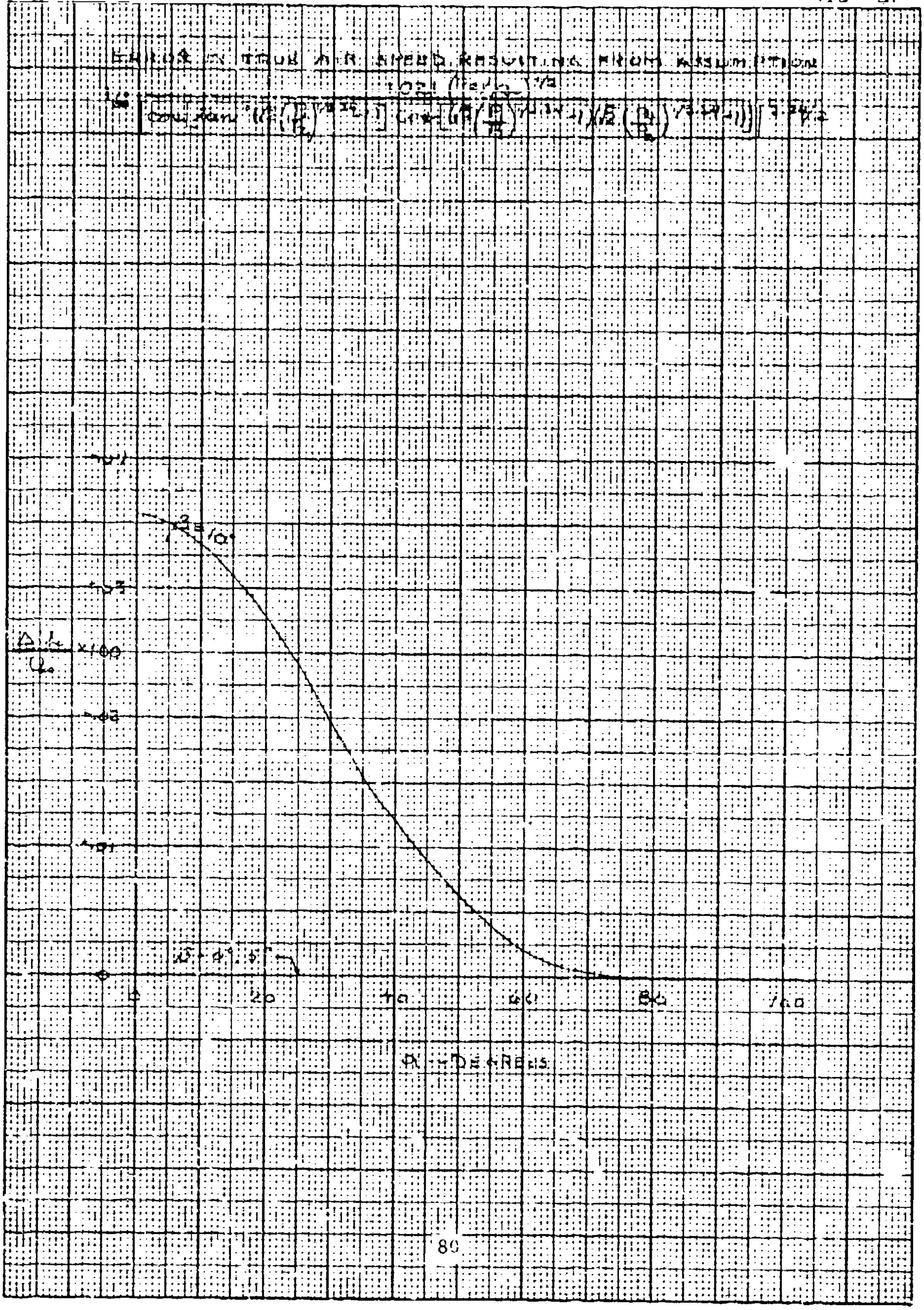
ERROR IN TRUE AIR SPEED RESULTING FROM ASSUMPTION
20
40
60
80
100
DEGREES

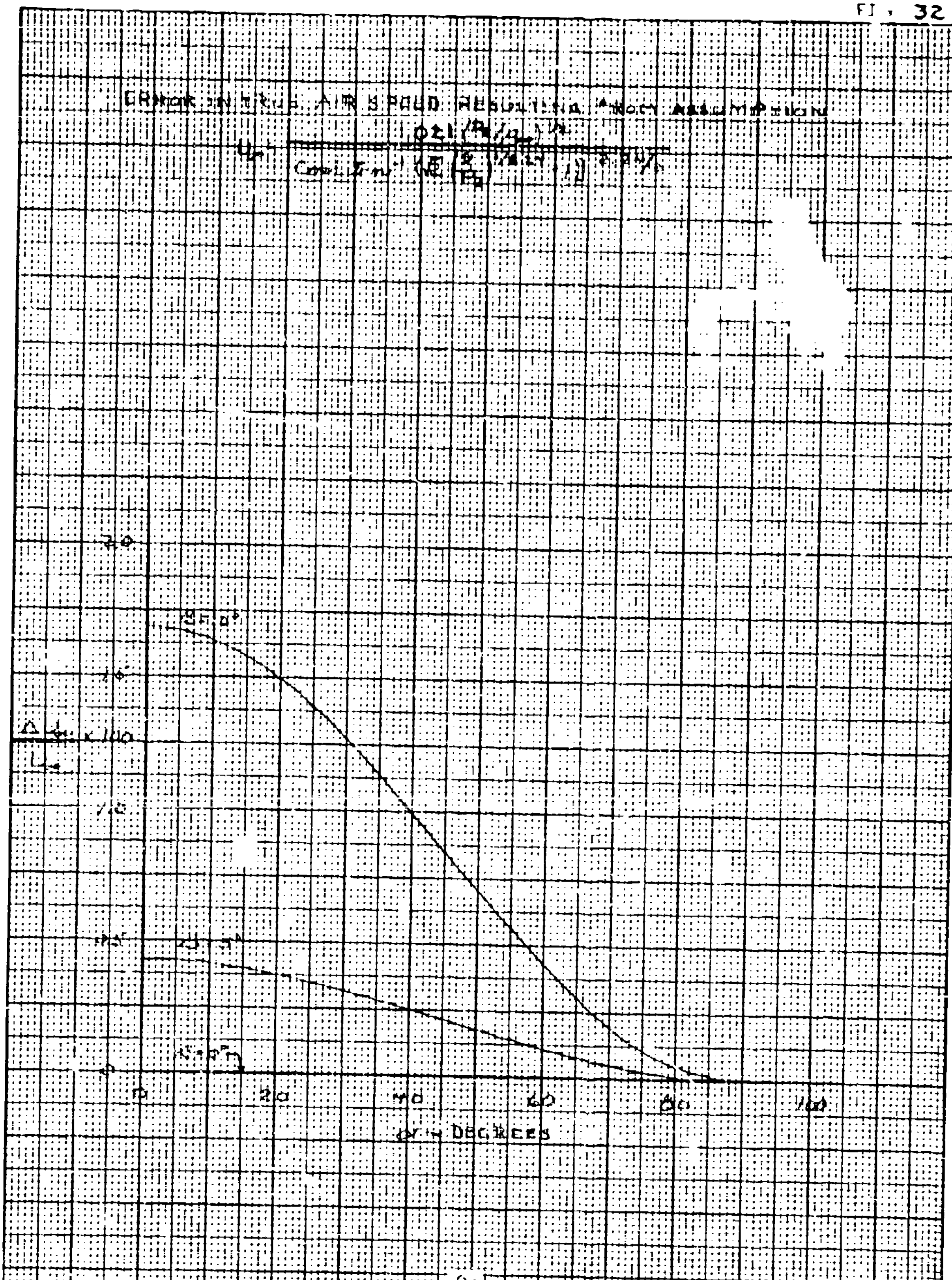
ERROR IN TRUE AIR SPEED RESULTING FROM ASSUMPTION
20
16
12
x 100
0
20
40
60
80
100
IN DEGREES

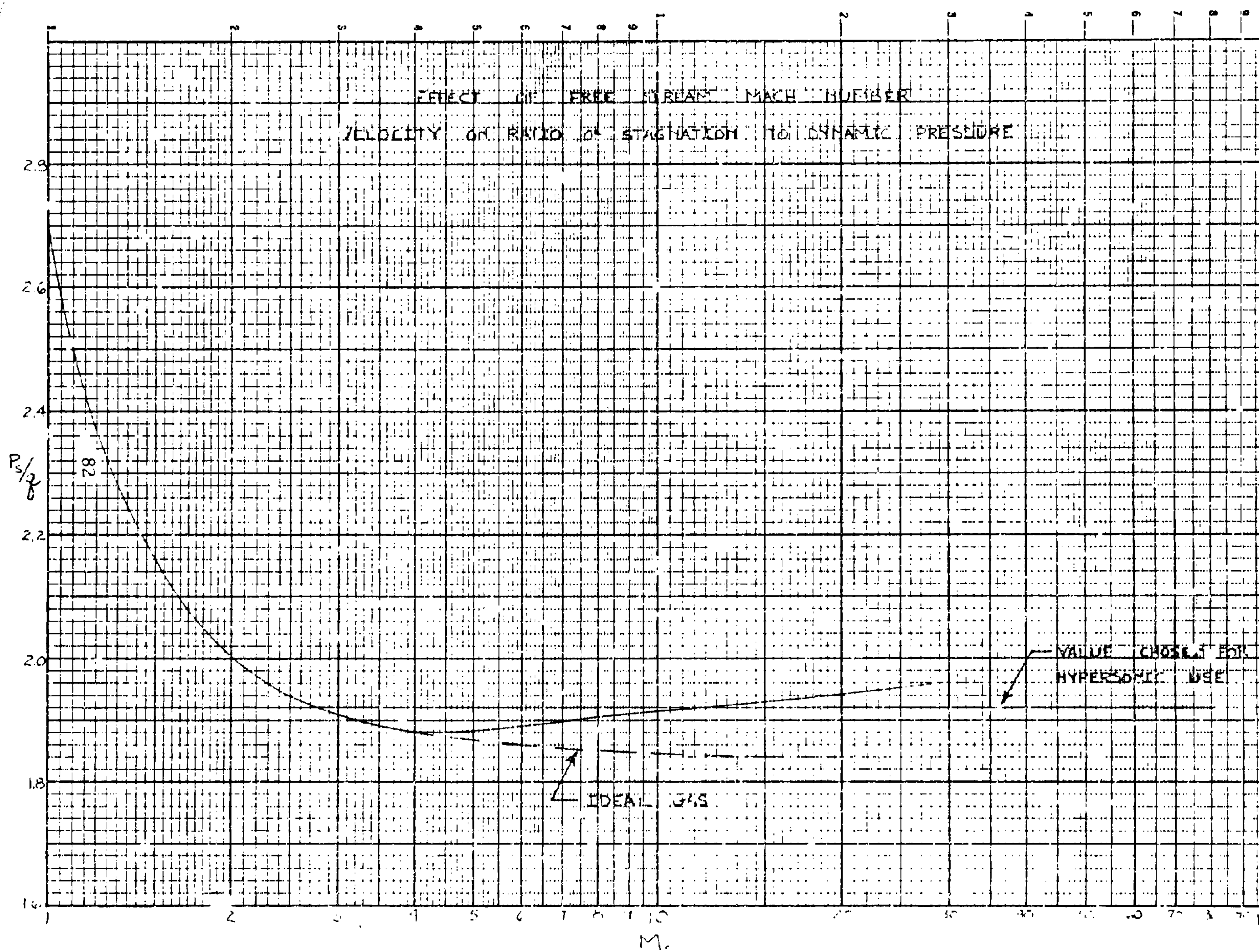
EFFECT OF FREE STREAM MACH NUMBER
VELOCITY ON RATIO OF STAGNATION TO DYNAMIC PRESSURE
VALUE CHOSEN FOR HYPERSONIC USE
IDEAL GAS
P_s/q
M.

FIG 33

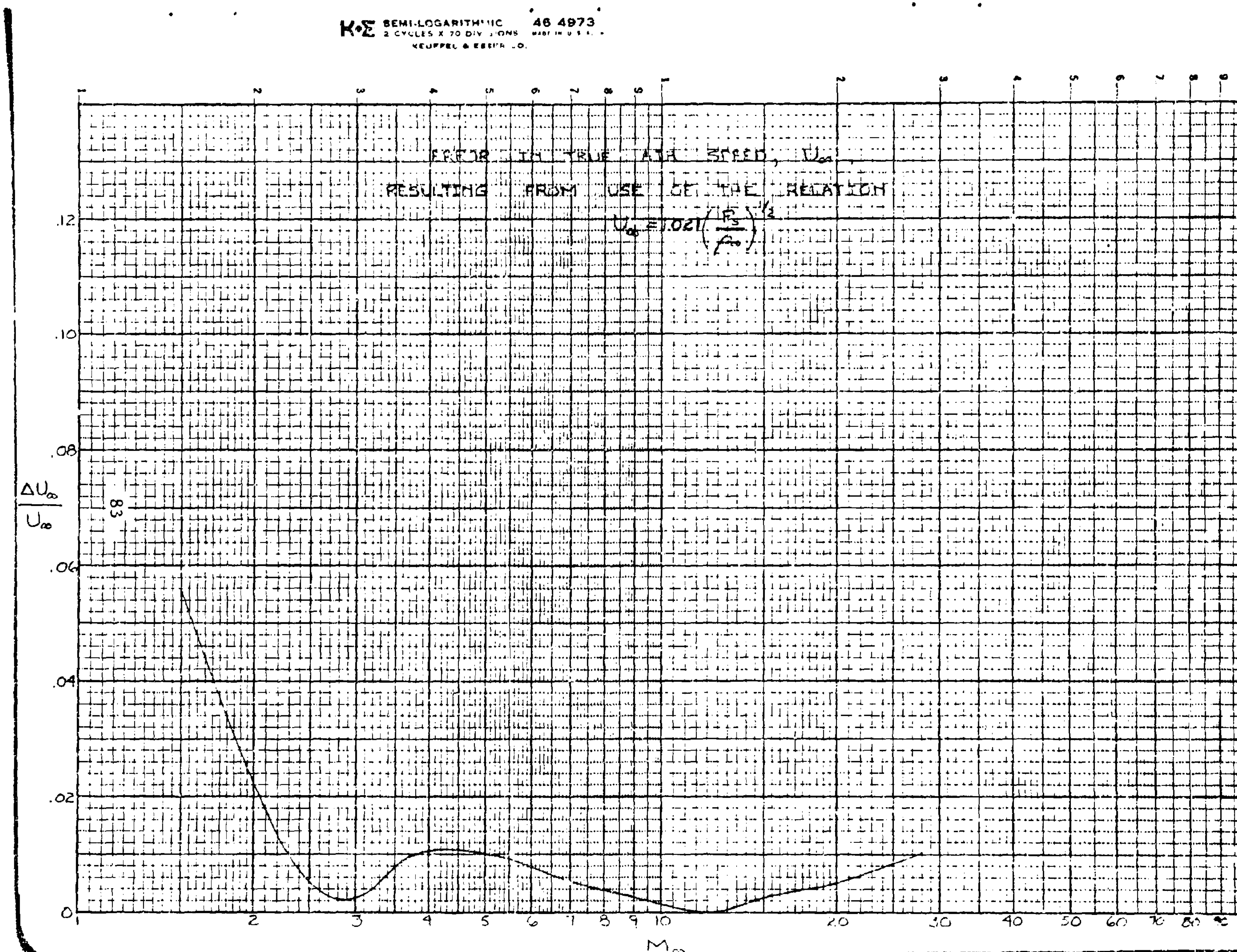
K+E SEMI-LOGARITHMIC 46 4973
2 CYCLES X 70 DIVISIONS MADE IN U.S.A.
KEUFFEL & ESSER CO.
ERROR IN TRUE AIR SPEED, U_∞
RESULTING FROM USE OF THE RELATION
$U_\infty = 1.021\left(\frac{P_s}{\rho_\infty}\right)^{1/2}$
$\frac{\Delta U_\infty}{U_\infty}$
M_∞

FIG. 34

MODEL DATE FIG. 35

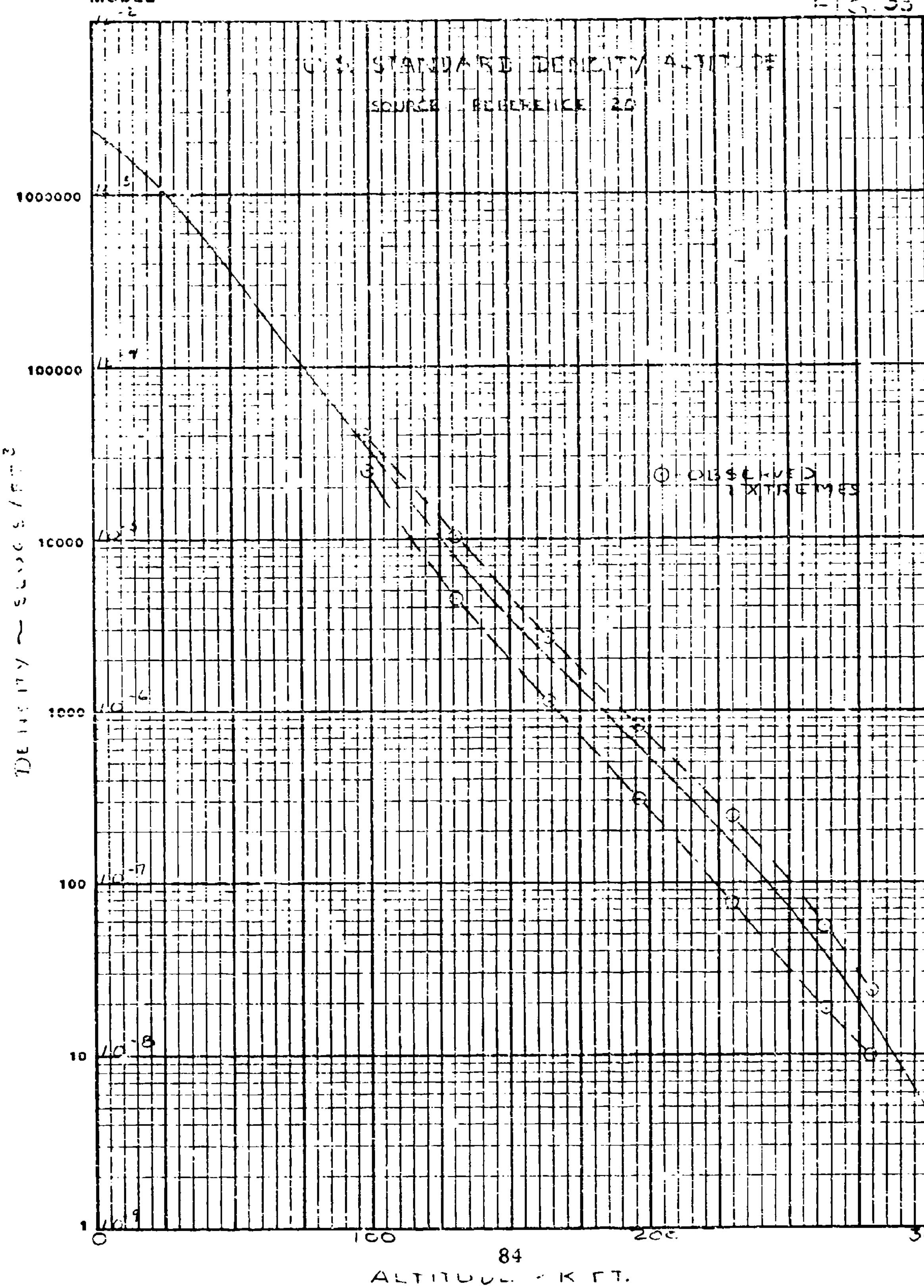

FIG 36

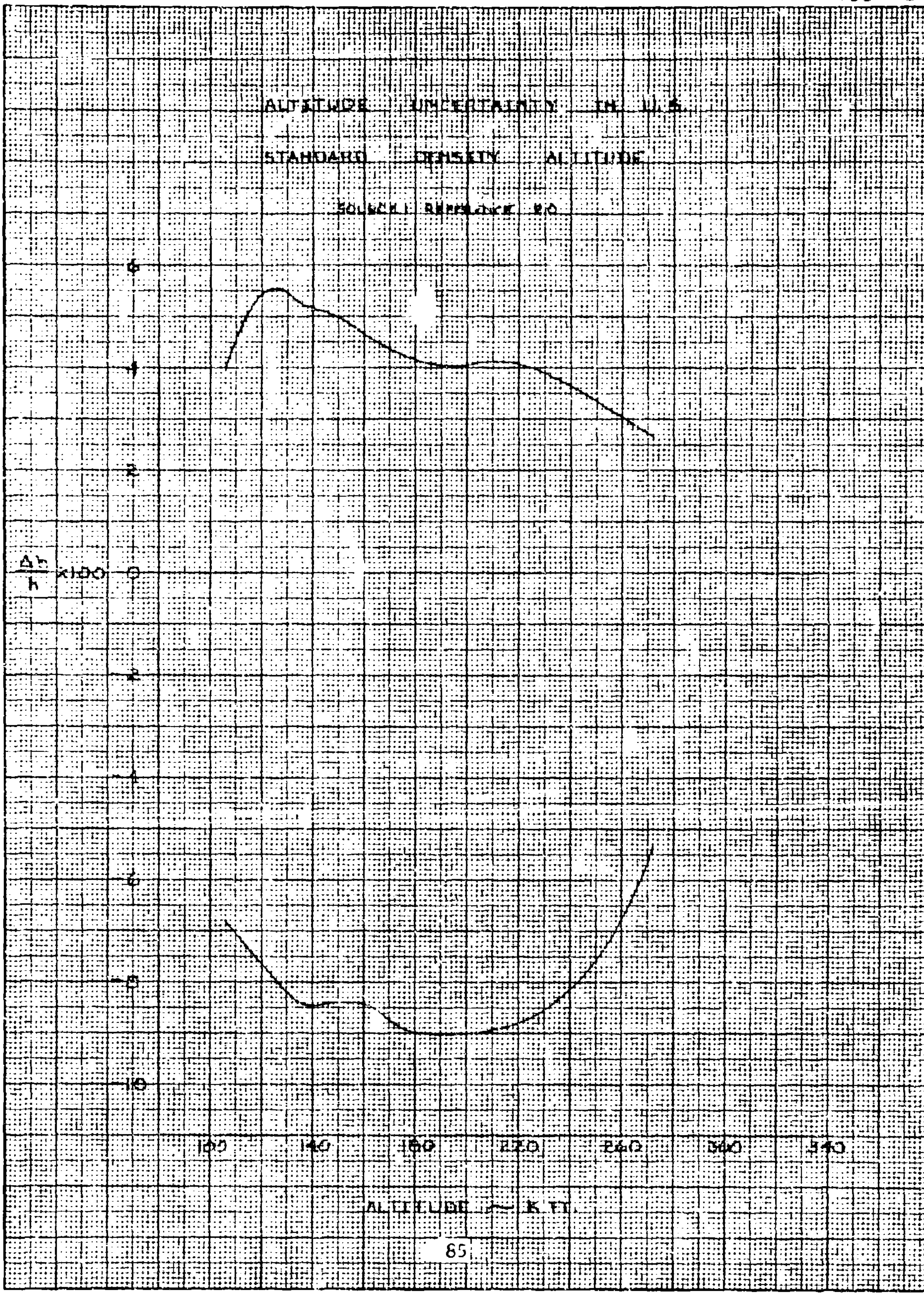
ALTITUDE UNCERTAINTY IN U.S.
STANDARD DENSITY ALTITUDE
SOURCE: REFERENCE 20
6
4
2
0
2
4
6
8
10
Δh/h ×100
100
140
180
220
260
300
340
ALTITUDE ~ K FT.

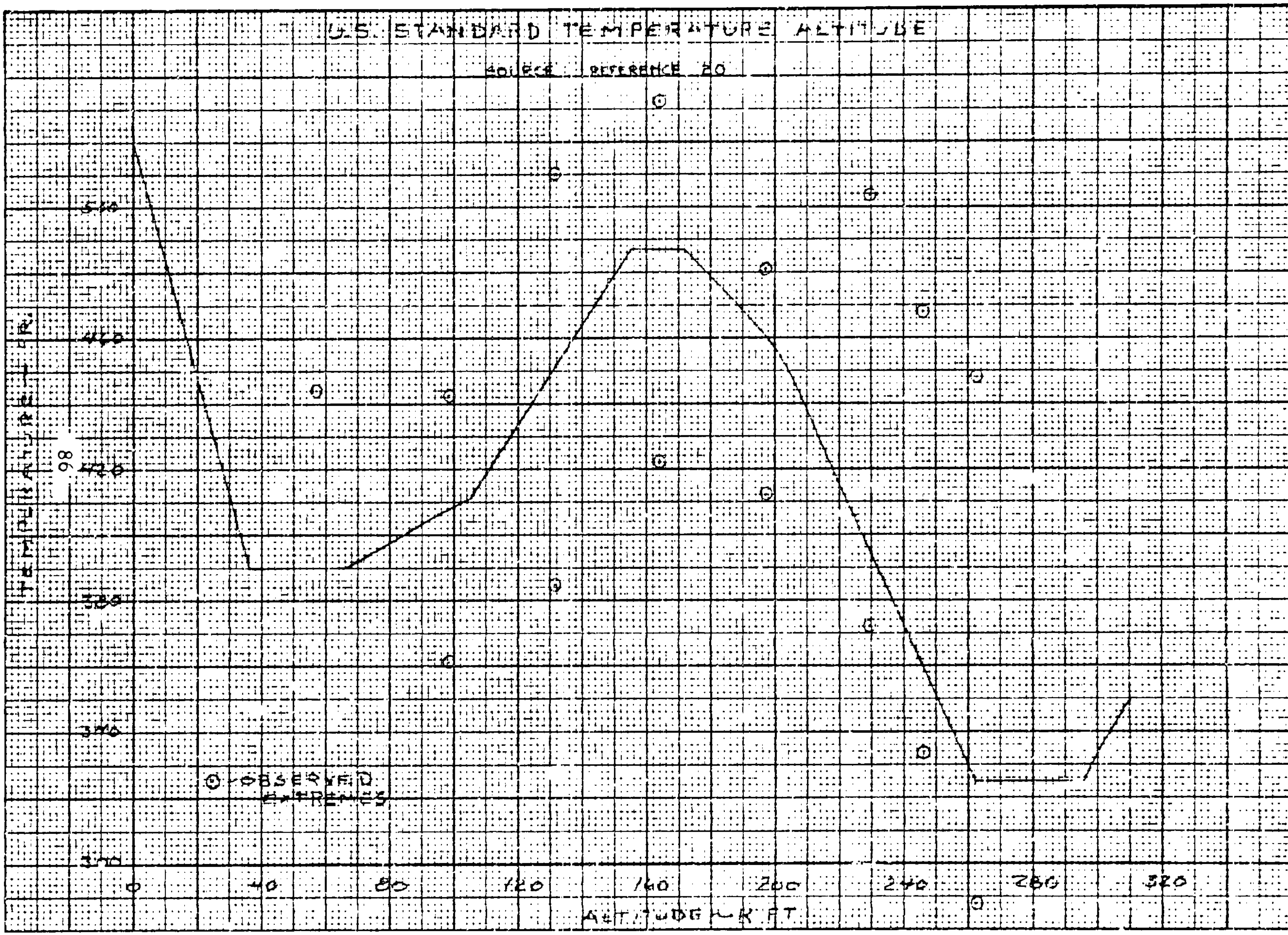
U.S. STANDARD TEMPERATURE ALTITUDE
SOURCE REFERENCE 20
TEMPERATURE — °R
500
460
420
380
340
300
0
40
80
120
160
200
240
280
320
ALTITUDE ~ K FT
⊙ - OBSERVED EXTREMES

FIG 37

K•E 10 X 10 TO THE CENTIMETER 46 1513
KEUFFEL & ESSER CO.

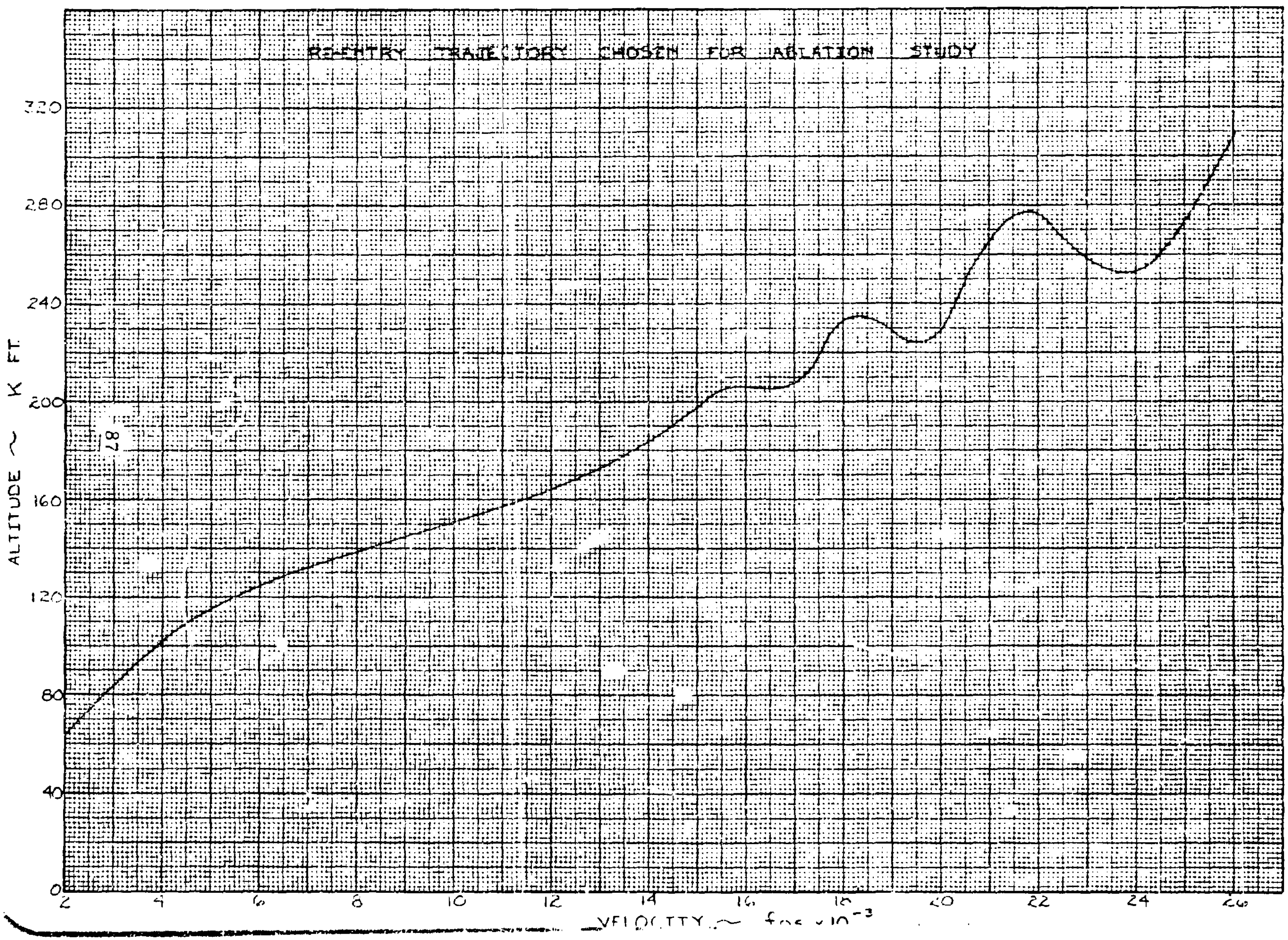

FIG 38

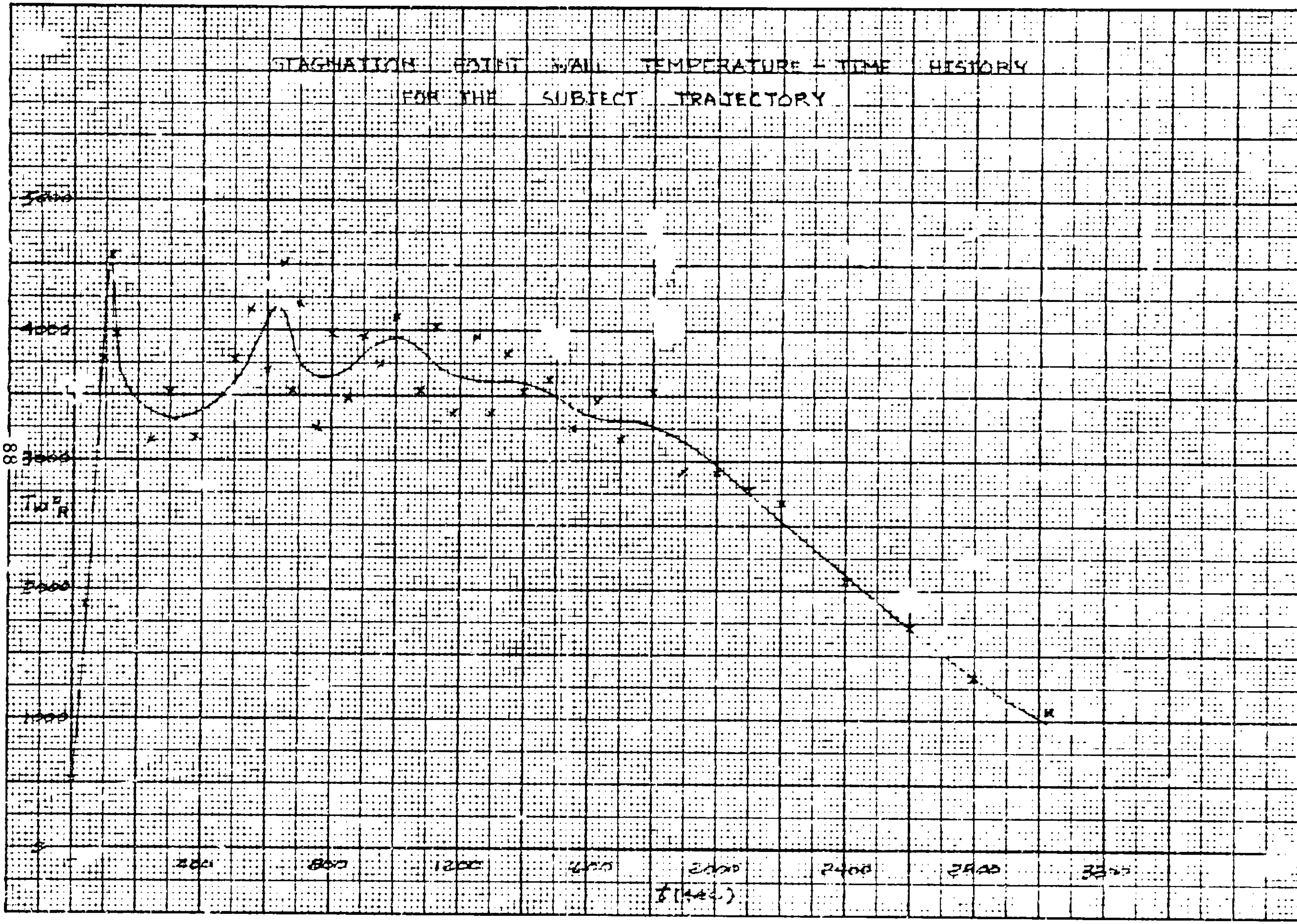
STAGNATION POINT WALL TEMPERATURE - TIME HISTORY
FOR THE SUBJECT TRAJECTORY
5000
4000
3000
Tw °R
2000
1000
400
800
1200
2000
2400
2800

FIG. 39

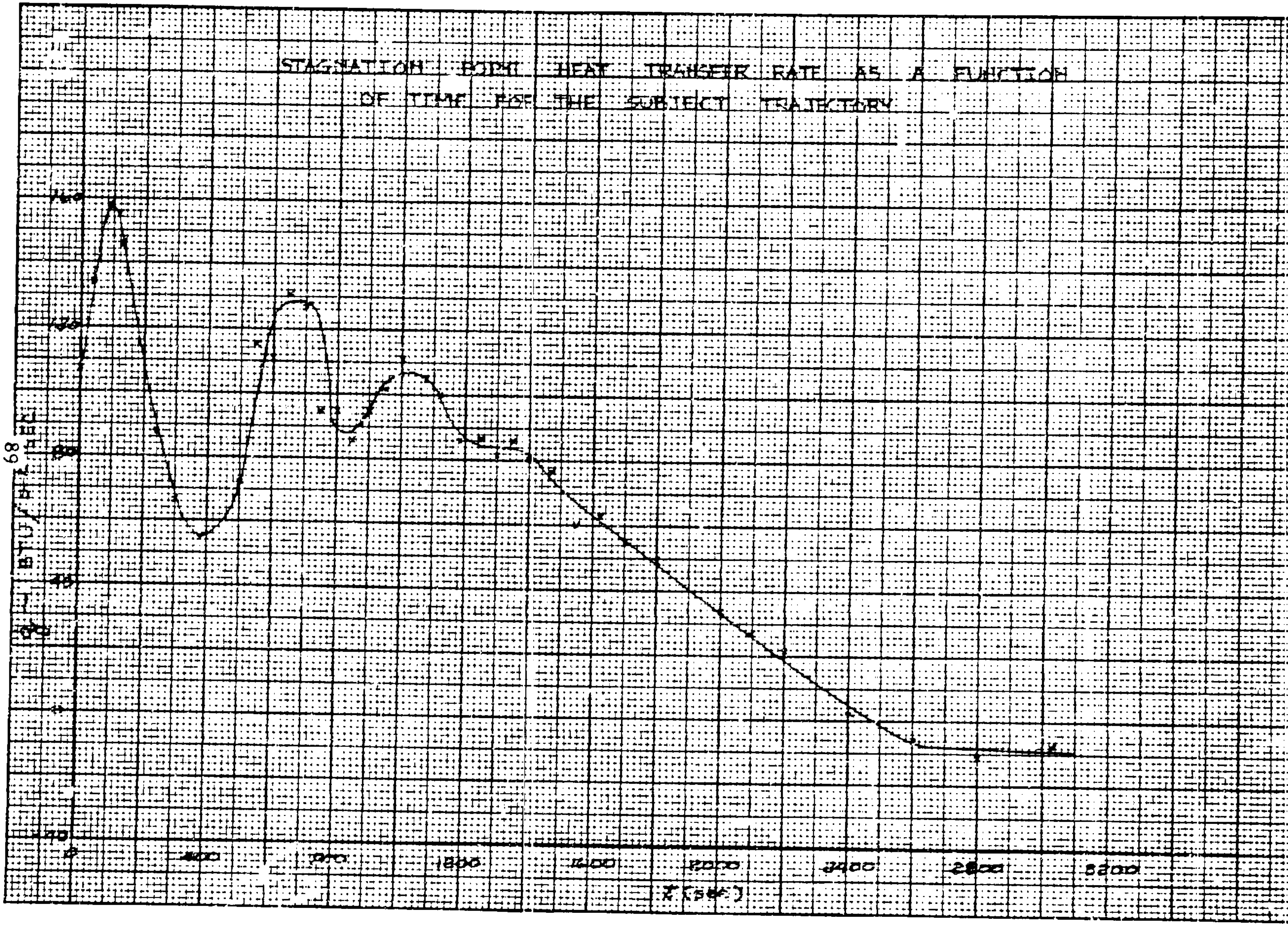
STAGNATION POINT HEAT TRANSFER RATE AS A FUNCTION
OF TIME FOR THE SUBJECT TRAJECTORY
160
120
80
40
0
400
800
1200
1600
2000
2400
2800
3200
BTU/FT² SEC

FIG 40

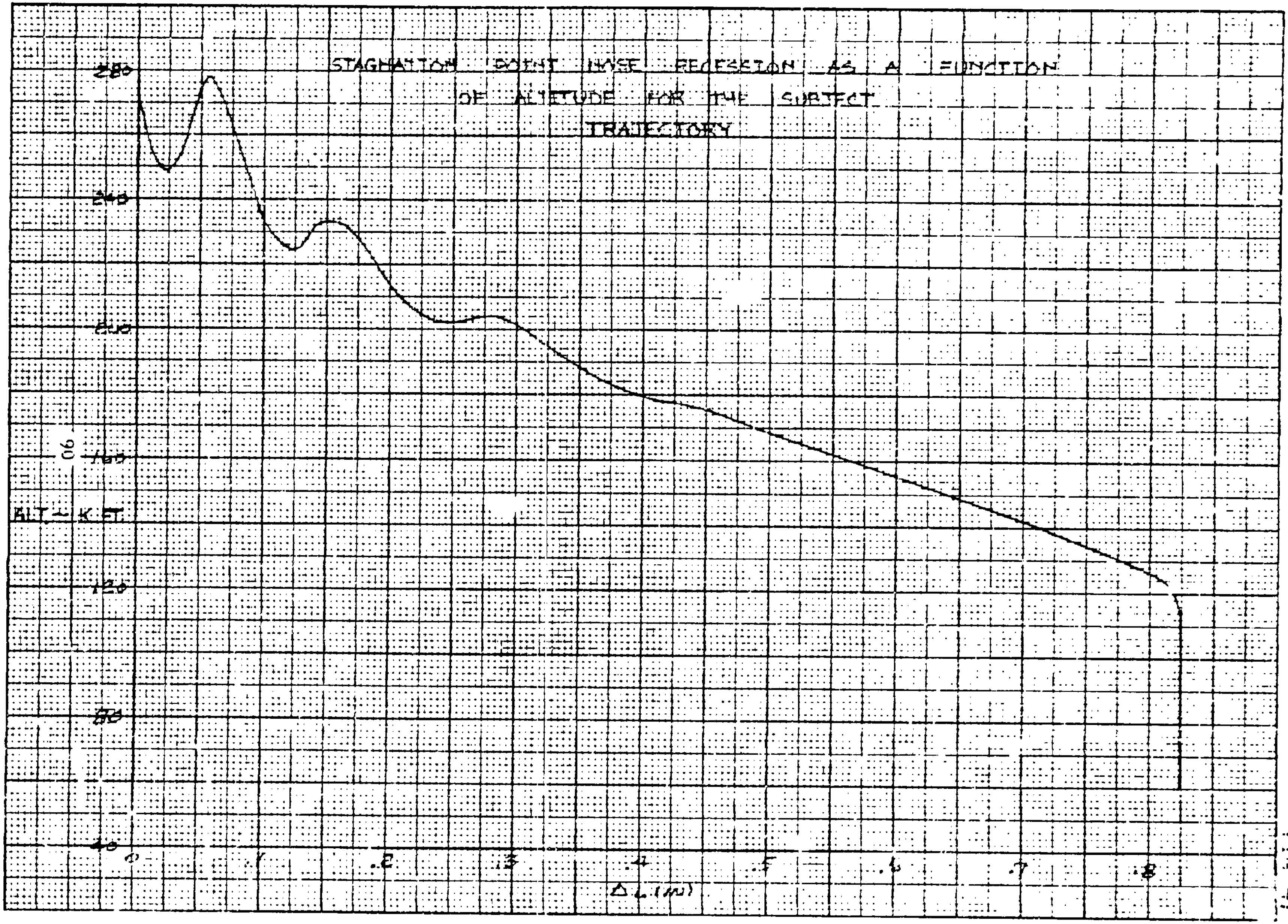
STAGNATION POINT NOSE RECESSION AS A FUNCTION
OF ALTITUDE FOR THE SUBJECT
TRAJECTORY
280
240
200
160
ALT ~ K FT
120
80
40
0
.1
.2
.3
.4
.5
.6
.7
.8
ΔL (IN)

FIG. 41

FIG 42

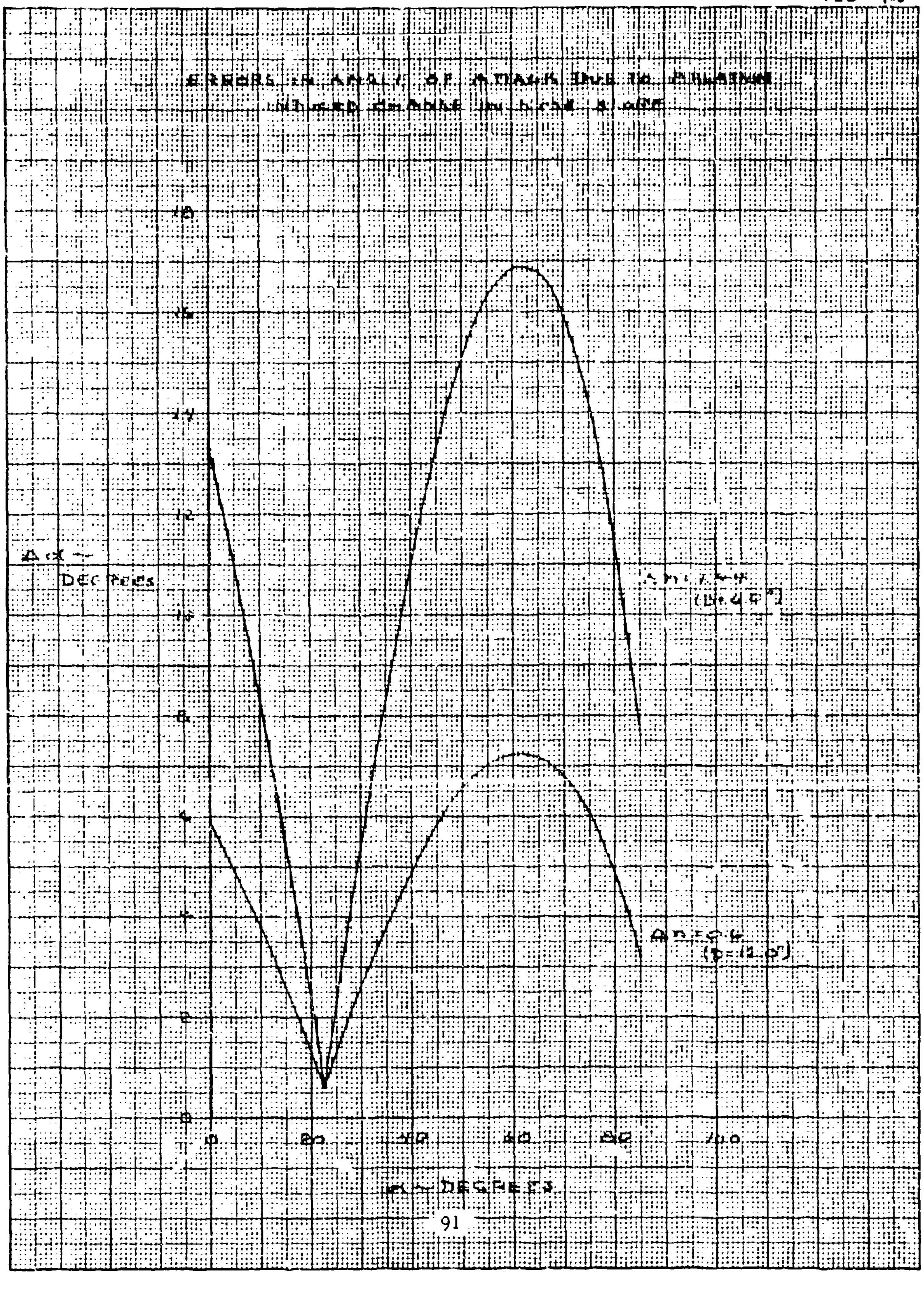

REFERENCES

1. Andersen, N. Y., "Validity of Air Data Equations at High Altitudes," CAL Report AF-1429-Y-1, June 1960.

2. Andersen, N. Y., "Final Report Transonic Flight Line Computer," CAL Report IH-933-P-2, October 1956.

3. Stillwell, W. H. and Larson, T. J., "Measurement of the Maximum Speed Attained by the X-15 Airplane Powered with Interim Rocket Engines," NASA Technical Note D-615, September 1960.

4. Stillwell, W. H. and Larson, T. J., "Measurement of the Maximum Altitude Attained by the X-15 Airplane Powered with Interim Rocket Engines," NASA Technical Note D-623, October 1960.

5. Larson, T. J. and Webb, L. D., "Calibrations and Comparisons of Pressure-Type Airspeed-Altitude Systems of the X-15 Airplane from Subsonic to High Supersonic Speeds," NASA Technical Note D-1724, February 1963.

6. Fischel, J. and Webb, L. D., "Flight-Informational Sensors, Display, and Space Control of the X-15 Airplane for Atmospheric and Near-Space Flight Missions," NASA Technical Note D-2407, August 1964.

7. Cary, J. P. and Keener, E. R., "Flight Evaluation of the X-15 Ball-Nose Flow-Direction Sensor as an Air-Data System," NASA Technical Note D-2923, July 1965.

8. Wolowicz, C. H. and Gossett, T. D., "Operational and Performance Characteristics of the X-15 Spherical Hypersonic Flow-Direction Sensor," NASA Technical Note D-3070, November 1965.

9. Zayas-Aguiar, H. A., "Angle of Attack from Pressure Measurements on a Fixed Ball Nose," NASA - FRC Memorandum, August 1, 1963.

10. Etkin, Bernard, Dynamics of Flight Stability and Control, John Wiley & Sons, Inc., New York, 1959.

11. Schuler, J. and Pritchard, F. E., "Six-Degree-of-Freedom Equations of Motion for a Maneuvering Re-Entry Vehicle," CAL Report No. TE-1411-F-1, 21 August 1961.

12. Boyer, D. W. and Bitikofer, D. R., "Analytical and Experimental Studies of Microwave Interaction with a Hypersonic Air Plasma," AF 19(628)-4968, Scientific Report No. 1, February 1967.

13. Inouye, Mamoru, "Numerical Solutions for Blunt Axisymmetric Bodies in a Supersonic Spherical Source Flow," NASA TN D-3383.

14. Roberts, J. F., Lewis, Clark H. and Reed, Marvin, "Ideal Gas Spherically Blunted Cone Flow Field Solutions at Hypersonic Conditions," AEDC-TR-66-121.

15. Beecham, L. J., "The Hemispherical, Differential Pressure Yawmeter at Supersonic Speed," Aeronautical Research Council Reports and Memoranda No. 3237, 1961.

16. Domasch, D. O., Sherby, S. S. and Connolly, T. F., "Airplane Aerodynamics," Pitman Pub. Co., 1957.

17. Bird, K. D., "Wind Tunnel Tests of a Pitot-Static Tube in the Subsonic and Lower Transonic Speed Range," JHU/APL/CF-1436, June 19, 1950, RESTRICTED.

18. Bird, K. D., "The Supersonic Calibration of Two Basic Pitot-Static-Yaw Tubes for Free-Flight Application," JHU/APL/CM 568, August 22, 1949, RESTRICTED.

19. "U.S. Standard Atmosphere, 1962: ICAO Standard Atmosphere to 20 Kilometers; Proposed ICAO Extension to 32 Kilometers; Tables and Data to 700 Kilometers," Prepared under sponsorship of NASA, USAF, United States Weather Bureau, December 1962.

20. Fukuzawa, Jun, and Smetana, F. O., "Feasibility Report Re-Entry Air Data Sensors," Prepared by Fairchild Camera and Instrument Corporation for Litton Systems, Inc., Canoga Park, California.

21. Experimental Facilities Division, Hypersonic Shock Tunnels Description and Capabilities, October 1964.

UNCLASSIFIED

Security Classification

DOCUMENT CONTROL DATA - R&D

(Security classification of title, body of abstract and indexing annotation must be entered when the overall report is classified)

1. ORIGINATING ACTIVITY (Corporate author) Cornell Aeronautical Laboratory, Inc. Buffalo, New York 14221	2a. REPORT SECURITY CLASSIFICATION UNCLASSIFIED 2b. GROUP N/A

3. REPORT TITLE

Analytical Study of Air Data Equations for a Hemispherical Pressure Through the Hypersonic Mach Number Range

4. DESCRIPTIVE NOTES (Type of report and inclusive dates)

Final Report

5. AUTHOR(S) (Last name, first name, initial)

Romeo, David J.

6. REPORT DATE	7a. TOTAL NO. OF PAGES	7b. NO. OF REFS
Sept. ber 1967		23

8a. CONTRACT OR GRANT NO. AF 33(615)-3554 b. PROJECT NO. 8222 c. Task No. 822207 d.	9a. ORIGINATOR'S REPORT NUMBER(S) CAL Report AA-2217-Y 9b. OTHER REPORT NO(S) (Any other numbers that may be assigned this report) AFFDL-TR-67-128

10. AVAILABILITY/LIMITATION NOTICES

This document is subject to special export controls and each transmittal to foreign governments or foreign nationals may be made only with prior approval of the Air Force Flight Dynamics Laboratory.

11. SUPPLEMENTARY NOTES	12. SPONSORING MILITARY ACTIVITY
N/A	Air Force Flight Dynamics Laboratory Air Force Systems Command Wright-Patterson AFB, Ohio 45433

13. ABSTRACT

Air data outputs obtainable from pressure measurements on a hemispherical probe were investigated analytically for Mach numbers of 0 to 20 and altitudes from 0 to 300,000 feet. Angles of attack from +50° to -20° and angles of sideslip up to ±15° are considered using a five orifice probe. Emphasis was placed on the hypersonic regime wherein air data parameters were shown to be obtainable by using a simplified set of pressure relations. Expressions for determining the uncertainties in the air data outputs resulting from both pressure measurement error and simplifying assumptions used in deriving the air data equations are presented. Errors resulting from changes in probe shape due to ablation are also considered. Finally, limitations in deriving air data information with this approach are presented.

Distribution of this Abstract is Unlimited.

DD FORM 1 JAN 64 1473

UNCLASSIFIED

Security Classification

14. KEY WORDS	LINK A		LINK B		LINK C	
	ROLE	WT	ROLE	WT	ROLE	WT
Supersonic/Hypersonic Air Data Sensing						
Hemispherical Pressure Distribution						
Air Data Equations						
Angle of Attack and Sideslip Measurement						
Velocity and Mach Number Measurement						

INSTRUCTIONS

1. ORIGINATING ACTIVITY: Enter the name and address of the contractor, subcontractor, grantee, Department of Defense activity or other organization *(corporate author)* issuing the report.

2*a*. REPORT SECURITY CLASSIFICATION: Enter the overall security classification of the report. Indicate whether "Restricted Data" is included. Marking is to be in accordance with appropriate security regulations.

2*b*. GROUP: Autor .ic downgrading is specified in DoD Directive 5200.10 and Armed Forces Industrial Manual. Enter the group number. Also, when applicable, show that optional markings have been used for Group 3 and Group 4 as authorized.

3. REPORT TITLE: Enter the complete report title in all capital letters. Titles in all cases should be unclassified. If a meaningful title cannot be selected without classification, show title classification in all capitals in parenthesis immediately following the title.

4. DESCRIPTIVE NOTES: If appropriate, enter the type of report, e.g., interim, progress, summary, annual, or final. Give the inclusive dates when a specific reporting period is covered.

5. AUTHOR(S): Enter the name(s) of author(s) as shown on or in the report. Enter last name, first name, middle initial. If military, show rank and branch of service. The name of the principal author is an absolute minimum requirement.

6. REPORT DATE: Enter the date of the report as day, month, year; or month, year. If more than one date appears on the report, use date of publication.

7*a*. TOTAL NUMBER OF PAGES: The total page count should follow normal pagination procedures, i.e., enter the number of pages containing information.

7*b*. NUMBER OF REFERENCES: Enter the total number of references cited in the report.

8*a*. CONTRACT OR GRANT NUMBER: If appropriate, enter the applicable number of the contract or grant under which the report was written.

8*b*, 8*c*, & 8*d*. PROJECT NUMBER: Enter the appropriate military department identification, such as project number, subproject number, system numbers, task number, etc.

9*a*. ORIGINATOR'S REPORT NUMBER(S): Enter the official report number by which the document will be identified and controlled by the originating activity. This number must be unique to this report.

9*b*. OTHER REPORT NUMBER(S): If the report has been assigned any other report numbers *(either by the originator or by the sponsor)*, also enter this number(s).

10. AVAILABILITY/LIMITATION NOTICES: Enter any limitations on further dissemination of the report, other than those imposed by security classification, using standard statements such as:

(1) "Qualified requesters may obtain copies of this report from DDC."

(2) "Foreign announcement and dissemination of this report by DDC is not authorized."

(3) "U. S. Government agencies may obtain copies of this report directly from DDC. Other qualified DDC users shall request through ________________."

(4) "U. S. military agencies may obtain copies of this report directly from DDC. Other qualified users shall request through ________________."

(5) "All distribution of this report is controlled. Qualified DDC users shall request through ________________."

If the report has been furnished to the Office of Technical Services, Department of Commerce, for sale to the public, indicate this fact and enter the price, if known.

11. SUPPLEMENTARY NOTES: Use for additional explanatory notes.

12. SPONSORING MILITARY ACTIVITY: Enter the name of the departmental project office or laboratory sponsoring *(paying for)* the research and development. Include address.

13. ABSTRACT: Enter an abstract giving a brief and factual summary of the document indicative of the report, even though it may also appear elsewhere in the body of the technical report. If additional space is required, a continuation sheet shall be attached.

It is highly desirable that the abstract of classified reports be unclassified. Each paragraph of the abstract shall end with an indication of the military security classification of the information in the paragraph, represented as *(TS)*, *(S)*, *(C)*, or *(U)*.

There is no limitation on the length of the abstract. However, the suggested length is from 150 to 225 words.

14. KEY WORDS: Key words are technically meaningful terms or short phrases that characterize a report and may be used as index entries for cataloging the report. Key words must be selected so that no security classification is required. Identifiers, such as equipment model designation, trade name, military project code name, geographic location, may be used as key words but will be followed by an indication of technical context. The assignment of links, roles, and weights is optional.